

**PERFORMANCE EVALUATION OF A MULTI-PORT DC-DC CURRENT
SOURCE CONVERTER FOR HIGH POWER APPLICATIONS**

A Thesis

by

BILLY FERRALL YANCEY III

Submitted to the Office of Graduate Studies of
Texas A&M University
in partial fulfillment of the requirements for the degree of

MASTER OF SCIENCE

May 2010

Major Subject: Electrical Engineering

**PERFORMANCE EVALUATION OF A MULTI-PORT DC-DC CURRENT
SOURCE CONVERTER FOR HIGH POWER APPLICATIONS**

A Thesis

by

BILLY FERRALL YANCEY III

Submitted to the Office of Graduate Studies of
Texas A&M University
in partial fulfillment of the requirements for the degree of

MASTER OF SCIENCE

Approved by:

Chair of Committee,	Mehrdad Ehsani
Committee Members,	Shankar Bhattacharyya
	Karen Butler-Purry
	Mark Holtzapple
Head of Department,	Costas Georghiades

May 2010

Major Subject: Electrical Engineering

ABSTRACT

Performance Evaluation of a Multi-port DC-DC Current Source Converter for High Power Applications. (May 2010)

Billy Ferrall Yancey III, B.S.E., Arkansas State University

Chair of Advisory Committee: Dr. Mehrdad Ehsani

With the ever-growing developments of sustainable energy sources such as fuel cells, photovoltaics, and other distributed generation, the need for a reliable power conversion system that interfaces these sources is in great demand. In order to provide the highest degree of flexibility in a truly distributed network, it is desired to not only interface multiple sources, but to also interface multiple loads. Modern multi-port converters use high frequency transformers to deliver the different power levels, which add to the size and complexity of the system. The different topological variations of the proposed multi-port dc-dc converter have the potential to solve these problems.

This thesis proposes a unique dc-dc current source converter for multi-port power conversion. The presented work will explain the proposed multi-port dc-dc converter's operating characteristics, control algorithms, design and a proof of application. The converter will be evaluated to determine its functionality and applicability. Also, it will be shown that our converter has advantages over modern multi-port converters in its ease of scalability from kW to MW, low cost, high power density and adaption to countless

combinations of multiple sources. Finally we will present modeling and simulation of the proposed converter using the PSIM[®] software.

This research will show that this new converter topology is unstable without feedback control. If the operating point is moved, one of the source ports of the multi-port converter becomes unstable and dies off supplying very little or no power to the load while the remaining source port supplies all of the power the load demands. In order to prevent this and add stability to the converter a simple yet unique control method was implemented. This control method allowed for the load power demanded to be shared between the two sources as well as regulate the load voltage about its desired value.

To my parents and my son

ACKNOWLEDGEMENTS

I would like to express my upmost gratitude to Dr. M. Ehsani for his support, guidance, and words of wisdom throughout the course of my graduate studies. I would also like to thank all of my committee members for their advice and assistance throughout this work. I also would like to convey my appreciation to the faculty and staff of the Electrical Engineering Department at Texas A&M University for their support and dedication to my education. I want to especially thank all of my current and former lab members with whom I have spent endless hours, and learned much: particularly Mr. R. Barazarte, Miss G. Gonzalez, Mr. S. Sarma, and Mr. A. Skorcz. Last but not least I would like to thank my family, my son, and Miss L. Durham for their neverending support and encouragement throughout my thesis work and my studies.

TABLE OF CONTENTS

	Page
ABSTRACT.....	iii
DEDICATION.....	v
ACKNOWLEDGEMENTS.....	vi
TABLE OF CONTENTS.....	vii
LIST OF FIGURES.....	ix
LIST OF TABLES.....	xiii
 CHAPTER	
I INTRODUCTION: DC-DC POWER CONVERTERS.....	1
A. Overview.....	1
B. Conventional DC-DC Converters.....	1
C. Multi-port DC-DC Converters.....	3
1. Multiple Inputs.....	3
2. Multiple Outputs.....	4
D. State of the Art Multi-port DC-DC Converters.....	5
1. Current Source Converters.....	6
2. Voltage Source Converters.....	8
E. Summary.....	9
II PREVIOUS RESEARCH.....	11
A. Inductor Converter Bridge (ICB).....	11
1. Analysis.....	11
2. Control Techniques.....	16
3. Multi-port ICB.....	17
B. Inverse Dual Converter (IDC).....	23
1. Analysis.....	24
2. Control Techniques.....	28
C. Summary.....	29

CHAPTER	Page
III	PROPOSED DC-DC CONVERTER TOPOLOGY..... 30
	A. Multi-Source IDC..... 30
	1. Basic Operation and Configuration..... 31
	B. Simulation Study..... 34
	1. Phase Difference Angle Variations..... 34
	2. Input Voltage Deviations..... 40
	3. Load Variations..... 40
	4. System Specifications and Control..... 41
	C. Modeling the System..... 43
	D. Summary..... 47
IV	PERFORMANCE RESULTS, ANALYSIS, AND CONTROL..... 48
	A. Operational Characteristics..... 48
	1. Phase Difference Angle Variation..... 48
	2. Input Voltage Deviation..... 62
	B. Control Results..... 65
	1. Input Voltage Deviation and Load Variation..... 65
	2. Input Voltage Deviation and Load Voltage Variations..... 68
	3. Input Voltage Deviation and Input Current Variations..... 71
	C. Summary..... 76
V	CONCLUSIONS AND FUTURE WORK..... 77
	A. Conclusions..... 77
	B. Future Work..... 78
	REFERENCES..... 79
	APPENDIX A..... 81
	APPENDIX B..... 88
	APPENDIX C..... 95
	APPENDIX D..... 98
	VITA..... 102

LIST OF FIGURES

FIGURE		Page
1	Conventional topology.....	2
2	Block diagram of a multi-input DC-DC converter.....	4
3	Block diagram of a multi-output DC-DC converter.....	5
4	Current source multi-port DC-DC converter.....	6
5	Multi-port DC-DC converter based on half bridge technique.....	7
6	Multi-port DC-DC converter based on flux additivity.....	8
7	Triple-active-bridge DC-DC converter.....	9
8	Inductor Converter Bridge (ICB).....	12
9	Timing diagram of load converter leading storage converter by φ	13
10	Three step phase shift from $\varphi = 0^\circ$ to $\varphi = -90^\circ$	17
11	Multi-port ICB with control variables defined.....	18
12	PSIM [®] model of multi-port ICB.....	20
13	Multi-port ICB source current calculated and simulated.....	21
14	Multi-port ICB load one current calculated and simulated.....	22
15	Multi-port ICB load two current calculated and simulated.....	22
16	Multi-port ICB currents for $\varphi_{12} \neq \varphi_{13}$	23
17	Inverse Dual Converter (IDC).....	24
18	Symbolic diagram of a gyrator.....	25
19	Examples of element gyrator transformation.....	26

FIGURE		Page
20	Gyrator equivalent IDC viewed from the source.....	26
21	Gyrator equivalent IDC viewed from the load.....	27
22	Voltage gain curve.....	29
23	Multi-source IDC.....	31
24	Input modules for S_{x14} switches conducting.....	36
25	Input modules for S_{x23} switches conducting.....	37
26	PSIM [®] model of Multi-source IDC with no controller.....	45
27	PSIM [®] model of Multi-source IDC with open loop control.....	45
28	PSIM [®] model of Multi-source IDC with feedback control.....	46
29	Converter currents for Scenario 1.....	50
30	Center link capacitor voltage for Scenario 1.....	50
31	Load voltage for Scenario 1.....	51
32	Original IDC converter currents.....	51
33	Magnitude of converter currents for Scenario 1.....	52
34	Magnitude of load voltage for Scenario 1.....	52
35	Converter currents for Scenario 2 mode 1 ($\varphi_{12} = 5^\circ$).....	54
36	Center link capacitor voltage for Scenario 2 mode 1 ($\varphi_{12} = 5^\circ$).....	54
37	Load voltage for Scenario 2 mode 1 ($\varphi_{12} = 5^\circ$).....	55
38	Magnitude of converter 1 current for increasing φ_{12}	55
39	Converter currents for Scenario 2 mode 1 ($\varphi_{12} = 80^\circ$).....	56
40	Center link capacitor voltage for Scenario 2 mode 1 ($\varphi_{12} = 80^\circ$).....	56

FIGURE		Page
41	Load voltage for Scenario 2 mode 1 ($\varphi_{12} = 80^\circ$).....	57
42	Converter currents for $\varphi_{12} = 0^\circ$ to $\varphi_{12} = 5^\circ$	58
43	Center link capacitor voltage for $\varphi_{12} = 0^\circ$ to $\varphi_{12} = 5^\circ$	58
44	Load voltage for $\varphi_{12} = 0^\circ$ to $\varphi_{12} = 5^\circ$	59
45	Converter currents for $\varphi_{12} = 0^\circ$ to $\varphi_{12} = 45^\circ$	60
46	Center link capacitor voltage for $\varphi_{12} = 0^\circ$ to $\varphi_{12} = 45^\circ$	61
47	Load voltage for $\varphi_{12} = 0^\circ$ to $\varphi_{12} = 45^\circ$	61
48	Converter currents for $V_2 = 25V$	62
49	Converter currents for $V_2 = 75V$	63
50	Load voltage for $R_L = 50\Omega$ to 45Ω	64
51	Load voltage for $R_L = 50\Omega$ to 55Ω	64
52	Source currents for 10% V_2 and 10% R_L variations.....	66
53	Center capacitor voltage for 10% V_2 and 10% R_L variations.....	66
54	Load current for 10% V_2 and 10% R_L variations.....	67
55	Load voltage for 10% V_2 and 10% R_L variations.....	67
56	Phase difference angles for 10% V_2 and 10% R_L variations.....	68
57	Source currents for 10% V_2 and 10% V_L variations.....	69
58	Center capacitor voltage for 10% V_2 and 10% V_L variations.....	69
59	Load current for 10% V_2 and 10% V_L variations.....	70
60	Load voltage for 10% V_2 and 10% V_L variations.....	70
61	Phase difference angles for 10% V_2 and 10% V_L variations.....	71

FIGURE		Page
62	Source currents for 10% V_2 and 25% I_2 variations.....	72
63	Load voltage for 10% V_2 and 25% I_2 variations.....	72
64	Phase difference angles for 10% V_2 and 25% I_2 variations.....	73
65	Source currents for 10% V_2 and ramp down I_2 variations.....	73
66	Load voltage for 10% V_2 and ramp down I_2 variations.....	74
67	Phase difference angles for 10% V_2 and ramp down I_2 variations.....	74
68	Source currents for 10% V_2 and ramp down and up I_2 variations.....	75
69	Load voltage for 10% V_2 and ramp down and up I_2 variations.....	75
70	Phase difference angles for 10% V_2 and ramp down/up I_2 variations...	76

LIST OF TABLES

TABLE		Page
1	Multi-port ICB simulation parameters.....	20
2	Multi-Source IDC simulation parameters.....	46

CHAPTER I

INTRODUCTION: DC-DC POWER CONVERTERS

This chapter will cover the evolution of multi-port DC-DC converters and their applications. An overview of multi-port DC-DC converter applications will be presented along with state of the art topologies being researched. Our research was motivated by the topics covered in this chapter.

A. Overview

In today's society the need for renewable energy sources is in high demand. Over the past few years technological advances have been made in wind power systems, photovoltaics, fuel cells, and hydroelectric power systems, just to name a few. With these advances comes the question of how to interface these for standalone power generation, whether it is one or all of these sources simultaneously. Along with interfacing multiple inputs, a growing need for interfacing multiple outputs has become an interesting topic in hybrid vehicles. One way to interface multiple inputs and multiple outputs is through the use of DC-DC converters.

B. Conventional DC-DC Converters

The first interface systems for renewable energy sources were constructed using the conventional topology, Fig.1 [1]. The conventional topology consists of multiple

This thesis follows the style and format of the *IEEE Transactions on Power Electronics*.

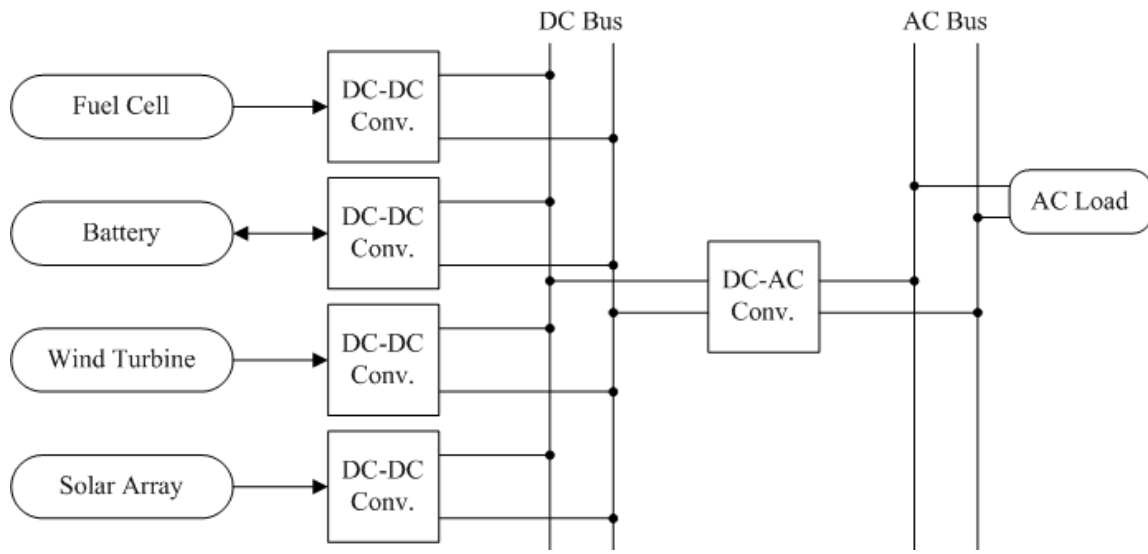


Fig. 1. Conventional topology [1].

energy inputs connected to a respective DC-DC converter with its own controller and storage element. Each DC-DC converter is connected to a common DC bus. The common DC bus is where the energy from each input is combined and then distributed to the loads through yet another DC-DC converter for each load. In a system of this nature, each DC-DC converter communicates with each other in order to control the power transferred from each input to its respective output. With this type of topology if one were to add multiple input modules, the overall system could become too large for its particular application where size and weight are an issue, i.e. hybrid vehicles. This conventional topology can also be used for multiple output systems. This is done by connecting each of the loads to the DC bus via a DC-DC converter or DC-AC converter.

C. Multi-port DC-DC Converters

The multi-port DC-DC converter topology is quickly becoming an alternative for renewable energy source interfacing [2], [3], [4]. A multi-port converter consists of multiple inputs or outputs, connected to its respective DC-DC converter. Each DC-DC converter is then connected to one overall energy storage element, as opposed to individual storage elements connected to a bus (conventional topology). The control of each DC-DC converter is then done by one controller to determine amount of power transferred from each input. This topology is specifically becoming interesting in hybrid vehicles where there are multiple inputs/outputs [4]. The reason for this interest is because hybrid vehicles currently have two voltage buses, 14V and 42V. The main bus is 42V and the 14V bus is then supplied by a DC-DC converter. Multi-level converters are currently being used to supply these voltages. However, a new bus voltage of 300V is needed to drive high voltage motor drives for active suspensions [5], and multi-level converters are not optimal for achieving voltage level differences of this magnitude (14V to 300V).

1. Multiple Inputs

A multiple input multi-port DC-DC converter is a converter having more than one energy source as its input. In this topology each input is connected to a DC-DC converter, then to an individual energy link. The energy link is then connected to another DC-DC converter, then to the output. A simple block diagram of this is shown in Fig. 2. A multi-input converter can be a four quadrant, a two quadrant or a single quadrant

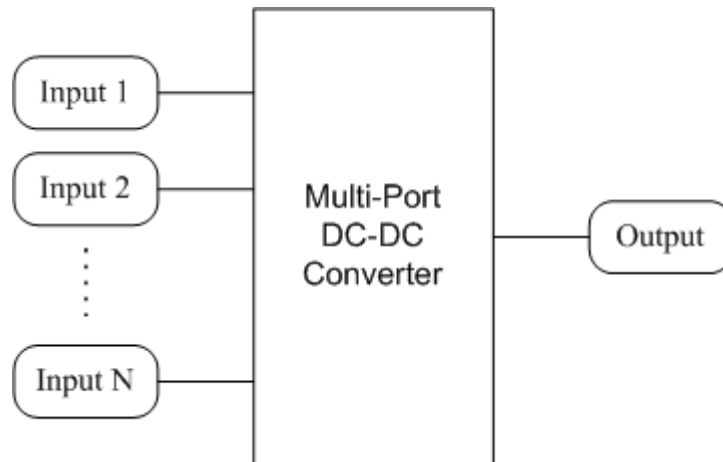


Fig. 2. Block diagram of a multi-input DC-DC converter.

converter. A four quadrant converter would consist of bidirectional current switches, i.e. BJTs, IGBTs, etc., and a two quadrant converter would consist of reverse blocking switches, i.e. SCRs, GTOs, etc. The use of two or four quadrant converters will allow for the inputs to send and receive power in either quadrants II and III or in all quadrants respectively. A single quadrant converter (diodes) will only allow power to be sent or received depending on the connection of the converter. A four quadrant converter can be useful in systems that have batteries, ultracapacitors, or other types of bidirectional current storage media. The two quadrant converter is useful in systems that do not require bidirectional current for storage, i.e. super magnetic energy storage.

2. *Multiple Outputs*

A multiple output multi-port DC-DC converter is defined as one having multiple outputs and is shown in Fig. 3. These multiple outputs are connected to an energy link through its respective DC-DC converter. One controller is used to monitor the amount

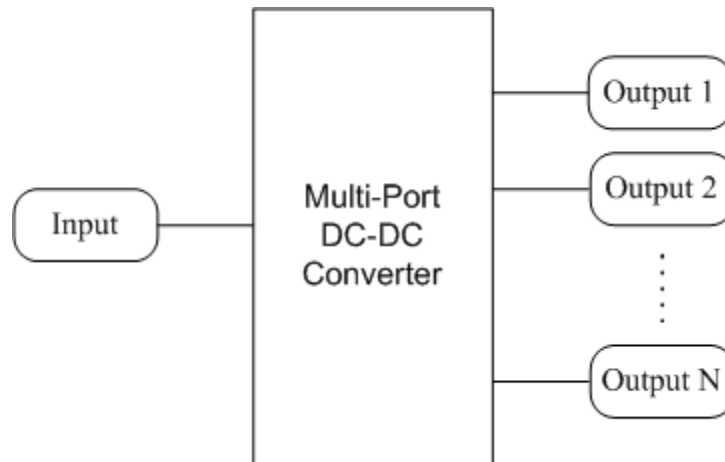


Fig. 3. Block diagram of a multi-output DC-DC converter.

of power transferred to each output from the input. This discussion will focus on hybrid vehicles with multiple outputs. In hybrid vehicles there are multiple dc buses that provide power for various electrical components of the vehicle. The big concern here is how to supply these dc buses as well as a much high dc bus. Multi-level converters are currently used for this, but are not optimal for large voltage differences between the levels. Multiple output DC-DC converters can supply these large voltage differences as well as get rid of multiple energy storage elements. Once this is accomplished in a cost effective manner, multi-port DC-DC converters will become standard for many applications.

D. State of the Art Multi-port DC-DC Converters

There are various topologies for multi-port DC-DC converters in today's market. Of these, the most interesting and similar to the proposed work will be discussed here.

These converters will be placed into two categories, current source converters and voltage source converters.

1. Current Source Converters

A current source converter (CSC) is one which determines current at the output and whose voltage is determined by the load. State of the art CSCs are voltage controlled current source converters. This means that a voltage source is placed in series with an inductor in order to simulate a current source. The size of the inductor determines how stiff the current is over one cycle. The current from this type of input is determined by the output. If this output is changed and the inductor is large enough the current will stay constant over one cycle. Therefore making it resemble a current source.

The first multi-port converter to be discussed is a CSC and is presented in [6]. This converter is made up of three active full bridges with voltage sources connected in series with inductors, Fig. 4. Each output is connected to a separate transformer with a

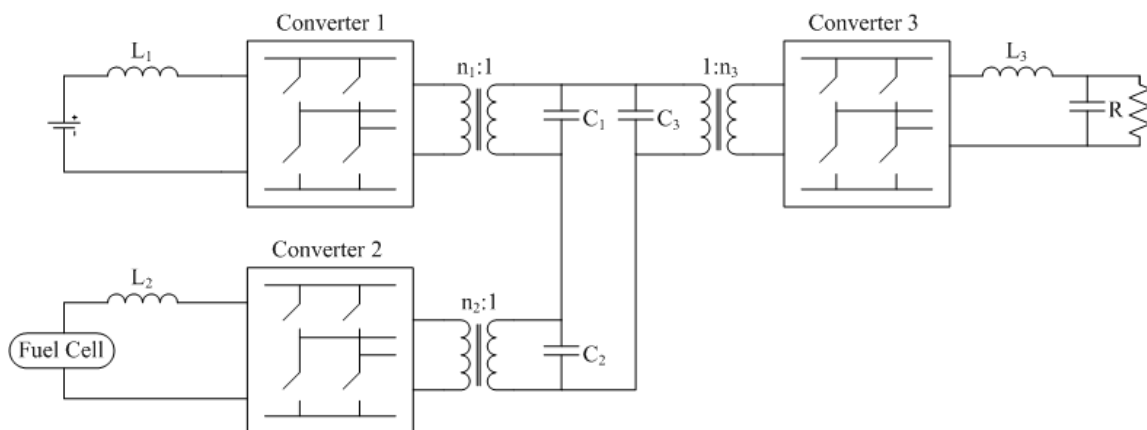


Fig. 4. Current source multi-port DC-DC converter [6].

capacitor across their respective terminals. The power transfer control strategy for this converter is done by shifting the timing of the bridges, leading or lagging, with respect to each other in order to transfer power. By adjusting this timing, the amount of power transferred will be changed. The power from each input is transferred through the transformer link.

A half bridge based multi-port converter is presented in [7], Fig. 5. This converter is based on a combination of dc-link and magnetic coupling through half bridge circuits. The operation of this topology consists of the switch timing of the three half bridges, HB1, HB2, and HB3. HB1 operates at a variable duty cycle based on whether it is sending or receiving power. Power flows from the input side of the circuit to the output by properly phase shifting HB2 and HB3. This control strategy is similar to the one stated above except it is performed on half bridges. The dc-link capacitors combine the power from the inputs (supercapacitor and fuel cell) and then the phase shift between HB2 and HB3 transfers the power by using the leakage inductance of the transformer.

A multi-port flux adding converter is shown in Fig. 6. This topology and control

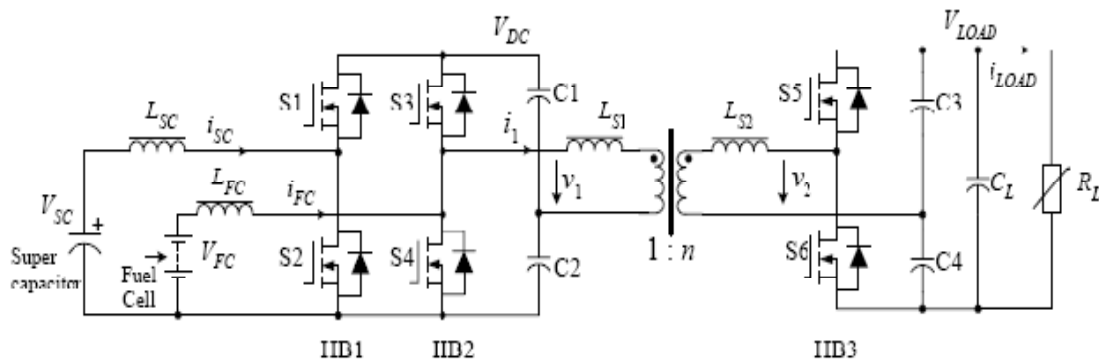


Fig. 5. Multi-port DC-DC converter based on half bridge technique [7].

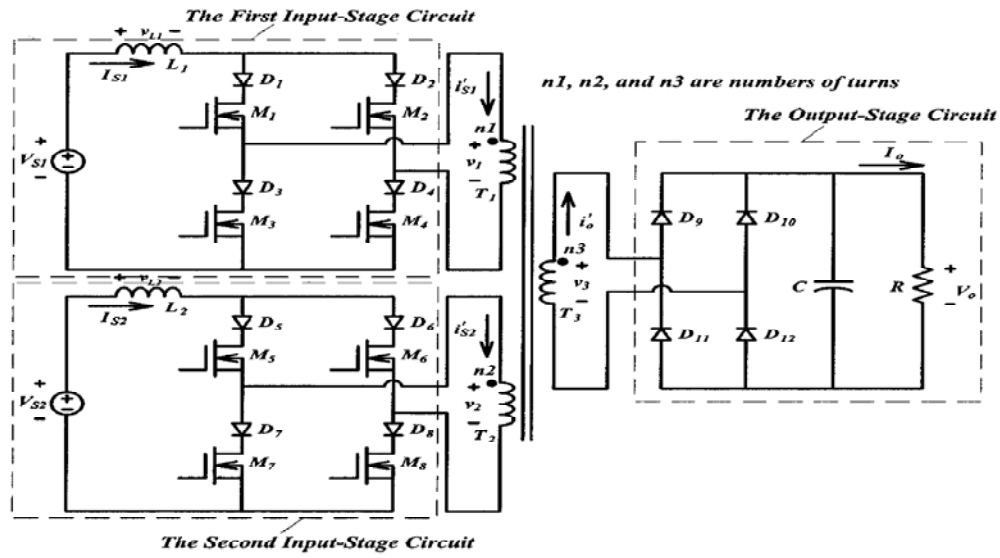


Fig. 6. Multi-port DC-DC converter based on flux additivity [8].

is similar to that of Fig. 4, but it uses the concept of flux additivity through a multi-wound transformer [8]. The power transfer control strategy for this topology is to combine the power sources in the magnetic form rather than in the electric form. This is done by phase shifting the full bridges' inputs based on power requirements of the output and then a current is injected into the terminals of the transformer, creating a flux in the magnetic core proportional to its current. The flux from both bridges is then added in the magnetic core and that flux produces a current of a proportional magnitude at the output terminal, i.e. supplying power to the output.

2. Voltage Source Converters

A voltage source converter (VSC) is one which determines voltage at the output and whose current is determined by the load. This type of converter is by far the most

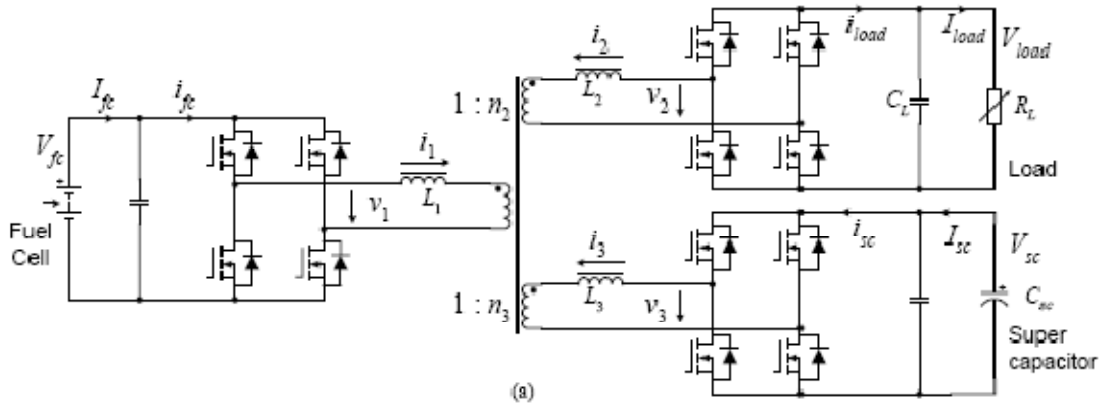


Fig. 7. Triple-Active-Bridge DC-DC converter.

widely used in DC-DC conversion. The triple-active-bridge (TAB) converter is introduced in [9], Fig. 7. This topology is an extension of the dual active bridge (DAB) proposed in [10]. The power transfer control strategy for this converter is very similar to the previous converters. The power flow is controlled by shifting the switch timing between the full bridges with respect to the other.

E. Summary

With the ever-growing developments of sustainable energy sources and the increasing amount of multiple output systems, the need for a multi-input interface system is a necessity. All of the multi-port converters discussed in this chapter are good candidates for these types of applications. The disadvantage of these converters is the transformer. By discarding the transformer, the size and weight of the converter will decrease. Also, the overall efficiency of the converter may increase because the losses of the transformer will not be present. Another disadvantage of these converters is extra

circuitry needed for soft switching. Therefore, a natural soft switching circuit would decrease the size and weight of the converter without increasing control.

CHAPTER II

PREVIOUS RESEARCH

This chapter will describe a family of voltage controlled, current source DC-DC converters. This family of converters is made up of topological variations of the Inductor Converter Bridge (ICB) and the Inverse Dual Converter (IDC). This family of converters is designed specifically for high power applications. The proposed topology, Multi-source IDC, belongs to this family and will be described in the next chapter. The objective of this chapter is to give an overview of the different converters in this family in order to obtain a better understanding of their operational characteristics.

A. Inductor Converter Bridge (ICB)

The ICB, Fig. 7, was originally designed for two quadrant power transfer between two superconducting magnets, L_S and L_L [11]. Each superconductive coil is connected to a full bridge converter made up of SCRs. The output of each bridge is attached to a high frequency AC capacitor link, which is used to temporarily store the energy to be transferred between these two superconductive coils. Power is transferred in this system by controlling the phase difference between the two converters switching sequences.

1. Analysis

In Fig. 8, the leftmost converter will be identified as the source and the rightmost

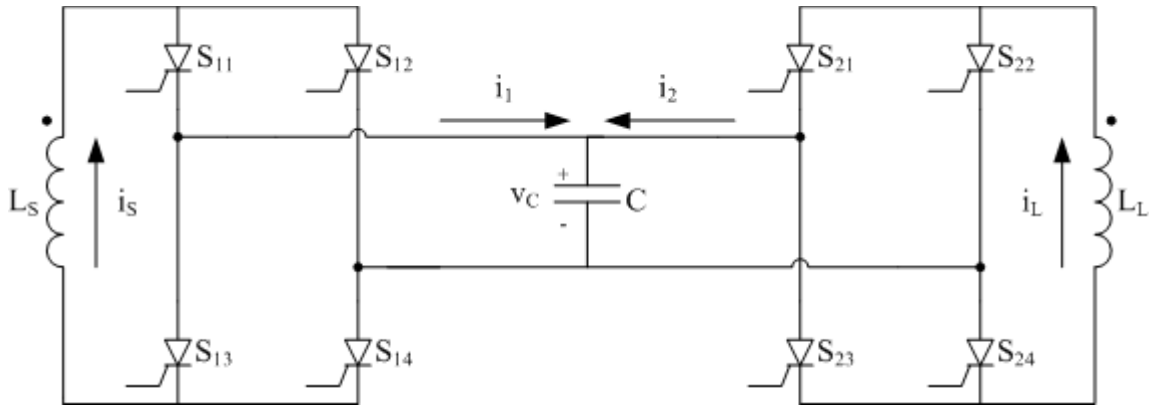


Fig. 8. Inductor Converter Bridge (ICB).

converter will be identified as the load. The switch timing of these converters will be referenced to the source converter. The switch timing of the source converter is the same as the load converter, i.e. $S_{11}S_{14}$, $S_{12}S_{13}$, $S_{11}S_{14}$, etc., and $S_{21}S_{24}$, $S_{22}S_{23}$, $S_{21}S_{24}$, etc., Fig. 9. A leading switch timing of less than half a cycle will cause a net energy transfer from source to load and a lagging switch timing will cause a net energy transfer from load to source. The leading or lagging switch timing difference between the two converters is denoted by the variable φ . The capacitor is used to temporarily store energy before it is transferred to the source or load. The switching frequency of this converter is high enough so that only a small fraction of the system's energy is stored in the capacitor every half cycle. In the other half cycle the energy stored in the capacitor is dissipated into the source or load. Therefore, over one full cycle there is no net energy storage in the capacitor. The importance of this will become apparent later when φ is

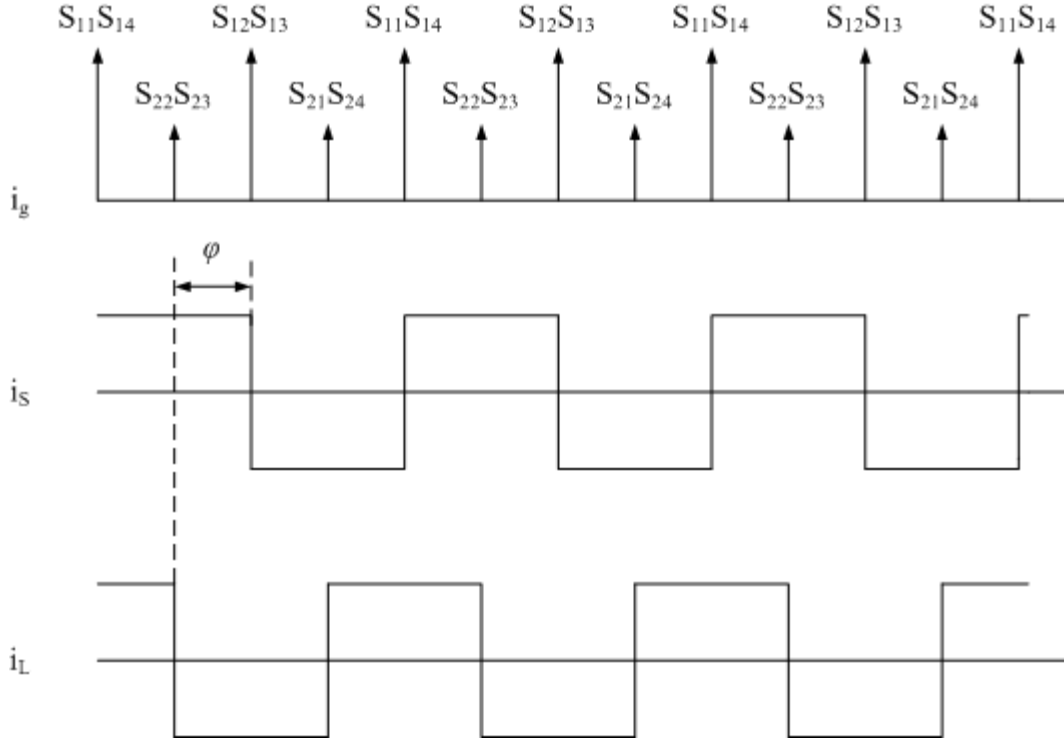


Fig. 9. Timing diagram of output converter leading input converter by φ .

changed during operation. The capacitor also supplies the reverse voltage necessary for the commutation of current between the switching events stated above [12].

Dynamic analysis of the ICB has previously been performed by means of fourier analysis, quadrometrics [12], and state space averaging [13]. The fourier analysis of the ICB gives an approximate expression for the average power transfer over one cycle from the source to the load.

$$\langle p_s \rangle = \sum_{n=1}^{\infty} \frac{4I_s I_L}{n^3 \pi^2 \omega C} [1 - (-1)^n] \sin(n\varphi) \quad (1)$$

where $\langle p_s \rangle$ is the average source power over one cycle, I_S and I_L are the average source and load currents, ω is the angular frequency of the converter and φ is the switch timing difference between the source and load converters.

State space averaging was used to obtain an averaged solution for the power transferred within the ICB. The coil currents are shown by the following equations.

$$\dot{I}_S = -\frac{k}{L_S} I_L \quad (2)$$

$$\dot{I}_L = \frac{k}{L_L} I_S \quad (3)$$

$$I_S(t) = I_O \cos\left(\frac{k}{\sqrt{L_S L_L}} t\right) \quad (4)$$

$$I_L(t) = I_O \sqrt{\frac{L_S}{L_L}} \sin\left(\frac{k}{\sqrt{L_S L_L}} t\right) \quad (5)$$

where,

$$k = \frac{\varphi - \frac{\varphi^2}{\pi}}{\omega C} \quad (6)$$

The coil voltages can be obtained from (2) and (3) as

$$V_S = -L_S \dot{I}_S = kI_L \quad (7)$$

$$V_L = -L_L \dot{I}_L = -kI_S \quad (8)$$

The rate of energy leaving the source is defined as positive power,

$$\langle p_S \rangle = -\frac{d}{dt} \left(\frac{1}{2} L_S I_S^2 \right) = -L_S I_S \dot{I}_S \quad (9)$$

Now substituting (2) into (9) we get the average power transferred from source to load is

$$\langle p_S \rangle = kI_S I_L = \frac{I_S I_L}{\omega C} \left(\varphi - \frac{\varphi^2}{\pi} \right) \quad (10)$$

The range of the phase difference angle, φ , is from $0^\circ - 180^\circ$ depending on the amount of desired power transfer, but it has been shown in [12] that the power transfer curve is symmetric about $\varphi = 90^\circ$.

Quadrometrics is a mathematical expression of the ICB phase currents as step functions and the capacitor voltage as a ramp function. Through this rigorous analysis, which can be seen in detail in [12], the same closed form solution was found for average power as in (10). Proof that (1) is equal to (10) is shown in [12]. In order to calculate maximum power transfer, one must take the derivative of (10) with respect to φ and set equal to zero and solve for φ .

$$0 = \frac{dp_s}{d\varphi} = \frac{d}{d\varphi} \left(\frac{I_s I_L}{\omega C} \left(\varphi - \frac{\varphi^2}{\pi} \right) \right) \Rightarrow \varphi = \frac{\pi}{2} \quad (11)$$

2. Control Techniques

For the ICB there are two variables that can be controlled to implement power transfer, phase difference angle φ and switching frequency f [12]. The preferred way to implement power transfer is through phase modulation because the phase difference angle φ is the only way one can change the direction of power transfer. When the amount of power transferred needs to be adjusted some sort of phase shifting is to be used to prevent overvoltages or voltage imbalances on the capacitor. This can be performed on either the source or the load converter. Phase shifting should be implemented in a minimum of a three step shift. For example, if a phase shift of $\Delta\varphi$ is to be implemented the timing sequence is as follows:

$$\Delta t_1 = \Delta t_1 - \frac{\Delta t_\varphi}{2} \quad (12)$$

$$\Delta t_2 = \Delta t_1 - \frac{\Delta t_\varphi}{2} \quad (13)$$

$$\Delta t_3 = \Delta t_1 \quad (14)$$

Note that a $\Delta\varphi$ phase shift corresponds to a Δt time shift, $\Delta\varphi/2\pi f$. Also, note that the phase angle will be positive for the load converter leading the source converter and vice versa. Fig. 10 shows that the source converter and load converter are in phase,

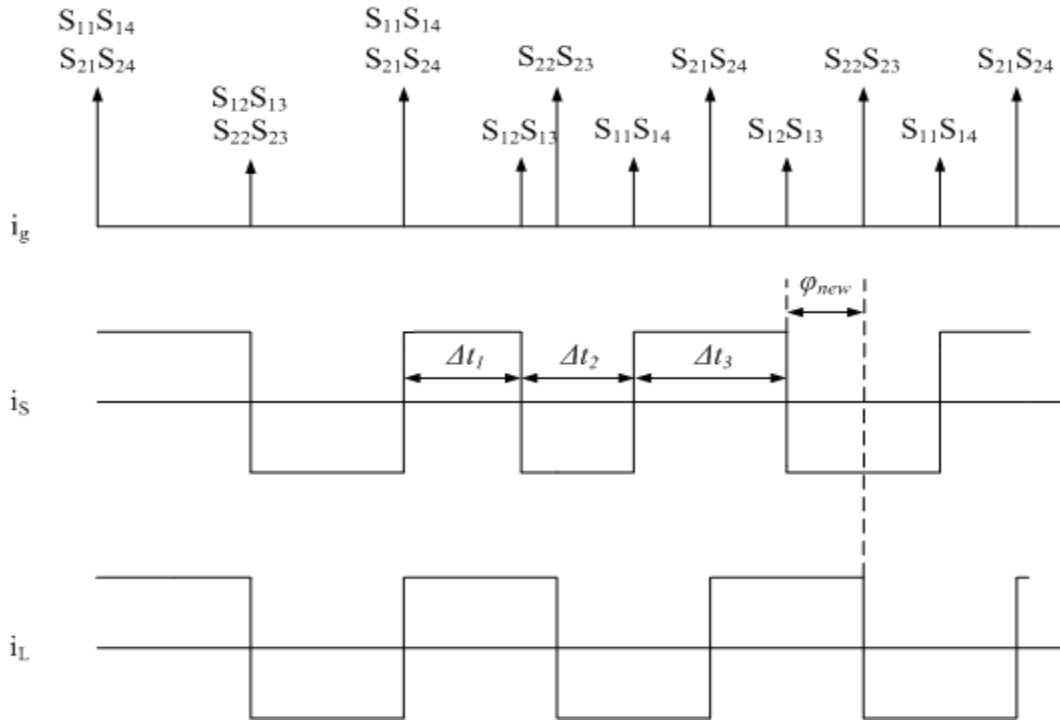


Fig. 10. Three step phase shift from $\varphi = 0^\circ$ to $\varphi = -90^\circ$.

$\varphi = 0^\circ$, and the new phase angle is $\varphi_{new} = 90^\circ$. A three step timing sequence should be implemented for every 90° phase shift to prevent capacitor spikes and voltage biasing. A bang-bang control technique that implements a phase shift from $\varphi = 90^\circ$ to $\varphi = -90^\circ$ was used to show that as well as transferring maximum power, one can control the current through a coil about a particular reference. This is significant if the load coil is supplying a current sensitive load.

3. Multi-port ICB

The multi-port ICB, Fig. 11, is an extension of the standard ICB discussed earlier. The multi-port ICB now has three phase difference angles, φ_{12} , φ_{13} , and φ_{23} .

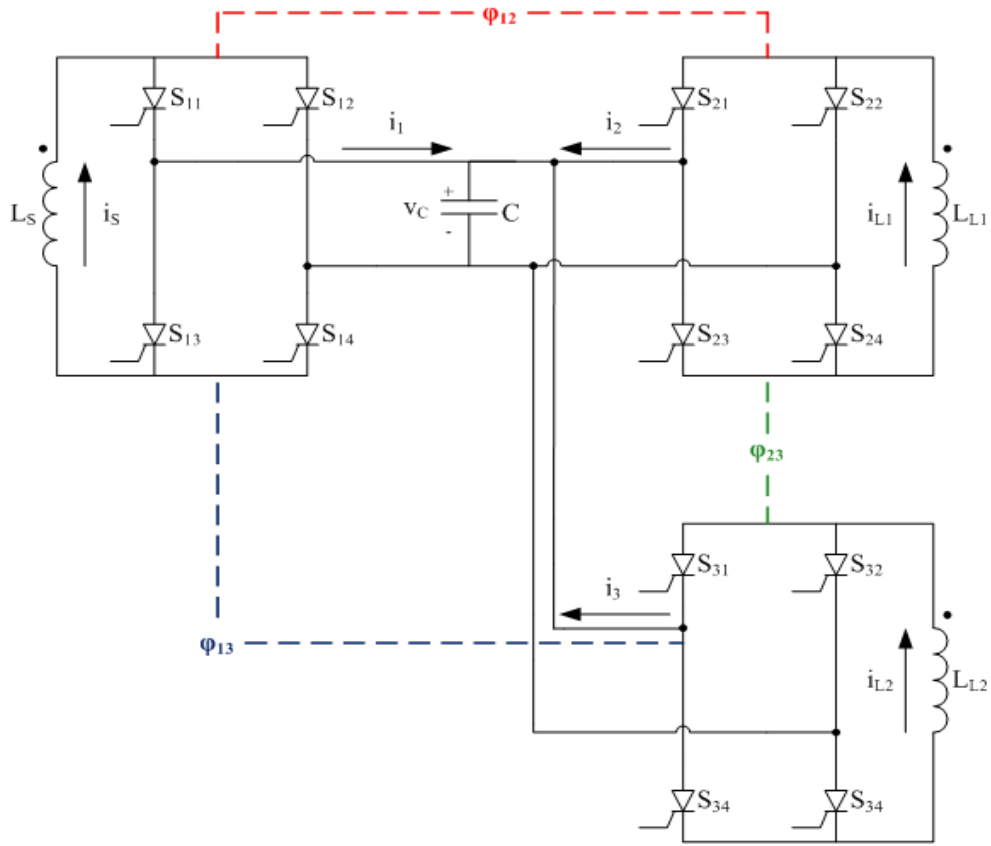


Fig. 11. Multi-port ICB with control variables defined.

With φ_{23} being the difference between φ_{12} and φ_{23} . The operation of this topology of the ICB is similar to the two port ICB except that the phase difference angle, φ , between the two load converters and the source converter need not be the same, i.e. $\varphi_{12} \neq \varphi_{13}$. To show the similarity between the multi-port ICB and the standard ICB the state space averaging technique was applied for $\varphi_{12} = \varphi_{13}$ and the details are shown in Appendix A. The results of this analysis are shown in (15) – (20). The differential equations for the three inductor currents are,

$$\dot{I}_1 = -\frac{k}{L_1} I_2 - \frac{k}{L_1} I_3 \quad (15)$$

$$\dot{I}_2 = \frac{k}{L_2} I_1 \quad (16)$$

$$\dot{I}_3 = \frac{k}{L_3} I_1 \quad (17)$$

where k is shown in (6) and through MATLAB's symbolic solver, the previous differential equations were solved and are shown in (18) – (20).

$$I_1 = I_o \cos\left(\frac{k\sqrt{L_2 + L_3}}{\sqrt{L_1 L_2 L_3}} t\right) \quad (18)$$

$$I_2 = I_o \frac{\sqrt{L_1 L_3}}{\sqrt{L_2} \sqrt{L_2 + L_3}} \sin\left(\frac{k\sqrt{L_2 + L_3}}{\sqrt{L_1 L_2 L_3}} t\right) \quad (19)$$

$$I_3 = I_o \frac{\sqrt{L_1 L_2}}{\sqrt{L_3} \sqrt{L_2 + L_3}} \sin\left(\frac{k\sqrt{L_2 + L_3}}{\sqrt{L_1 L_2 L_3}} t\right) \quad (20)$$

These equations were simulated from $t = 0 - 10s$ and compared with a simulated multi-port model in PSIM[®] shown in Fig. 12. The specifications for a predesigned multi-port ICB are given in Table 1.

Table 1. Multi-port ICB simulation parameters

Parameter	Symbol	Value	Units
Initial Storage Current	I_0	100	A
Source Inductor	L_S	4	H
Load Inductor 1	L_{L1}	4	H
Load Inductor 2	L_{L2}	4	H
AC Link Capacitor	C	250	μF
Phase Difference	φ_{12} & φ_{13}	85	$^\circ$

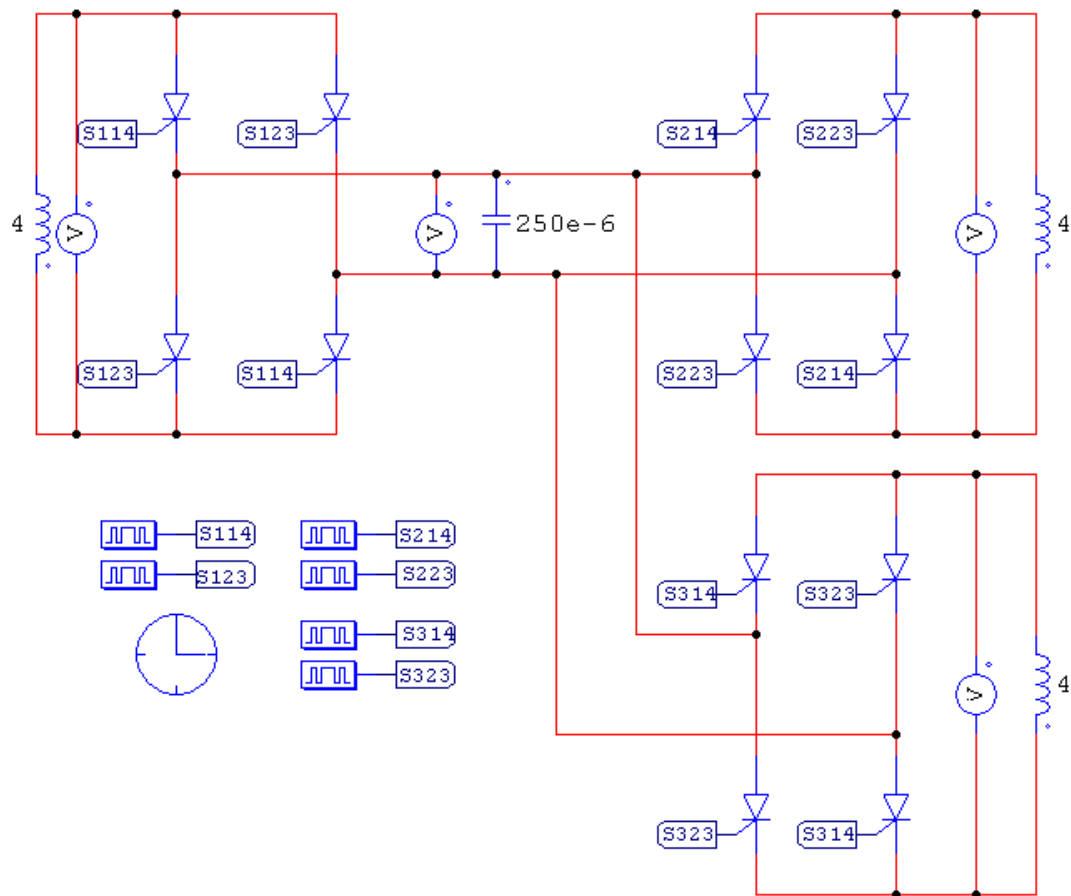


Fig. 12. PSIM model of multi-port ICB.

The results from the simulation are shown in Figs. 13 – 15. These figures show the calculated inductor currents and simulated inductor currents. As can be seen, the equations from the state space analysis describe the transients of the current from the source inductor to the load inductors. Therefore, these equations accurately describe the transient operation of the circuit.

The PSIM[®] model shown in Fig. 12 was simulated again with the same parameters shown in Table 1 except the phase differences between the converters were changed to the following: $\varphi_{12} = 90^\circ$, $\varphi_{13} = 75^\circ$, and $\varphi_{23} = 15^\circ$. The inductor currents are shown in Fig. 16. This figure indicates that power is being transferred at different rates to the two respective loads, as would be expected from the phase differences stated above. It can also be seen that at approximately 8 seconds the load inductors have

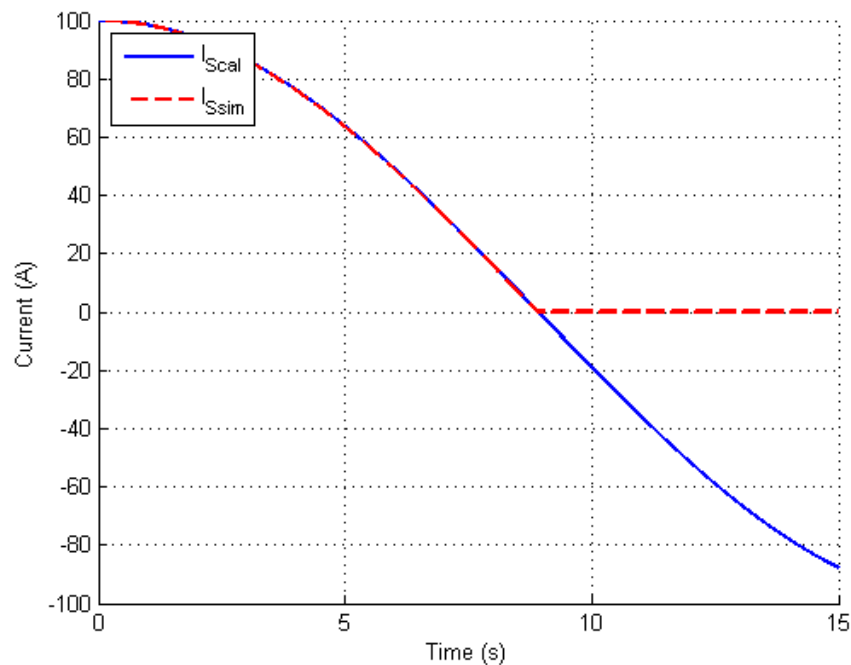


Fig. 13. Multi-port ICB source current calculated and simulated.

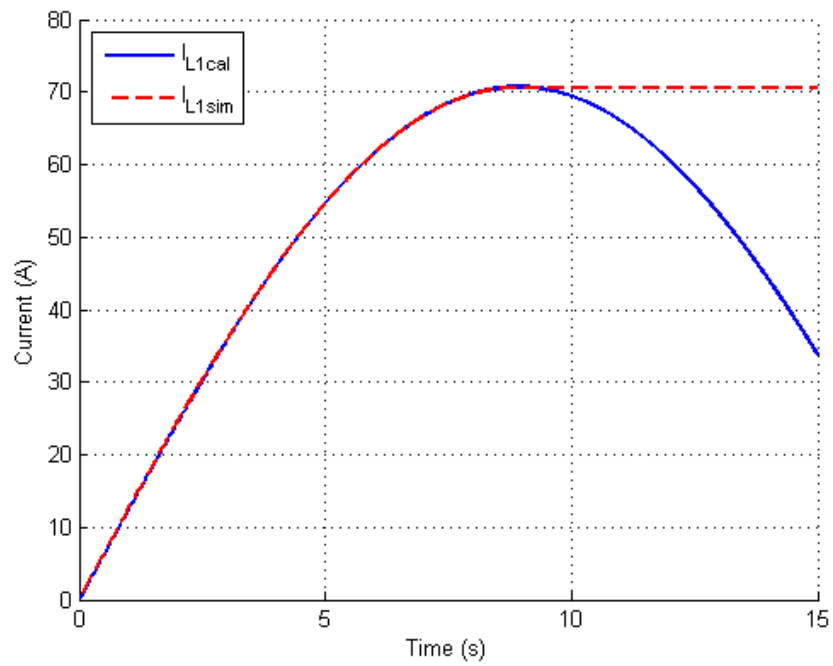


Fig. 14. Multi-port ICB load one current calculated and simulated.

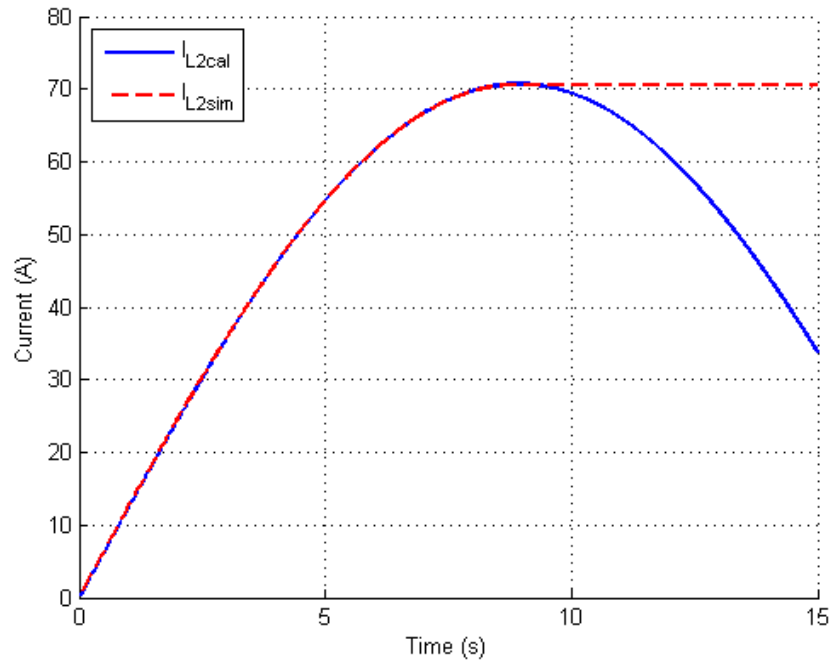


Fig. 15. Multi-port ICB load two current calculated and simulated.

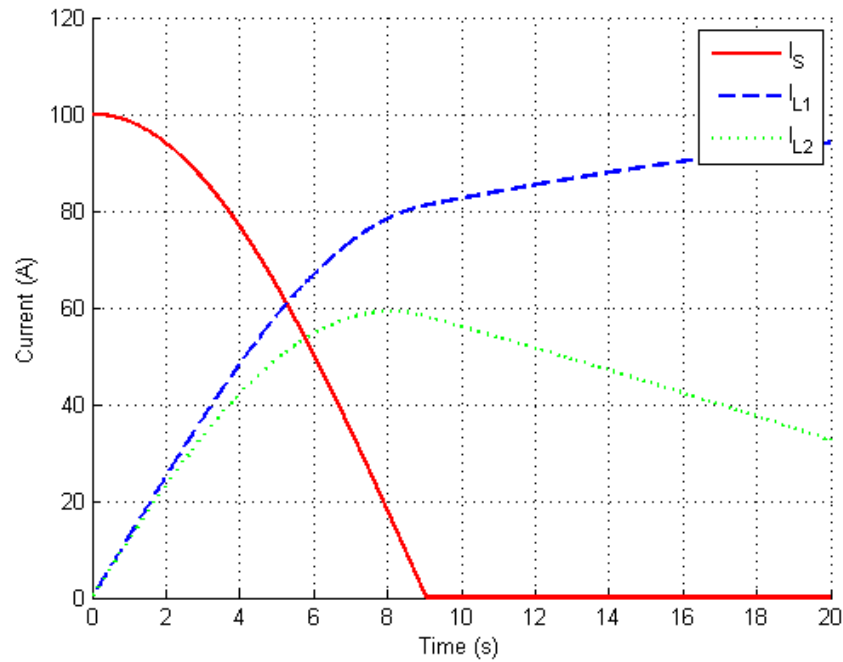


Fig. 16. Multi-port ICB currents for $\varphi_{12} \neq \varphi_{13}$.

reached their steady state. This means that the energy in the two load inductors is equal to that of the original energy in the source inductor. After the load inductors reach this point there is now a phase difference between the two loads such that load two is leading load one. This will cause power transfer from load two to load one. Since this phase difference is small, it will take some time for all of the energy to be transferred to load 1 from load 2.

B. Inverse Dual Converter (IDC)

The Inverse Dual Converter (IDC) is an extension of the ICB shown in Fig. 8. The IDC is a voltage controlled current source DC-DC converter shown in Fig. 17 [14].

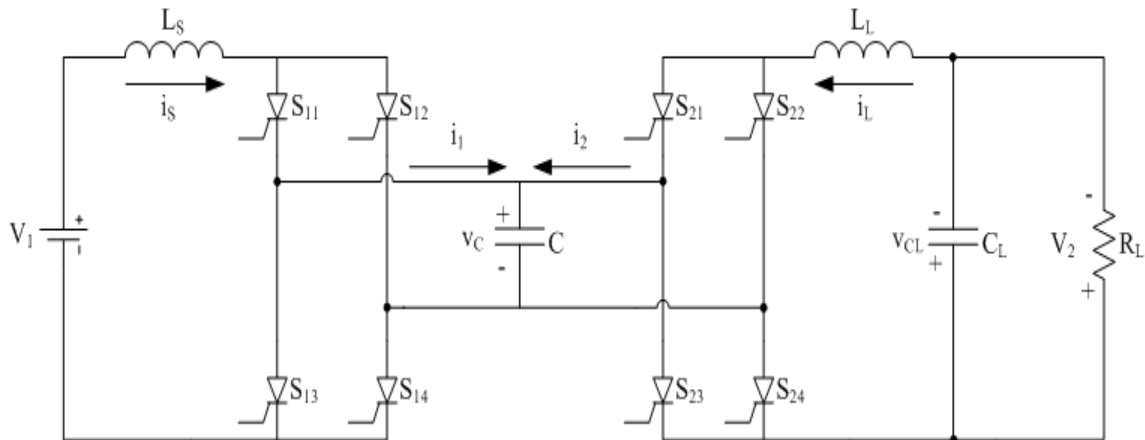


Fig. 17. Inverse Dual Converter (IDC).

The operation of the IDC is similar to the ICB. The IDC is a capacitor commutated converter with the capacitor acting as the voltage transfer element. Since the commutation is controlled by the capacitor, SCR's can be used as the switching element. With the use of SCR's the power rating can be scaled up to MWs rather easily.

1. Analysis

The analysis of the IDC was done using gyrator theory. A gyrator is defined as a two-port lossless storage less system that transforms one port into its dual with respect to the gyration coefficient. For example, a voltage source connected to one port would look like a current source if viewed from the second port and vice versa. The basic diagram for a gyrator is shown in Fig. 18. The equations for this system are shown in (21) and (22) [15]. Basic conversions of elements are shown in Fig. 19. These were used to get the equivalent circuits referred to the load and source side, respectively.

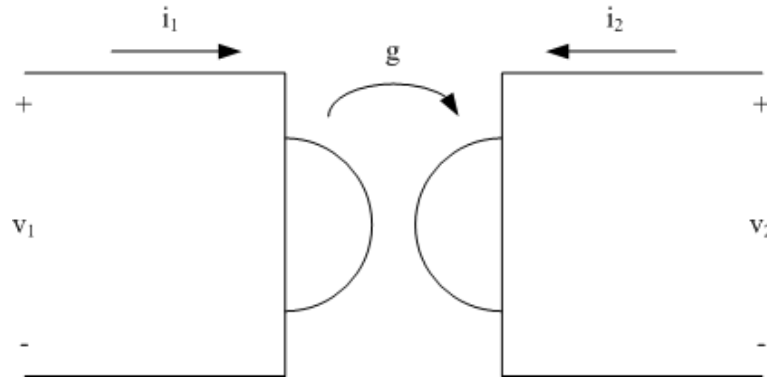


Fig. 18. Symbolic diagram of a gyrator.

$$i_1 = gv_2 \quad (21)$$

$$i_2 = -gv_1 \quad (22)$$

These circuits are used in the analysis of the IDC to determine source current, load current, and voltage gain. Now using the IDC model in Fig. 17 and using the gyrator conversions in Fig. 19 one can obtain two circuits for the IDC. Fig. 20 viewed from the source side and Fig. 21 viewed from the load side. From Fig. 20 the steady state source current can be calculated and is

$$I_s = \frac{V_i}{\frac{1}{g^2 R}} = V_i g^2 R \quad (23)$$

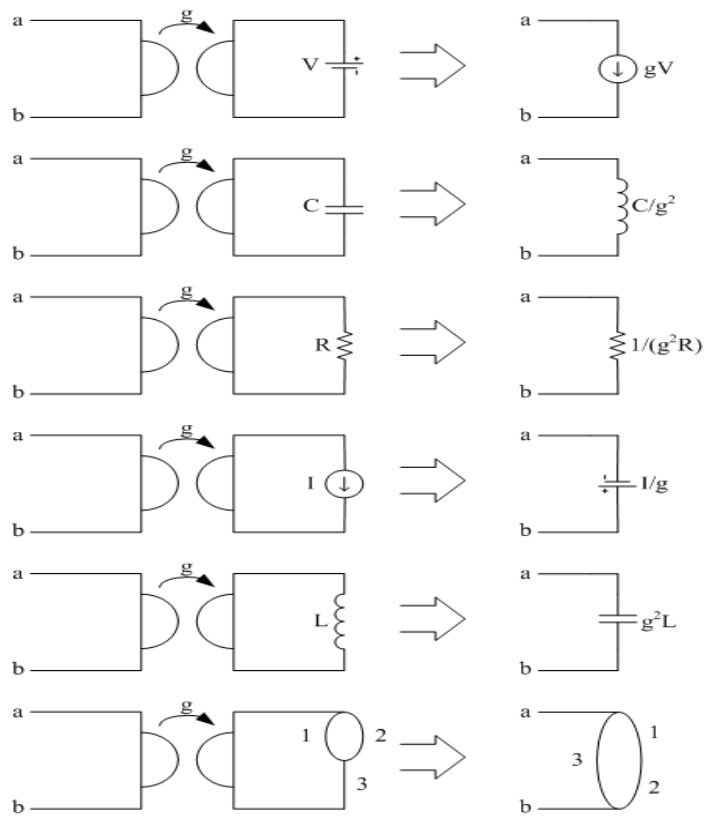


Fig. 19. Examples of element gyrator transformation.

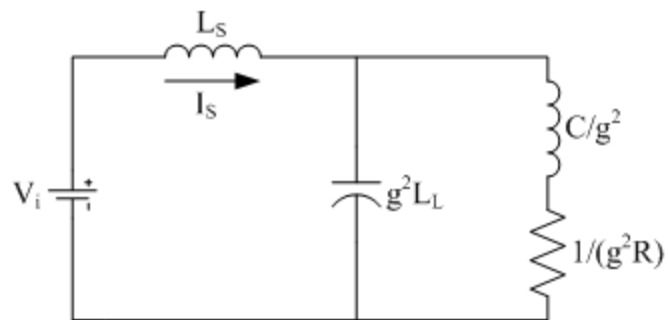


Fig. 20. Gyrator equivalent IDC viewed from the source.

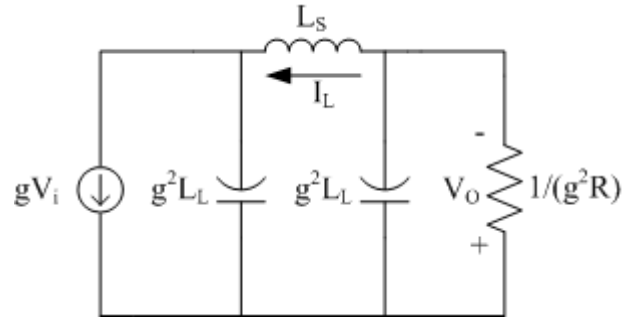


Fig. 21. Gyrator equivalent IDC viewed from the load.

From Fig. 21 one can calculate the steady state output current and output voltage, shown in (24) and (25) respectively.

$$I_L = gV_i \quad (24)$$

$$V_o = I_L R = gV_i R \quad (25)$$

The power transfer equation is shown in (26).

$$\langle P \rangle = \frac{I_S I_L}{g} = \frac{I_S I_L}{\omega C} \left(\varphi - \frac{\varphi^2}{\pi} \right) \quad (26)$$

Using equations (23) – (26) control techniques can be performed dependently or independently of the load.

2. Control Techniques

The control variables for this converter are the same as for the ICB, φ and f . By adjusting these variables the output voltage and current will be dynamically controlled. The voltage gain is shown in (27).

$$\frac{V_o}{V_i} = gR = \frac{\omega C}{\varphi - \frac{\varphi^2}{\pi}} R \quad (27)$$

To get a better feel for this equation it was plotted for $\varphi = 0^\circ$ to $\varphi = 90^\circ$ for $R = 1\Omega$, Fig. 22. This shows that when φ is chosen to be close to zero the voltage gain becomes infinite. This is the unstable region of the graph. If a voltage gain in the unstable region or below the curve is desired the frequency can be dynamically adjusted to shift this curve up or down. This type of control will not be used in this research. By adjusting φ , one can only achieve voltages on this curve and it is recommended to stay out of the unstable region. Also the load resistance is directly proportional to the gain so if it changes then the overall gain will change. This means that if the output voltage is being regulated then φ would have to change to bring the gain back to its previous value. Therefore, the IDC is designed to be able to achieve a certain voltage range within the stable region of φ .

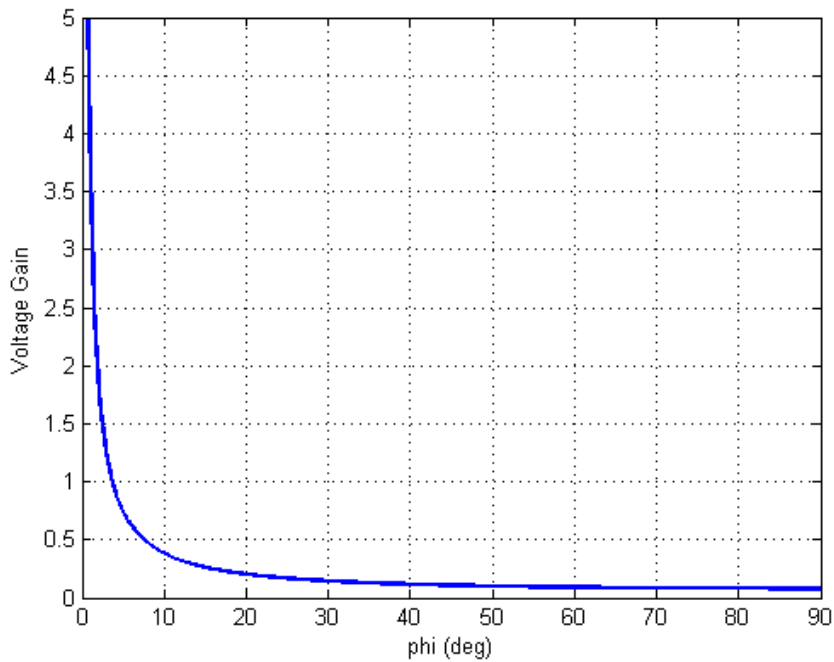


Fig. 22. Voltage gain curve.

C. Summary

This chapter has shown three DC-DC converter topologies, i.e. ICB, multi-port ICB, and IDC. All of these converters are capable of being used in high power applications. These converters are capable of two quadrant power transfer with no net storage element. The IDC is capable of voltage step up or step down over a wide range without the use of a transformer.

CHAPTER III

PROPOSED DC-DC CONVERTER TOPOLOGY

This chapter will discuss a case study performed on the proposed multi-port power converter. This case study will involve a topological variation of the Inductor Converter Bridge (ICB) family of converters shown in Chapter II, in particular the Inverse Dual Converter (IDC). The IDC will be manipulated into a multi-source converter and various simulation study methods will be presented in this chapter that will determine various operational characteristics of this converter in order to aid in the development of a control strategy.

A. Multi-Source IDC

The multi-port IDC is first presented as a multi-load topological variation of the original IDC in [16]. The multi-port IDC is being expanded into a converter that can support multiple sources, i.e. Multi-source IDC, Fig. 23. This will allow for multiple energy sources, renewable or nonrenewable, to be connected and controlled to supply a load. This will also help in instances where the load power demanded is too great for just one connection and must be split into two.

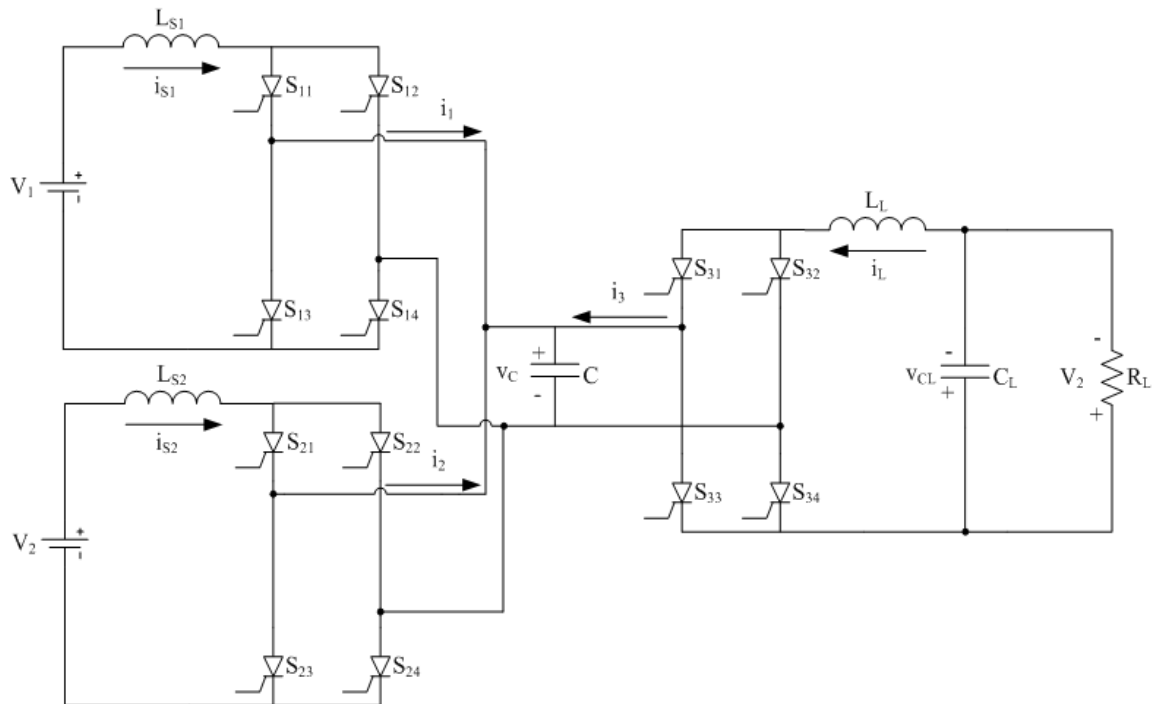


Fig. 23. Multi-source IDC.

1. Basic Operation and Configuration

The Multi-source IDC is made up of three ports with key components being a single phase thyristor bridge, inductor and center link capacitor, as shown in Fig. 23. The importance of the inductance in the modules is based on the fact that the core technology for this family of converters, the ICB, is of current source type as was shown in Chapter II. As can be seen these ports or modules are very similar to one another regardless of the type of connection, source or load. Therefore, each of these modules, thyristors and inductance, can be designed for the load or source that will occupy that port. More modules can be added to the system by connecting the AC terminals of the thyristor bridge in parallel with the center link capacitor. The center link capacitor plays

an important role in this converter by temporarily storing energy every half cycle before dispersing it to the load. With this know the operation of the Multi-source IDC is very similar to the IDC with added control for the extra modules added to the system.

As was shown in Chapter II the key variables for power transfer were the phase difference angle φ and the switching frequency f . For the purpose of this thesis only φ was manipulated to control the power transfer of the Multi-source IDC. The variable φ_{ij} is defined as the difference between the firing angles for the i converter thyristor pair (α_{i14} or α_{i23}) and the j converter thyristor pair (α_{j14} or α_{j23}). If φ_{ij} is positive then power is transferred from the i converter to the j converter and if it is negative power is transferred from the j converter to the i converter. In order to number the converter modules accordingly a standard top to bottom left to right method will be used. For instance in Fig. 23, this means that converter 1 is in the top left, converter 2 is in the bottom left, and converter 3 is in the top right. If there were another converter on the right then it would be numbered after the top right converter. This means for the standard IDC presented in Chapter II there is only one phase difference angle where $\varphi_{ij} = \varphi_{ji}$ or vice versa depending on the initial firing angles of the respective converters. For the Multi-source IDC there can be as many phase difference angles as there are ports. For example in Fig. 23 there is φ_{13} , φ_{23} , and φ_{12} , assuming that the load leads both sources and that converter 2 leads converter 1. For power transfer to occur the load converter must lead the source converter. The source port cannot receive power because the unidirectional switches will not allow for the current to change directions and flow into the source. Therefore, the only way for the source port to receive power is to

reverse the connection of the source such that the current remains in the same direction, but is fed into the positive terminal of the source which would add complexity.

At first glance the source port of the Multi-source IDC looks like a current source feeding a capacitor and then feeding a load, but in reality it is a voltage controlled current source. This means that the voltage at the input has control over the instantaneous current delivered through the inductor by the equations,

$$\frac{di_s}{dt} = \frac{v_s - v_C}{L_s} \quad (28)$$

$$\frac{di_s}{dt} = \frac{v_s + v_C}{L_s} \quad (29)$$

where (28) is for a source port whose conducting switches are 1 and 4 and (29) is for switches 2 and 3 conducting. These equations will cause three different instances during one half cycle to occur: $v_s > v_C$, $v_s = v_C$, or $v_s < v_C$. For the first of the three instances, the current in the source inductor will be rising from its previous starting value. This will continue until the second instance occurs, causing the current to reach its peak value for that half cycle. Next, the third instance occurs causing the inductor current to fall. As the current is falling the converter is switched from one pair of switches to the other, i.e. for converter 1 S_{114} to S_{123} . For transient periods, like start up and phase shifting, the starting current in the inductor is different from the final current during the half cycle, creating a rising or falling net current in the inductor. During these times of operation the time constant of the switching frequency is faster than the time constant of the

system to reach steady state. This process will continue until the circuit reaches steady state. Once steady state is reached, the current at the start and end of the half cycle to be the same. This basic operation will be important for phase control of the multi-port IDC. Also, note that unidirectional switches are being used. Therefore current cannot change directions from what is shown in Fig. 23.

B. Simulation Study

In order to obtain a better understanding of the operational and possible control characteristics of the Multi-source IDC a simulation study was performed. This converter is made up of two DC voltage sources each connected to a single phase thyristor bridge through an inductor respectively. Each of these modules are then connected in parallel to the AC link capacitor. The AC link capacitor is then connected to another single phase thyristor bridge that is connected to an inductor capacitor filter and then to a resistive load. This converter will be simulated in the PSIM[®] software package. PSIM[®] is a simulation software specifically designed for power electronics and motor control. This software will allow for easier control of the Multi-source IDC through programming in C in order to control the on/off timing of the thyristors.

1. Phase Difference Angle Variations

There are multiple aspects of this converter to be looked at in order to obtain a thorough understanding of its operational characteristics. One of these aspects is the phase difference angles φ_{13} , φ_{23} , and φ_{12} . These phase difference angles are controlled

by controlling the firing angle of the thyristors between the respective converters as stated earlier. For the Multi-source IDC the phase difference angle φ can be used to control how much power each source will send to the load. Therefore, φ_{13} and φ_{23} will be controlled and φ_{12} is a consequence of these by taking the difference between the two. The input and load response will be studied by applying the following scenarios for the phase difference angles mentioned above:

- Scenario 1: $(\varphi_{13} = \varphi_{23}) > 0$ ($\varphi_{12} = 0$)
- Scenario 2: $\varphi_{13} > 0, \varphi_{23} > 0$ ($\varphi_{12} > 0$ and $\varphi_{12} < 0$)
- Scenario 3: $\varphi_{13} > 0$ and $\varphi_{23} = 0$ ($\varphi_{12} > 0$)
- Scenario 4: $\varphi_{13} = 0$ and $\varphi_{23} > 0$ ($\varphi_{12} < 0$)
- Scenario 5: $\varphi_{13} > 0$ and $\varphi_{23} < 0$ ($\varphi_{12} > 0$)
- Scenario 6: $\varphi_{13} < 0$ and $\varphi_{23} > 0$ ($\varphi_{12} > 0$)
- Scenario 7: $\varphi_{13} < 0$ and $\varphi_{23} = 0$ ($\varphi_{12} < 0$)
- Scenario 8: $\varphi_{13} = 0$ and $\varphi_{23} < 0$ ($\varphi_{12} > 0$)
- Scenario 9: $\varphi_{13} < 0$ and $\varphi_{23} < 0$ ($\varphi_{12} > 0$ and $\varphi_{12} < 0$)

These scenario studies were simulated with equal source voltages and a constant resistive load, i.e. $V_1 = V_2$ and $R_{L1} = 50\Omega$. From above Scenario's 7 – 9 do make sense due to the fact that for power transfer to occur the load must be leading at least one of the sources. Otherwise the load will be required to send power to the sources, which cannot happen because the voltage source doesn't change polarity, current direction does not change, and a resistive load cannot generate power. Scenario's 3 – 6 also do not

make sense and this will be shown during the explanation of Scenario 2. Therefore only Scenario's 1 and 2 will be shown in greater detail.

Scenario 1 is the most obvious of all the scenarios with the phase difference angles equal. Since $\varphi_{13} = \varphi_{23}$ and both are greater than zero, power will be transferred from both sources to the load. For this scenario both of the source converters are switching the same set of switches at the same time, i.e. S_{114} , S_{214} and S_{123} , S_{223} . From this it can be seen that at any given time the two source modules are in exact parallel, i.e. the cathode of the switch combinations S_{11} , S_{21} and S_{12} , S_{22} are always connected and the anode of the switch combinations S_{14} , S_{24} and S_{13} , S_{23} are always connected in their respective switching sequence. This is shown in Figs. 24 and 25. Also connected to this is a load module as shown in Fig. 23. For this scenario the load module will be switched such that the switch timing is leading the source modules switch timing, i.e.

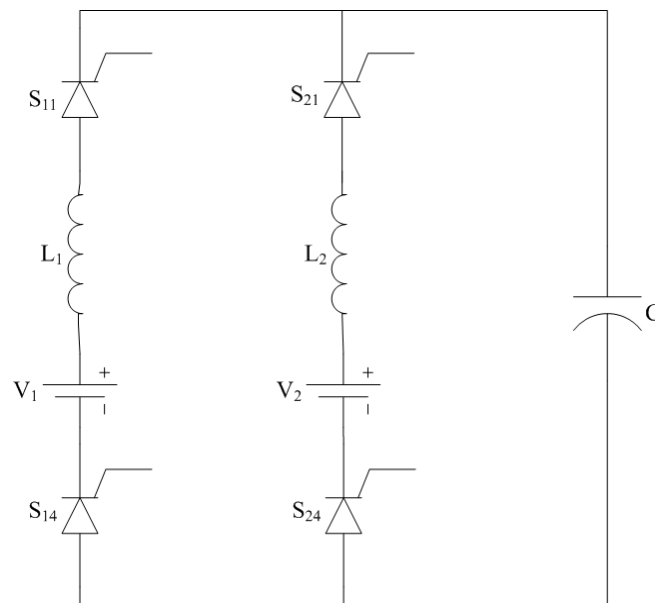


Fig. 24. Input modules for S_{x14} switches conducting.

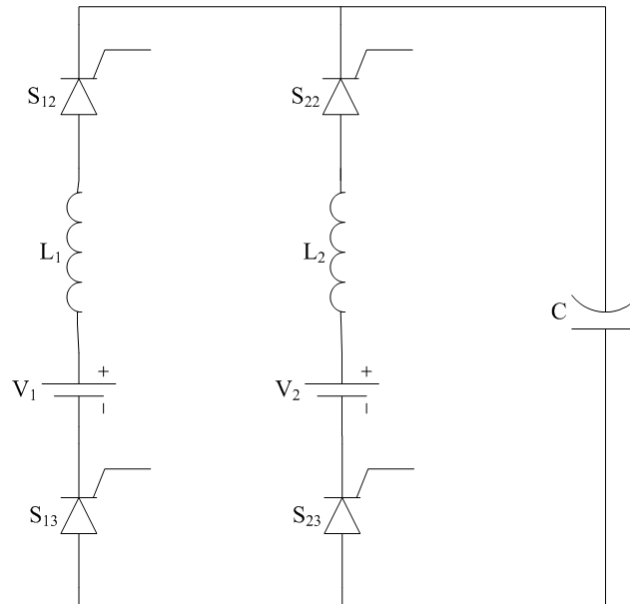


Fig. 25. Input modules for S_{x23} switches conducting.

switch on/off time for the source modules and load module are $\alpha_{x14} = 0^\circ/180^\circ$ and $\alpha_{314} = 0^\circ/135^\circ$ and $315^\circ/360^\circ$. Where each switch combination is on for half the period and $\varphi_{13} = \varphi_{23} = 45^\circ$ is chosen in order to make a comparison between the Multi-source IDC and the original IDC. Also, the phase difference angle was swept from $5^\circ - 85^\circ$ to observe the operational characteristics of the converter. It can also be noted that, either the source converter firing angles or the load firing angles can be changed to obtain the desired phase difference angle between the source modules and load module. This means that the phase shifting technique shown in Chapter II can be performed on the source or load modules. If this technique is not performed properly this can cause problems by causing a net charge to be stored in the capacitor, which is not desired.

From observation of the switching topology, it can be inferred that the load will behave the same as in the original IDC presented in Chapter II. The only difference is

that now there are two sources connected in exact parallel at all times. This means for any given phase difference angle such that $\varphi_{13} = \varphi_{23}$ the input current will be exactly split between the two sources. Therefore the same amount of energy is being stored every half cycle in the capacitor as was for the original IDC case with half coming from each source. This scenario is considered the most stable operating mode of the Multi-source IDC and will be used as the basis for conducting the phase shifting technique to change the phase difference angle of one source module or both source modules simultaneously. The control and simulations for this scenario will be shown in more detail in Chapter IV.

Scenario 2 has two different modes that were studied. The first of the two is the case where $(\varphi_{13} > \varphi_{23}) > 0^\circ$, making $\varphi_{12} > 0^\circ$. This shows that power is to be transferred from converter 1 and 2 to converter 3 and from converter 1 to converter 2. As stated earlier power transfer between source converters cannot occur because the voltage or current cannot change directions. In order to observe the behavior of this scenario the firing angle of the load was set at $\alpha_{314} = 0^\circ/180^\circ$ and $\alpha_{323} = 180^\circ/360^\circ$ respectively. The source modules were started at $\varphi_{12} > 5^\circ$ with firing angles of $\alpha_{114} = 45^\circ/225^\circ$ and $\alpha_{214} = 40^\circ/220^\circ$. It was observed that the current in module 1 fell to near zero with module 2 carrying the majority of the current to drive the load at $\varphi_{23} > 40^\circ$. This was repeated for $\varphi_{12} > 10^\circ$ by changing $\alpha_{114} = 50^\circ/230^\circ$. This showed that the current in module 1 was even closer to zero and the input of converter 2 and output started to resemble that of the original IDC presented in Chapter II. The phase difference angle was then swept in 5° increments in order to observe the lowest average input current of converter 1.

The second mode is the case where $(\varphi_{13} < \varphi_{23}) > 0^\circ$, making $\varphi_{12} < 0^\circ$. This mode was simulated with $\varphi_{12} = -5^\circ$ with firing angles of $\alpha_{114} = 40^\circ/220^\circ$ and $\alpha_{214} = 45^\circ/225^\circ$. From this simulation it was observed that the exact opposite occurred, i.e. converter 2 current went to near zero and converter 1 supplies the load. In order to be complete with the study this mode was simulated the same as the previous. From these observations it can be determined that if converter 1 leads converter 2, converter 1 will supply the load alone. If converter 2 leads converter 1 it will supply the load alone. For control purposes this can be seen as a way to increase or decrease current in either of the converters.

From this assumption, Scenario's 3 – 6 can now be shown to make no sense. Scenario 3 and 4 are similar in that one of the two phase differences is equal to 0° . Firstly, 0° is an unstable operating point for a single load IDC, therefore in order to make it semi-stable the point will have to be moved to approximately 10° . Once this is done, it can be seen that both of these scenarios resemble Scenario 2. Therefore is of no use. Scenario's 5 and 6 do not make any sense because of the observations seen in Scenario 2. Both Scenario 5 and 6 have a positive and negative phase difference. From Scenario 2, the converter that is lagging the other converter will go to near zero current. This means that if the phase difference is negative, the positive phase difference will be lagging causing it to go to near zero current. Then power is to be transferred from the load to the source because of the negative phase difference but this cannot happen because of the reasons mentioned earlier.

2. Input Voltage Deviations

To further understand the operation of this converter the input voltages were made unequal for both Scenario's 1 and 2. For Scenario 1, converter 2 input voltage was swept from 25V to 100V in 25V increments. This showed that the larger voltage of converter 1 caused converter 2 to go to near zero current, i.e. converter 2 has minimal current with respect to converter 1. The same was shown to happen when the voltage sweep was performed on converter 1 while keeping converter 2 constant. Further details on this occurrence will be presented in Chapter IV. This was also done for Scenario 2. The overall result of this was that if $V_1 > V_2$ then converter 1 supplies max current for the load and converter 2 goes to near zero. The opposite occurs for $V_1 < V_2$. This will be shown in Chapter IV.

3. Load Variations

In most applications the sources load is allowed to vary while continuing to send it power. If this load is a voltage sensitive load, it is desirable to send power at a fixed voltage and varying current. In order to do this the load voltage must be regulated for any change in load. For the Multi-source IDC this load is a simple resistive element. An increase or decrease of the element should not result in an increase or decrease in output voltage. If it does then there should be an adjustment to ϕ_{13} in order to keep this voltage within its predetermined range. By knowing how the load voltage varies with increasing or decreasing R_L , ϕ_{13} can be adjusted to compensate the voltage back to its desired value. This is shown in Chapter IV.

4. *System Specifications and Control*

For most systems it is desirable to regulate or control certain characteristics of the converter, whether it be source current or load voltage during disturbances. The Multi-source IDC will have two sources, one of which is an unlimited energy source while the other is limited or determined to be depleting. The load will be a simple resistive element that will be varied to demonstrate voltage regulation. It is also known that in most real world applications two sources are never exactly the same, i.e. voltage variations.

For control of the Multi-source IDC it was decided that the output voltage be regulated about a particular voltage with a peak to peak hysteresis ripple of 5%. Also, when one of the sources vary from the other it is not desired that current to go to near zero values. Therefore, the phase difference angle φ will be adjusted in such a way to keep the input current of converter 2 about a particular reference with a peak to peak hysteresis ripple of 5%. Converter 1 will be allowed to send any amount of energy necessary to supply the load based on the limitations from of converter 2. Since there are two variables that need to be controlled there needs to be two degrees of freedom. The control variables will be φ_{13} and φ_{23} . Since converter 1 is acting like an unlimited energy source it will be considered the primary control for the system. Since converter 1 will always be available, it will be in charge of the output voltage regulation and converter 2 will control it power transfer to the load by controlling the current sent to the load by φ_{23} . Voltage regulation of the load will be a first priority with the current regulation second. If the load changes while the input current is being regulated, the

controller will briefly step out of this routine and compute the new phase difference angle to meet the voltage criterion. Once this is done, current regulation will continue.

In order to achieve voltage regulation of the output one needs to incorporate a feedback loop of the output voltage. The instantaneous average voltage is measured and sent to the controller for comparison with the reference voltage desired. The phase difference angle φ_{13} is then adjusted. The algorithm for this is as follows:

$$\varphi_{ratio} = \frac{V_o}{V_{O,ref}} \quad (30)$$

$$\varphi_{13,new} = \varphi_{ratio} \times \varphi_{13,old} \quad (31)$$

$$\varphi_{23} = \varphi_{13,new} \quad (32)$$

This set of equations follows the voltage gain curve shown in Chapter II. This shows that if the measured output voltage rises above or falls below the reference voltage the phase angle difference will increase or decrease respectively. If this voltage continues to rise or fall the algorithm will continue to adjust to keep the average voltage within a hysteresis band of 5%. Also note that φ_{23} is set equal to φ_{13} to readjust the base point for determining current regulation of converter 2.

Current regulation of converter 2 is achieved using a bang-bang type of control. This type of control changes the control value based on whether the measured value is above or below the targeted average plus hysteresis band. For this case φ_{23} will be increased or decreased depending on if the measured converter 2 current is above or

below the hysteresis band respectively. Due to the fact that the load voltage is the first priority, φ_{23} is set equal to φ_{13} every time the output voltage needs to be regulated within its band. Then φ_{23} is adjusted around φ_{13} in order to keep the input current of converter 2 within its operational limits. If converter 2 cannot operate at its predetermined current it will be reduced or turned off and converter 1 will take over and power the load on its own. The control logic is as follows:

$$\text{if } (I_2 > I_{2,ref} + I_{rip}) \Rightarrow \varphi_{23} = \varphi_{23,old} + 1$$

$$\text{if } (I_2 < I_{2,ref} - I_{rip}) \Rightarrow \varphi_{23} = \varphi_{23,old} - 1$$

With this logic φ_{23} will be stepped by one until it reaches a point where it will alternate between two values. The controller code is presented in Appendix B.

C. Modeling the System

To fully understand the operation of this converter and compare results with past research, the system and its control was modeled and simulated. Three different simulation models were developed based on the results to be shown. For a basic simulation of constant φ over the simulation time the model in Fig. 26 was used. If a complex control of φ was to be simulated, the model in Fig. 27 was used. If a feedback control method was used, Fig. 28 was used. A 7.2kW system was designed with an input voltage (V_1 and V_2) of 100V and is shown in Figs. 26, 27, and 28. The system

components of Figs. 26, 27, and 28 will be designed based on these parameters and the equations developed in [14] and are shown in (35), (36), and (37).

$$L_S = \frac{1}{32C\tau f^2} \quad (35)$$

$$L_L = \frac{n}{32C\tau f^2} \quad (36)$$

$$C_L = \frac{\Delta i_L}{8f_r \Delta V_{CL}} \quad (37)$$

where

- τ is the ripple factor $\frac{\Delta i_S}{I_S}$ or $\frac{\Delta i_L}{I_L}$.
- f is the switching frequency.
- n is the ratio of average input current divided by average output current.
- f_r is the ripple frequency.
- Δi_L is the peak to peak current in the load.
- ΔV_{CL} is the peak to peak voltage in the load capacitor.

From these equations a base model was designed for simulation of this converter and these component values are shown in Table 2.

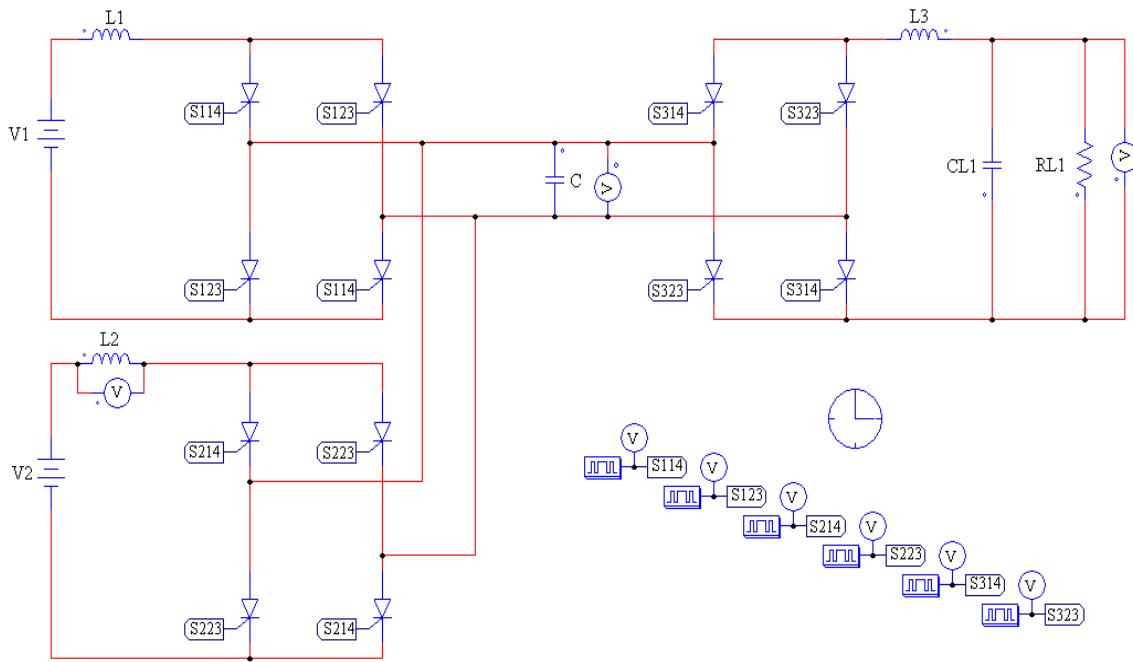


Fig. 26. PSIM[®] model of Multi-source IDC with no controller.

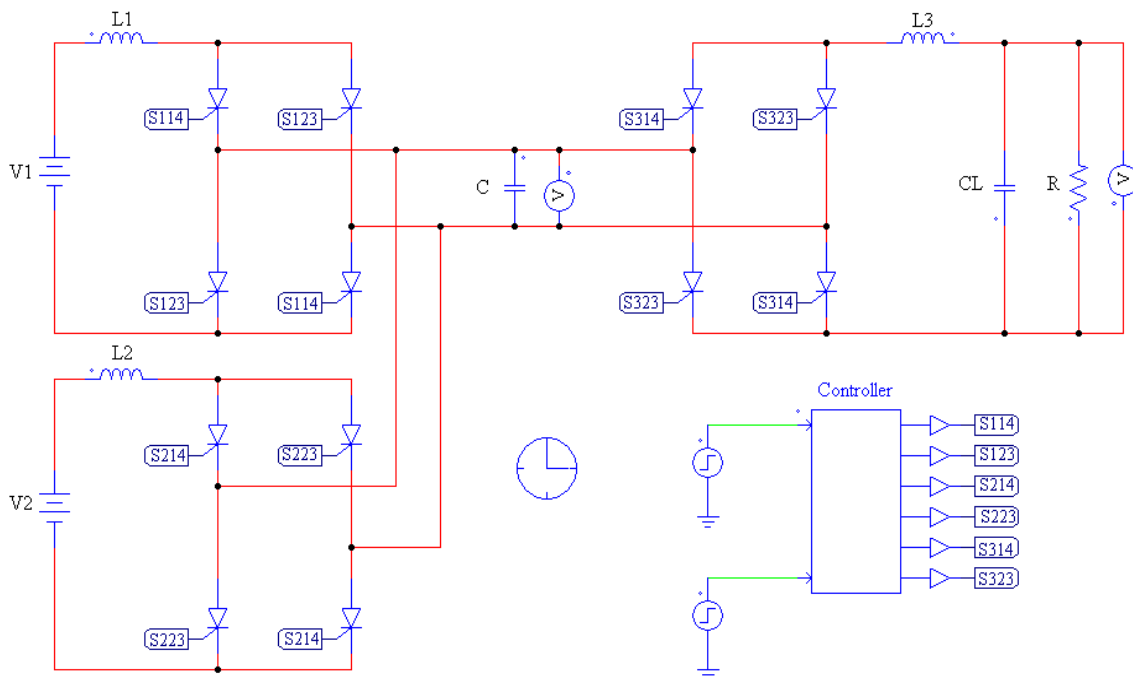


Fig. 27. PSIM[®] model of Multi-source IDC with open loop control.

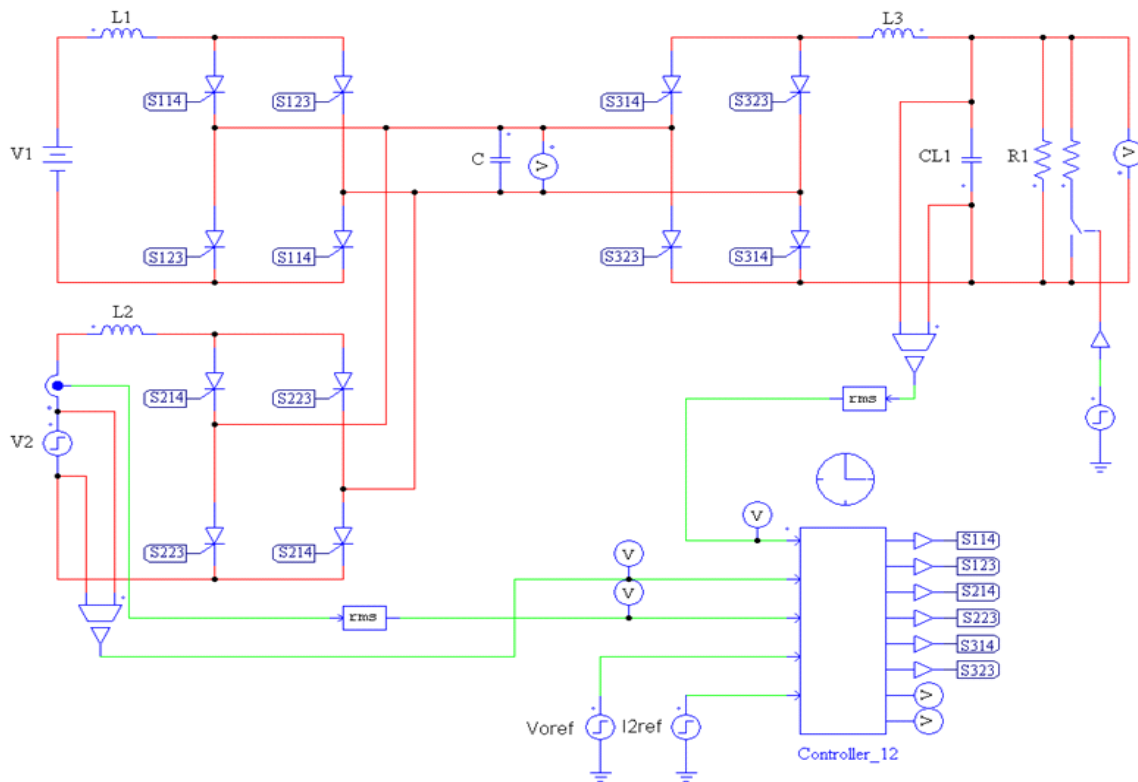


Fig. 28. PSIM[®] model of Multi-source IDC with feedback control.

Table 2. Multi-source IDC simulation parameters

Parameter	Symbol	Value	Units
Power Rating	P_{\max}	7200	W
Input Voltage	V_1 & V_2	100	V
Output Voltage	$V_{O,\max}$	500	V
Output Voltage Ripple	$V_{O,\text{ripple}}$	5	%
Input Current Ripple	τ	10	%
Output Current Ripple	τ	10	%
Switching Frequency	f	5	kHz
Ripple Frequency	f_r	10	kHz
AC Link Capacitor	C	2	μF
Source Inductance	L_1 & L_2	10	mH
Load Inductance	L_3	40	mH
Filter Capacitor	C_L	0.5	μF
Resistive Load	R	50	Ω

D. Summary

This chapter has introduced a new multi-port converter, Multi-source IDC, to study and analyze. In order to obtain an understanding of its operation, different circuit variations were studied: phase difference angle variations, input voltage variations, and load variation. From these studies, control strategies were able to be developed to regulate the output voltage and converter 2 input current by actively controlling φ_{13} and φ_{23} respectively.

CHAPTER IV

PERFORMANCE RESULTS, ANALYSIS, AND CONTROL

In this chapter the simulation results from the Multi-source IDC will be presented and discussed. All of the simulations presented are based on the specifications discussed in Chapter III. This chapter will consist of the operational characteristics and control strategy based on the behavior of the Multi-source IDC.

A. Operational Characteristics

In order to better understand the operational characteristics of the Multi-source IDC it was simulated under various conditions. These conditions include the variation of phase difference angle, φ , between each converter, variation of the each source voltage (V_1 and V_2), and load variation (R_L). From these simulation studies, a control method can be determined in order to keep the converter at a stable operating point while maintaining output voltage regulation and converter 2 current regulation. This converter was simulated in PSIM[®].

1. Phase Difference Angle Variation

The first simulation study of this converter consists of directly controlling φ by controlling the respective firing angles for each converter and switch. These firing angles are α_{1XX} , α_{2XX} , and α_{3XX} , where XX stands for the switch pair per converter. The phase difference angle φ between two converters is just the difference of these firing

angles. For this simulation, the model shown in Fig. 26 from Chapter III was simulated. For Scenario 1 α_{1XX} and α_{2XX} are set equal to one another and α_{3XX} was varied in order to change φ between the two source converters and the load converter. For example, the firing angles for converters 1 and 3 would be $\alpha_{114} = 0^\circ/180^\circ$ (on/off) and $\alpha_{314} = 0^\circ/135^\circ$ and $315^\circ/360^\circ$ (on/off and on/off). From these firing angles one can see that the converter 3 leads converter 1, therefore power will be transferred from converter 1 to converter 3. Also the phase difference angle for these firing angles is $\varphi_{13} = 180^\circ - 135^\circ = 45^\circ$. Fig. 26 was simulated for $V_1 = V_2 = 100V$, $\varphi_{13} = \varphi_{23} = 45^\circ$ and $\varphi_{12} = 0^\circ$ for a time of 0.15s at a sample rate of 1E-8s and the converter currents, capacitor voltage, and load voltage are shown in Figs. 29 – 31.

In Fig. 29 the larger current is both input currents overlapping one another. From this it was determined that as long as $\varphi_{13} = \varphi_{23}$ and $V_1 = V_2$ or ideal operating conditions the two sources will exactly split the current of the original IDC shown in Fig. 32. Fig. 30 also shows that the capacitor voltage is not biased with an average over a period equal to zero. The smaller current in Fig. 29 is the load current and Fig. 31 shows the load voltage, both of which are the same as the original IDC for the same phase angle difference of 45° . As $\varphi_{13} = \varphi_{23}$ was swept from $5^\circ - 85^\circ$ the shape of the currents and voltages remained the same with the steady state magnitude changing as shown in Figs. 33 and 34. From these figures it can be seen that as $\varphi_{13} = \varphi_{23}$ increases the converter currents and voltages decrease. These curves are monotonically decreasing meaning the slope of the function is always negative. This will be used as a control method later in the chapter.

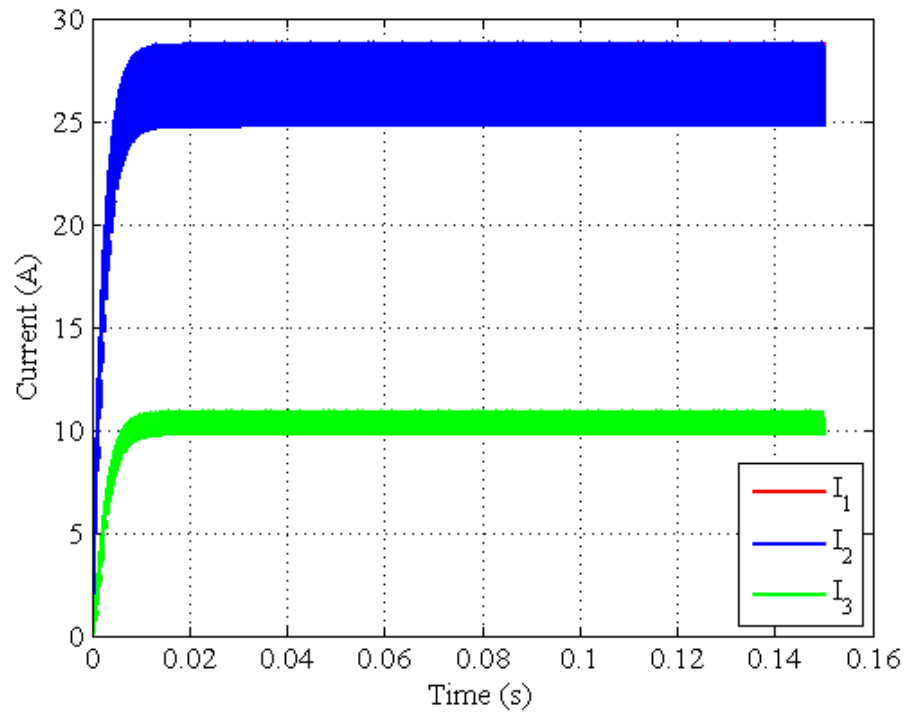


Fig. 29. Converter currents for Scenario 1.

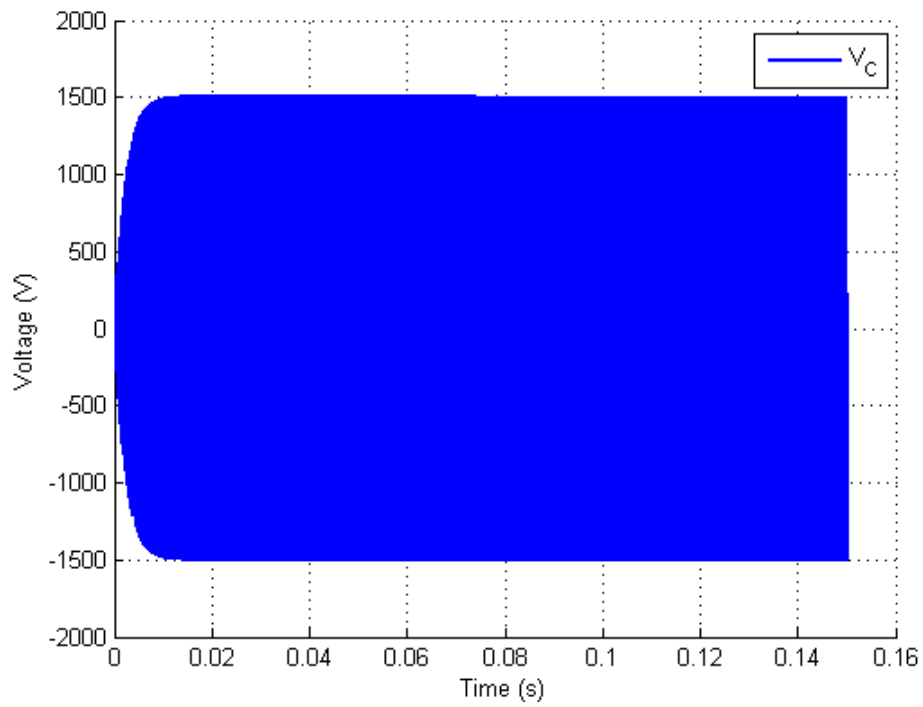


Fig. 30. Center link capacitor voltage for Scenario 1.

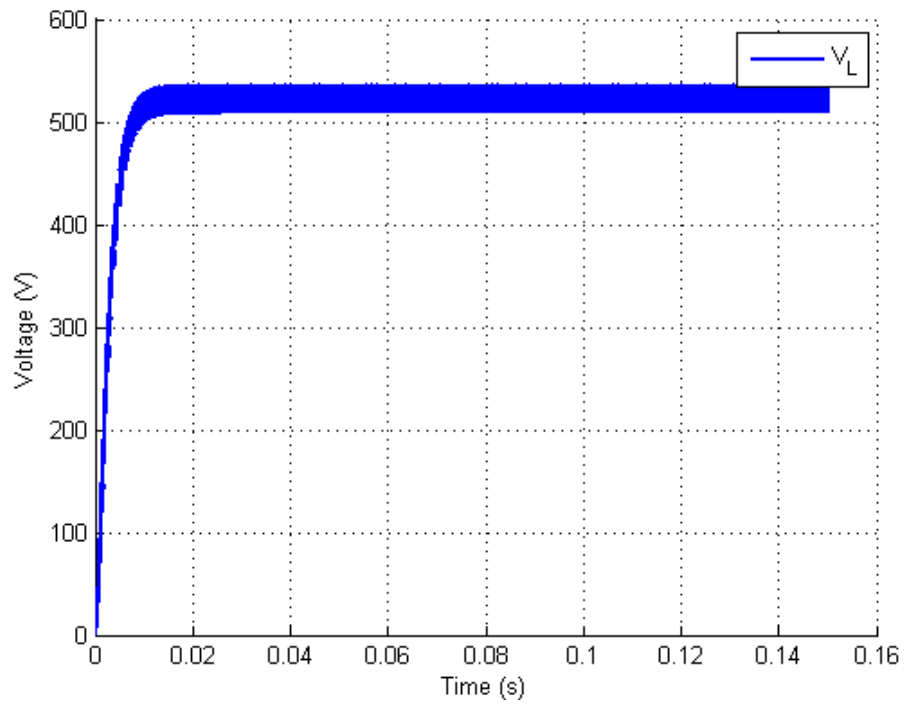


Fig. 31. Load voltage for Scenario 1.

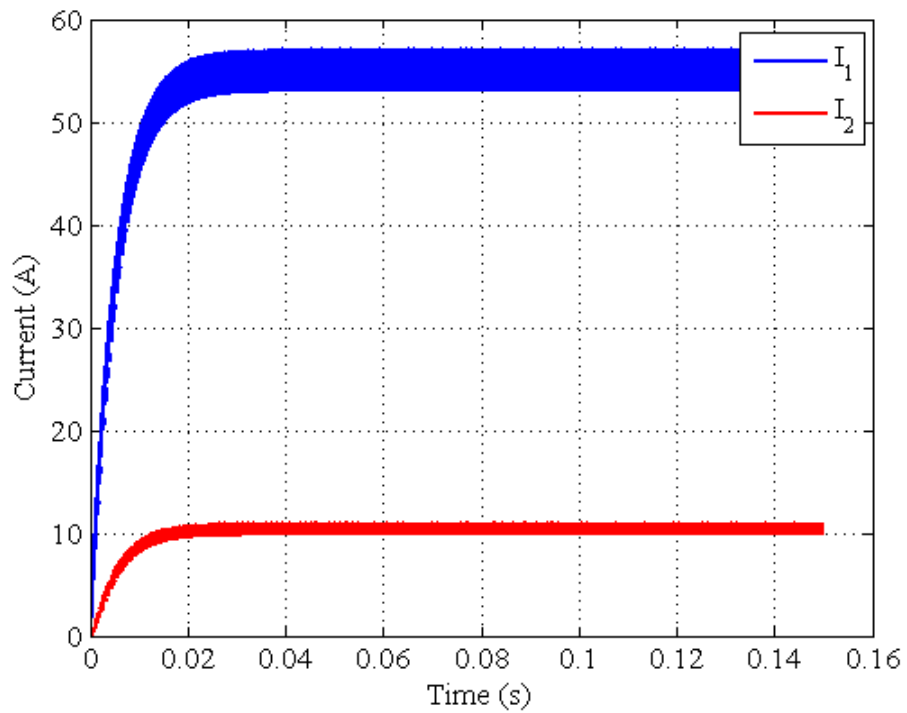


Fig. 32. Original IDC converter currents.

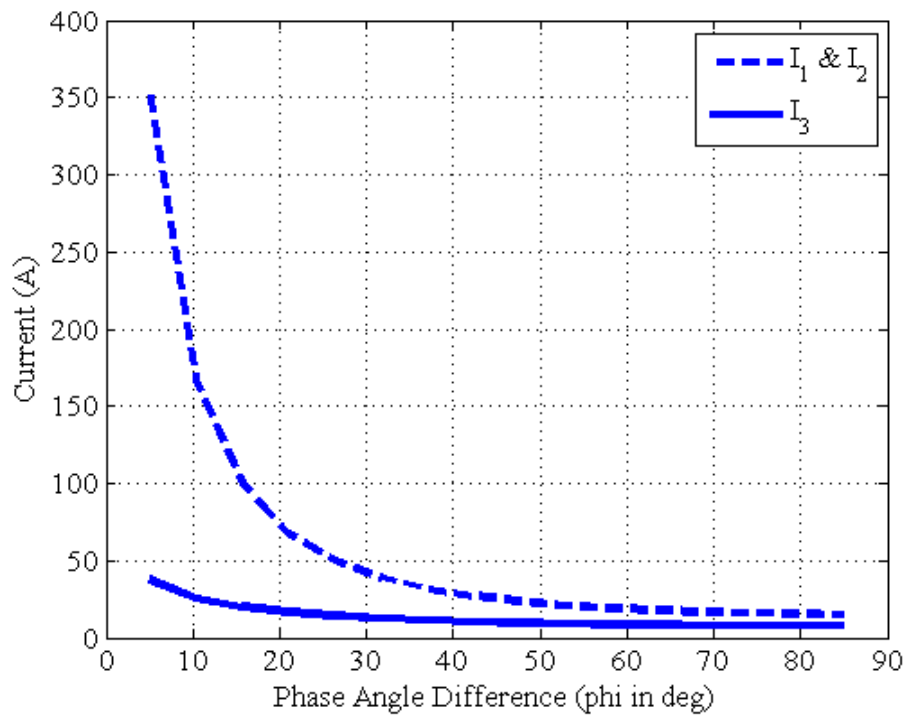


Fig. 33. Magnitude of converter currents for Scenario 1.

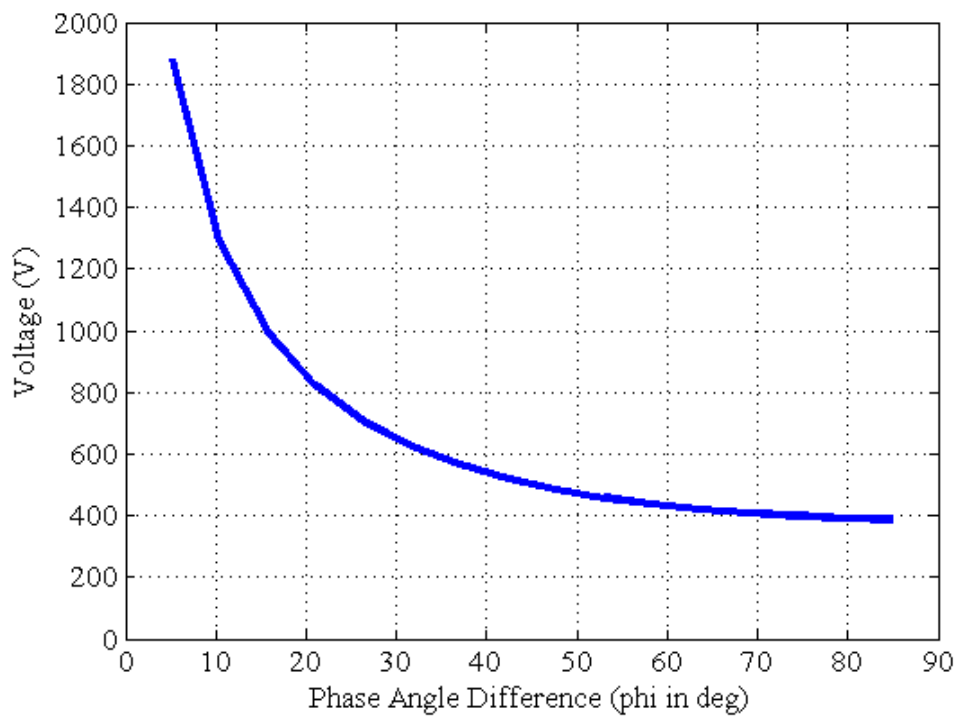


Fig. 34. Magnitude of load voltage for Scenario 1.

Scenario 2 has two different modes that were studied. For mode 1 the phase angle differences are $(\varphi_{13} > \varphi_{23}) > 0^\circ$, making $\varphi_{12} > 0^\circ$. This was shown with two different methods of simulation: non-controlled simulation, Fig. 26 and controlled simulation, Fig. 27. For the non-controlled simulation, φ_{12} was initially chosen to be 5° with $\alpha_{114} = 50^\circ/230^\circ$ and $\alpha_{214} = 45^\circ/225^\circ$. This mode caused the source current in converter 1 to go to near zero. Next φ_{12} was swept from $5^\circ - 80^\circ$ by adjusting the firing angle values accordingly to observe the magnitude of converter 1 current as φ_{12} increased and φ_{23} stayed constant. The converter currents, capacitor voltage and load voltage are shown in Figs. 35 – 37 for $\varphi_{12} = 5^\circ$. For the swept values of φ_{12} , only the magnitude of converter 1 current is shown because the magnitude of converter 2 and 3 currents and load voltage stayed the same over the simulation. This magnitude change is shown in Fig. 38. Also, the converter currents, capacitor voltage, and load voltage for $\varphi_{12} = 80^\circ$ is shown in Figs. 39 – 41 respectively.

Using the operational characteristics from the original IDC that has been shown in Chapter III, if the load converter leads the source converter, power will be transferred from source to load. For Scenario 2 mode 1 it can be seen that converter 2 leads converter 1 so power should have been transferred from converter 1 to converter 2. This was not the case. The source converters cannot accept power because the current in the converter would have to change directions to charge the voltage source. What actually happens in the Multi-source IDC is that converter 1 basically stops sending power to the load and converter 2 takes over. The reason for this is that if one looks closely at the source

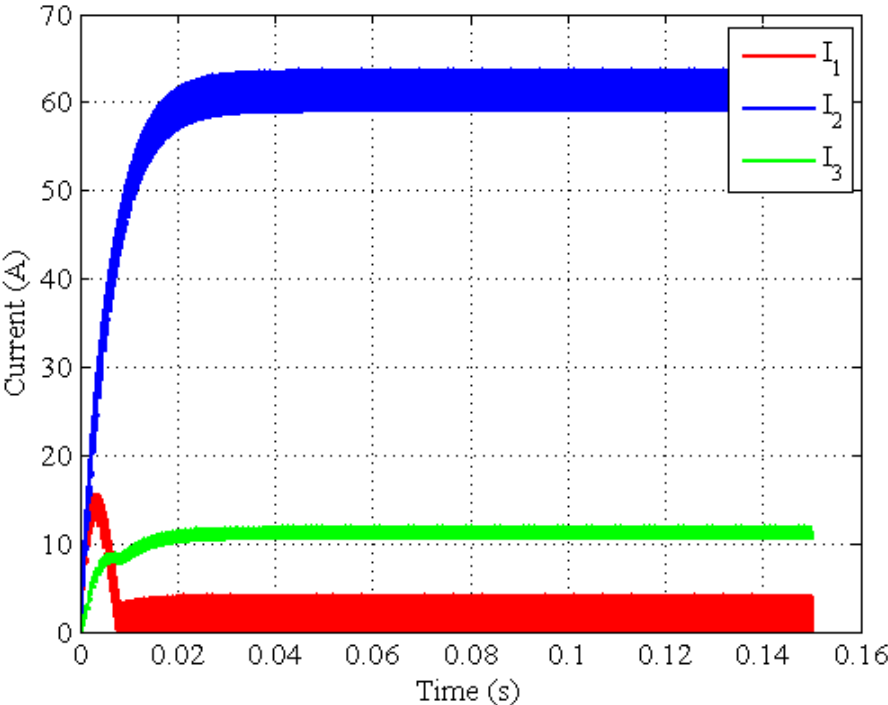


Fig. 35. Converter currents for Scenario 2 mode 1 ($\phi_{l2} = 5^\circ$).

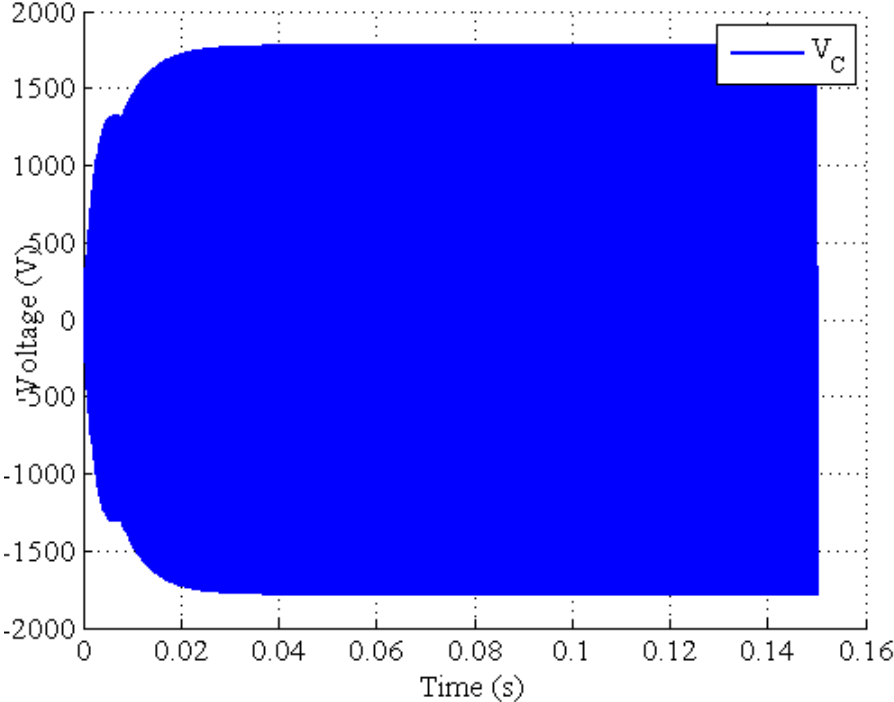


Fig. 36. Center link capacitor voltage for Scenario 2 mode 1 ($\phi_{l2} = 5^\circ$).

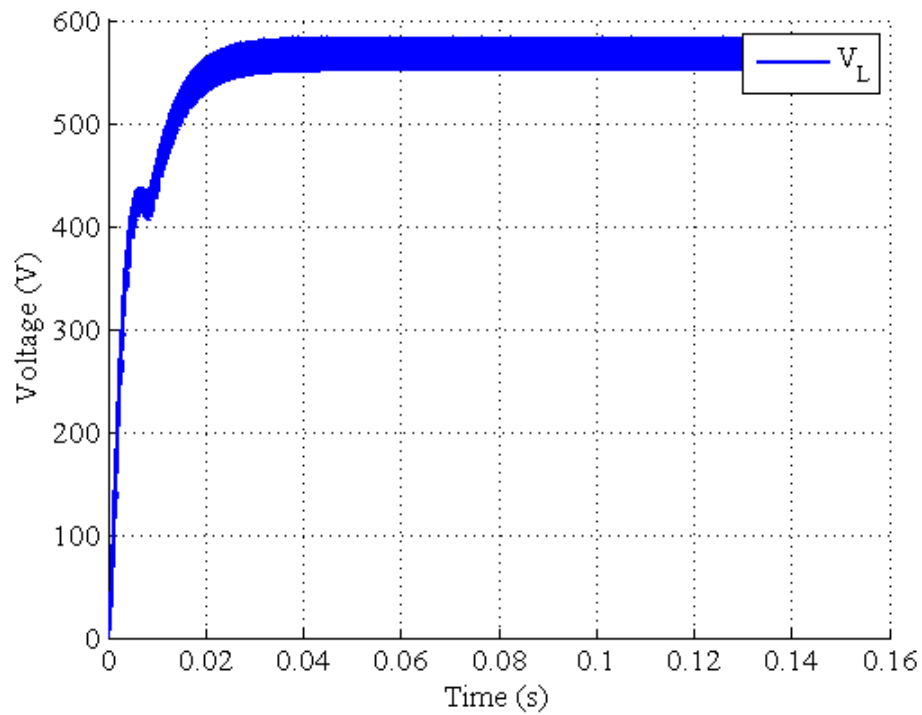


Fig. 37. Load voltage for Scenario 2 mode 1 ($\phi_{12} = 5^\circ$).

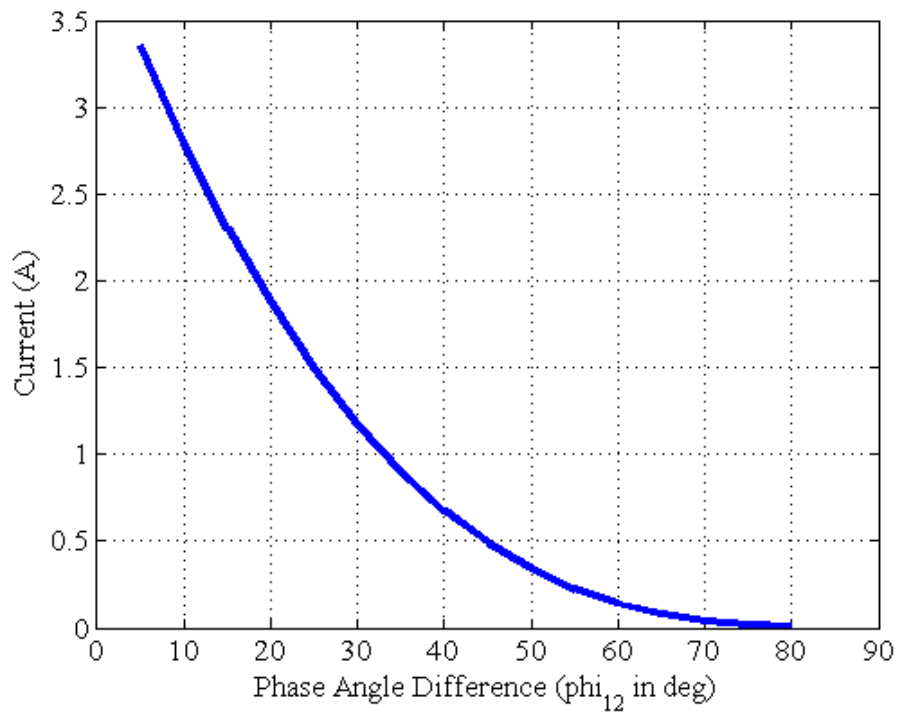


Fig. 38. Magnitude of converter 1 current for increasing ϕ_{12} .

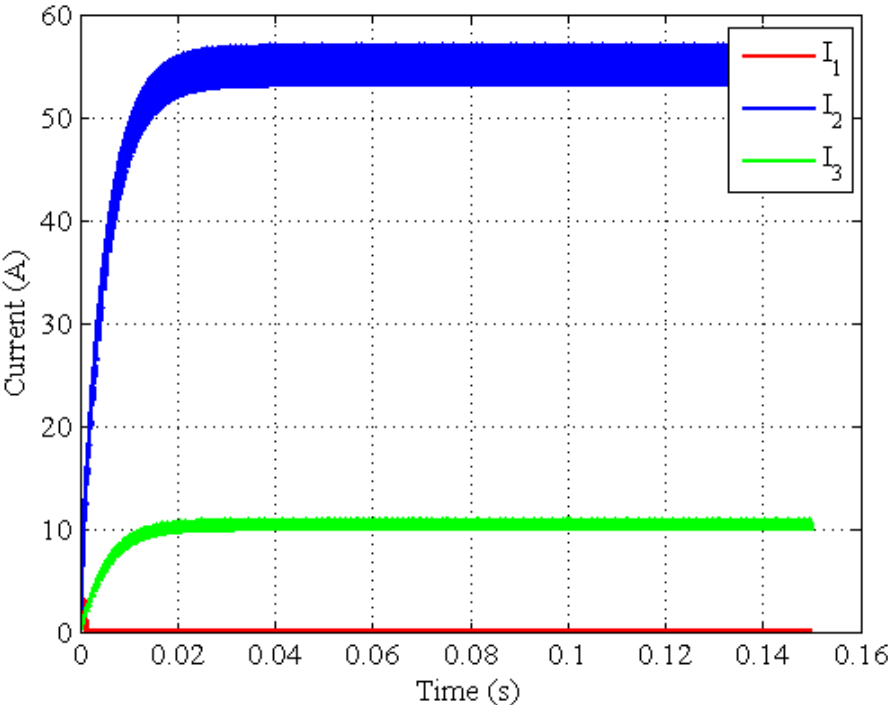


Fig. 39. Converter currents for Scenario 2 mode 1 ($\varphi_{12} = 80^\circ$).

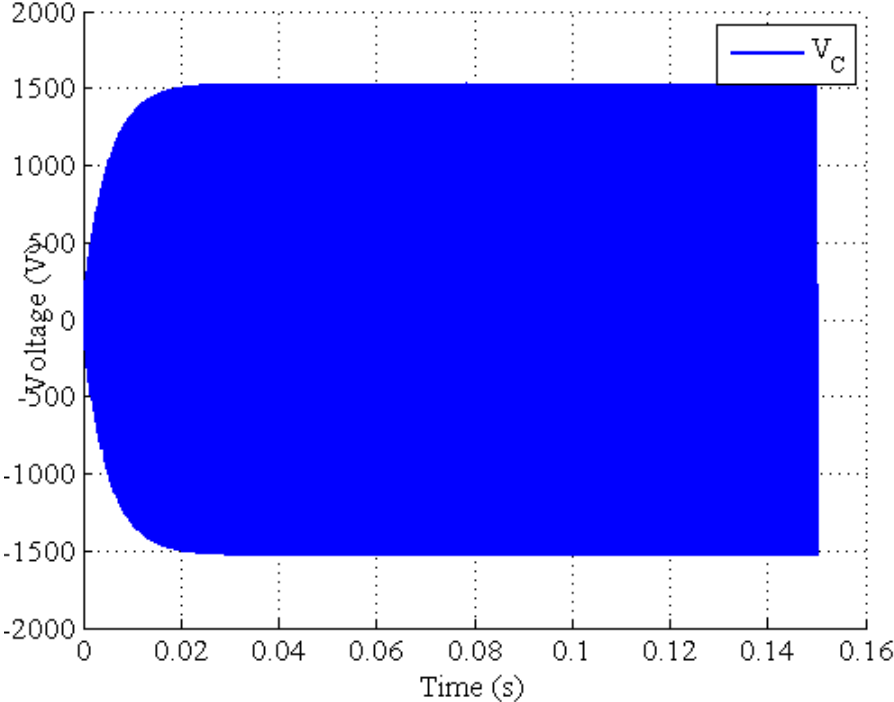


Fig. 40. Center link capacitor voltage for Scenario 2 mode 1 ($\varphi_{12} = 80^\circ$).

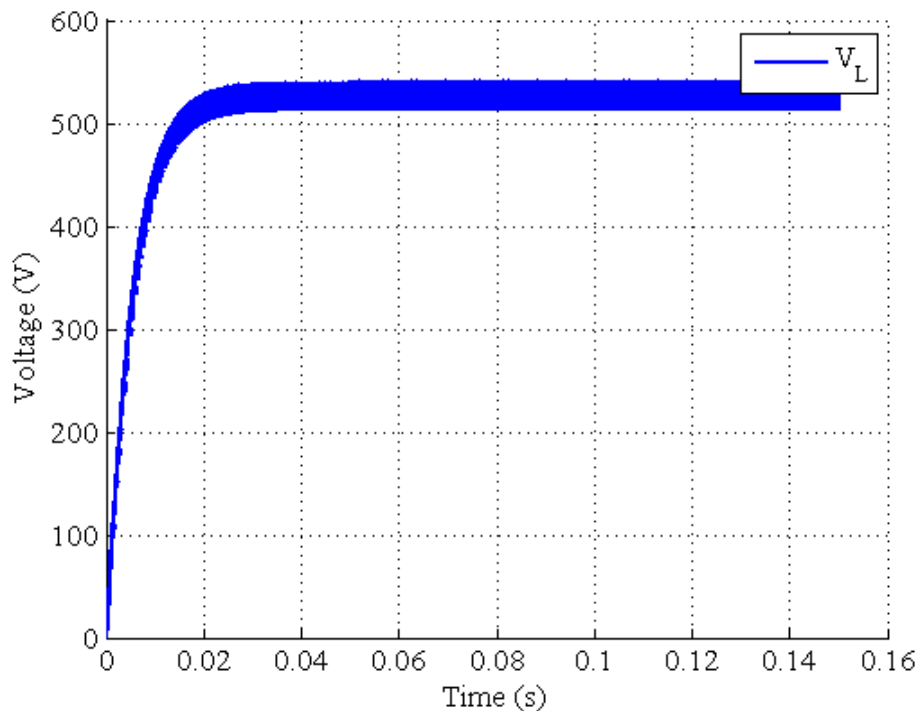


Fig. 41. Load voltage for Scenario 2 mode 1 ($\varphi_{12} = 80^\circ$).

converters it can be seen that it is just a switched LC circuit. From a steady state operating point where $\varphi_{13} = \varphi_{23}$ to a new operating point where $\varphi_{13} > \varphi_{23}$ the cause for the current decrease in converter 1 can be seen more clearly. This simulation was done from the open loop controlled PSIM[®] model by step changing $\varphi_{13} = 45^\circ$ to 50° and leaving φ_{23} the same. This is shown in Figs. 42 – 44. What happens is that at the steady state operating point of $\varphi_{13} = \varphi_{23}$ the source converter currents are identically equal. This means that the inductor currents are starting their charge cycle from the same point at the same time, reaching their peak at the same time, and reaching their final value at the same time for that switching instance. Once a switching instance occurs, i.e. S_{114} to S_{123} , this process repeats until φ_{13} steps to 50° . Now the firing angle for converter 1 has changed.

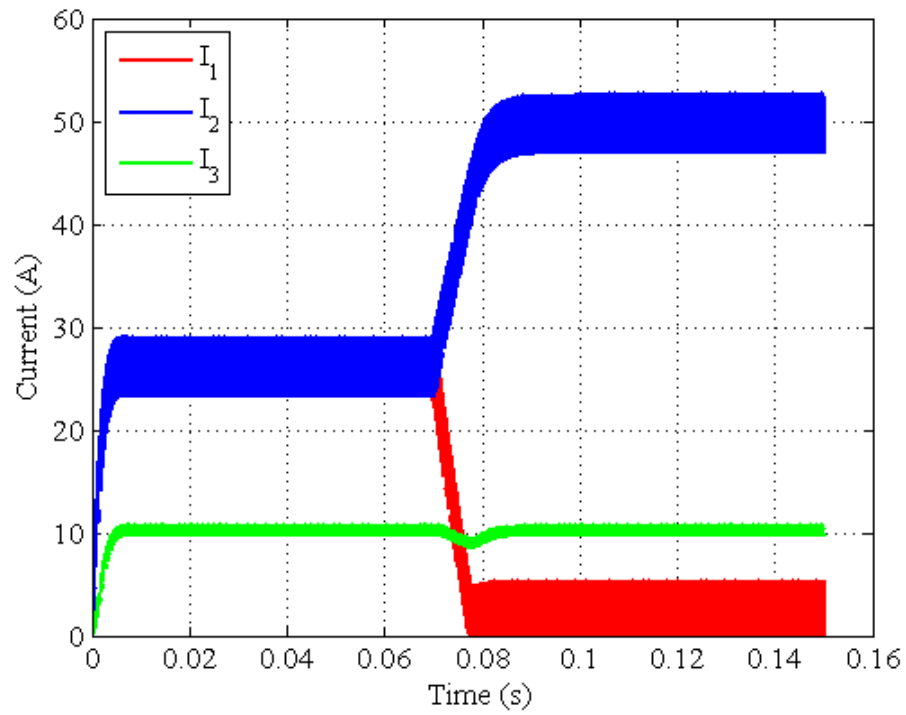


Fig. 42. Converter currents for $\varphi_{12} = 0^\circ$ to $\varphi_{12} = 5^\circ$.

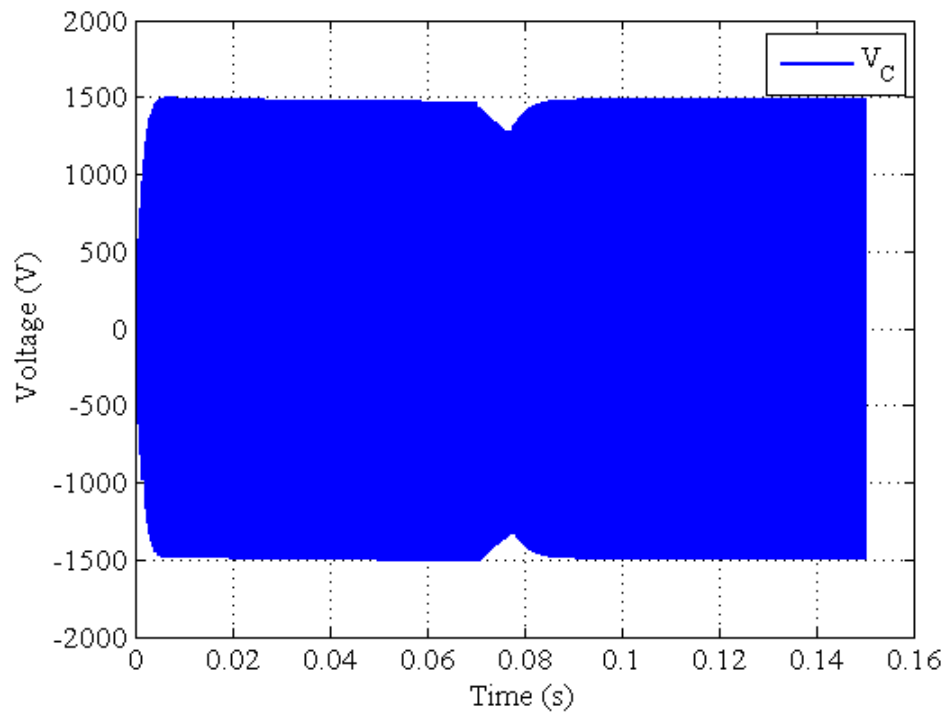


Fig. 43. Center link capacitor voltage for $\varphi_{12} = 0^\circ$ to $\varphi_{12} = 5^\circ$.

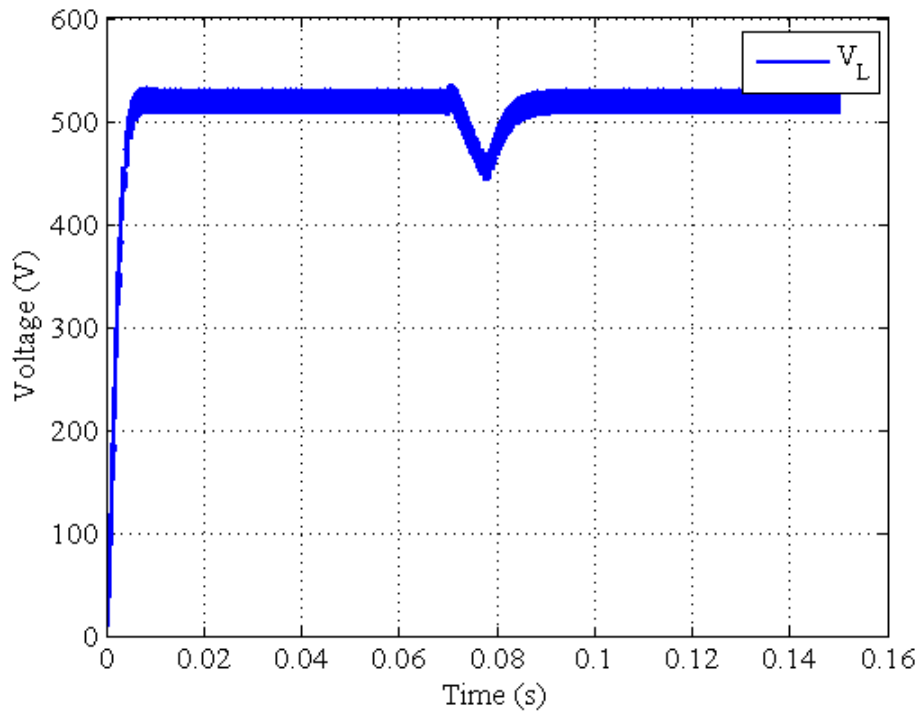


Fig. 44. Load voltage for $\varphi_{12} = 0^\circ$ to $\varphi_{12} = 5^\circ$.

This change causes converter 1 switch timing to lag converter 2 switch timing i.e. converter 2 changes switch pairs before converter 1. Once a converter changes switch pairs the current in the inductor begins to rise due to the voltage difference between the voltage source and the capacitor voltage. If the other converter continues with its previous switch pair then the inductor current continues to fall because the capacitor voltage is greater than the source voltage. So for this case converter 1 current continues to fall while converter 2 current begins to rise because the firing time for converter 2 to change switch pairs is before converter 1. This causes the average current of the two converters to be slightly different, i.e. the current decrease from average of converter 1 has now been added to converter 2. Now that these currents are not equal every time a switching instance

occurs the currents will not cancel each other out while charging the center capacitor, converter 2 will dominate the charging. Now the time for converter 1 inductor current to reach its peak value is slightly shorter than the time it takes to fall back to its original starting point for that switching instance. This causes the current in converter 1 to continue to fall until it reaches near zero. As ϕ_{12} increases this process happens quicker. This is shown in Figs. 45 – 47. Since mode 2 of Scenario 2 is the opposite of the first mode it was concluded that converter 2 will cease to send power to the load and converter 1 will continue to supply at max power.

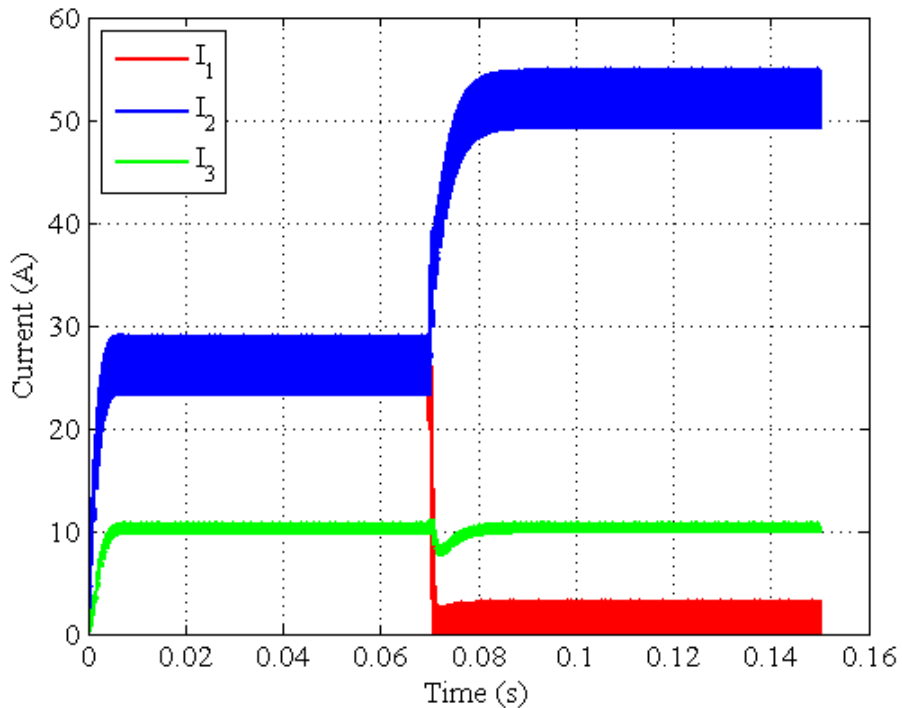


Fig. 45. Converter currents for $\phi_{12} = 0^\circ$ to $\phi_{12} = 45^\circ$.

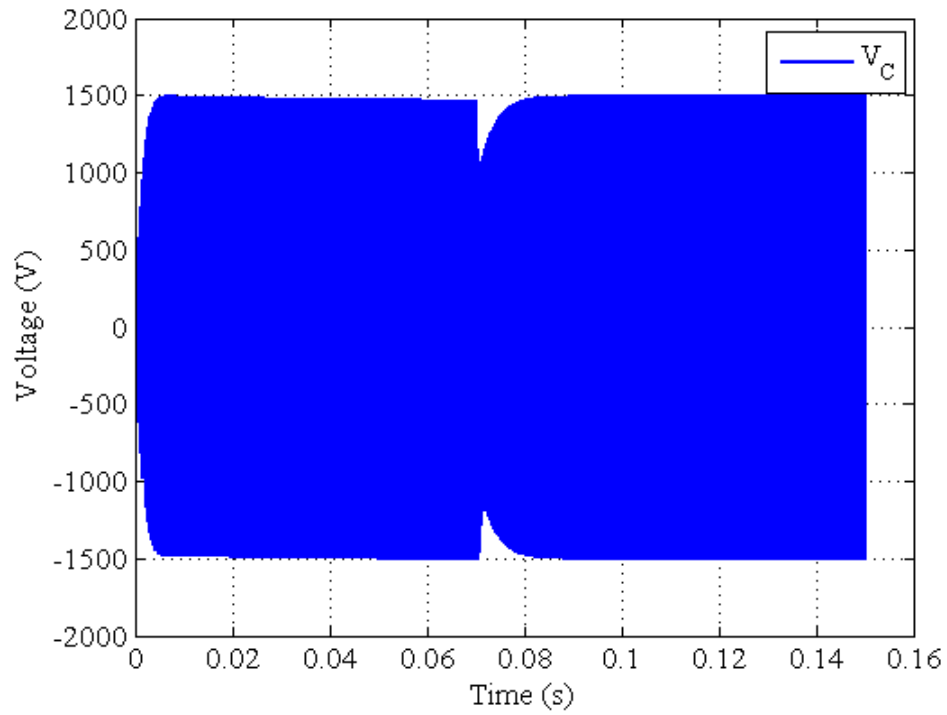


Fig. 46. Center link capacitor voltage for $\varphi_{12} = 0^\circ$ to $\varphi_{12} = 45^\circ$.

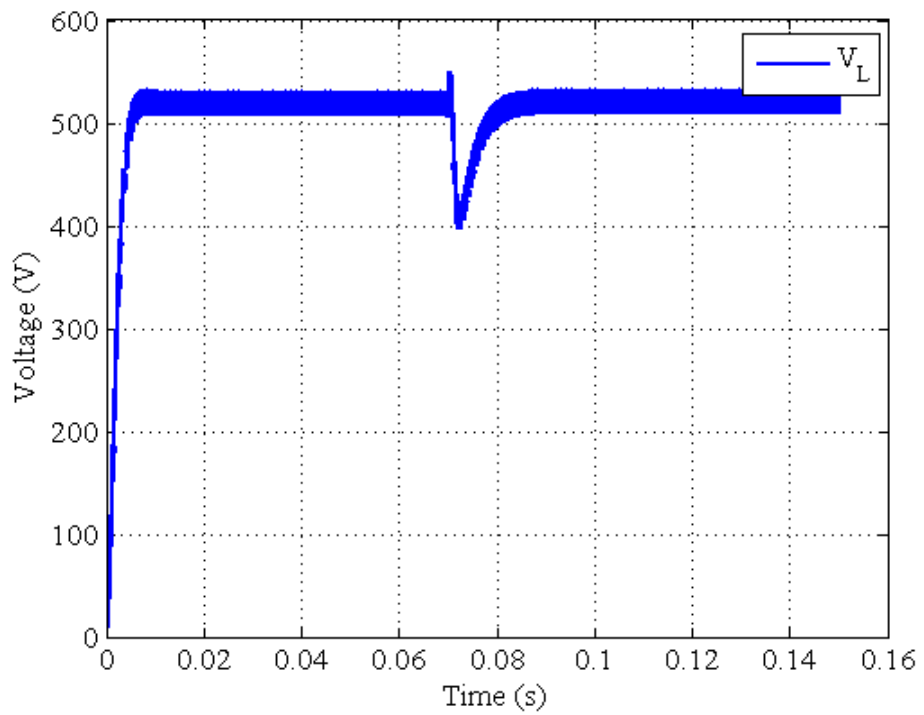


Fig. 47. Load voltage for $\varphi_{12} = 0^\circ$ to $\varphi_{12} = 45^\circ$.

2. Input Voltage Deviation

Input voltage deviation is a very important issue because two sources are hardly every exactly equal to one another. Therefore, to see how this affects the Multi-source IDC, converter 2 was adjusted from 25V to 100V to see how the converter would react. This was done in two different methods just like the phase angle difference variation. As can be seen in Fig. 48, converter 2 source current goes to near zero and converter 1 supplies all the current necessary to drive the load. The reason for this goes back to the switched LC circuit for both of the source converters. Since the source of converter 1 is higher it has a longer current charge time than converter 2, i.e. $V_1 > v_C$. This causes the peak inductor current per half cycle to be less in converter 2. This causes the fall time of

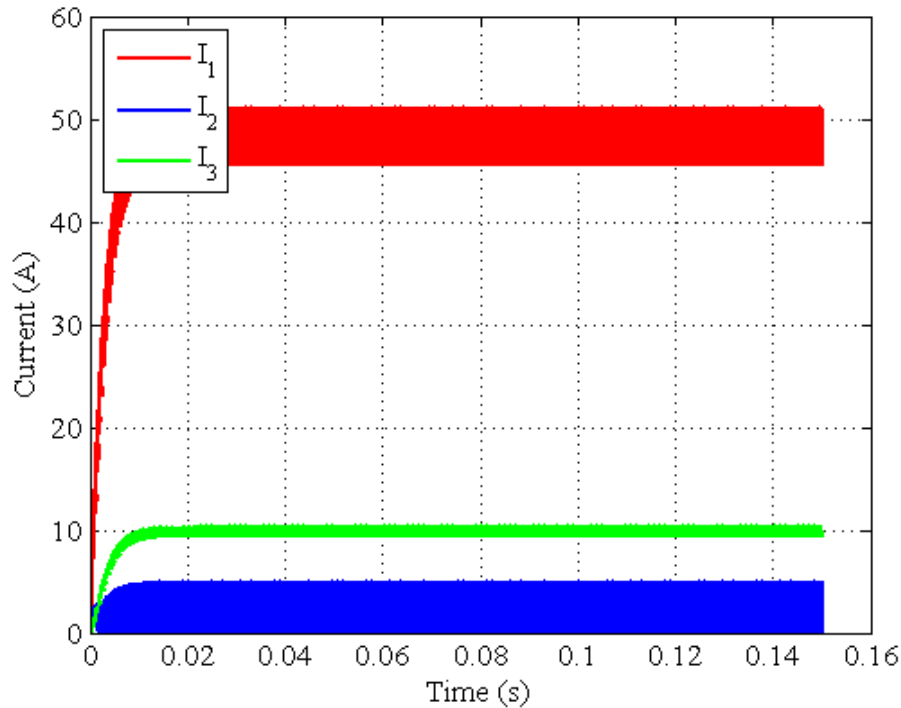


Fig. 48. Converter currents for $V_2 = 25V$.

the inductor current from peak to minimum to be longer than its charge time, therefore causing the current to go to near zero values. As V_2 was increased closer to V_1 the time for converter 2 current to go to zero increased and can be seen in Fig. 49.

To further understand the operation of the Multi-source IDC the load was increased and decreased for a constant phase difference angle, $\varphi_{13} = \varphi_{23}$, and source voltages equal, $V_1 = V_2$. Since the load is modeled as a resistor, $R_L = 50\Omega$, it was increased and decreased by 10%, 5Ω . This can be seen in Figs. 50 and 51. The variation of the phase difference angle, input voltage, and load resistance has given insight on how to control the Multi-Source converter for such instances.

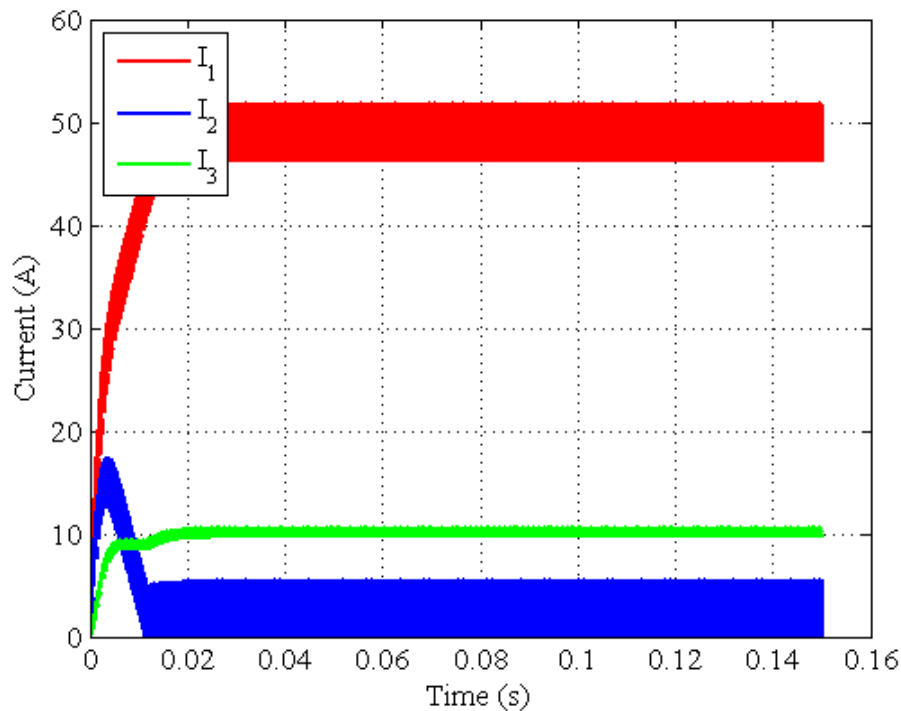


Fig. 49. Converter currents for $V_2 = 75V$.

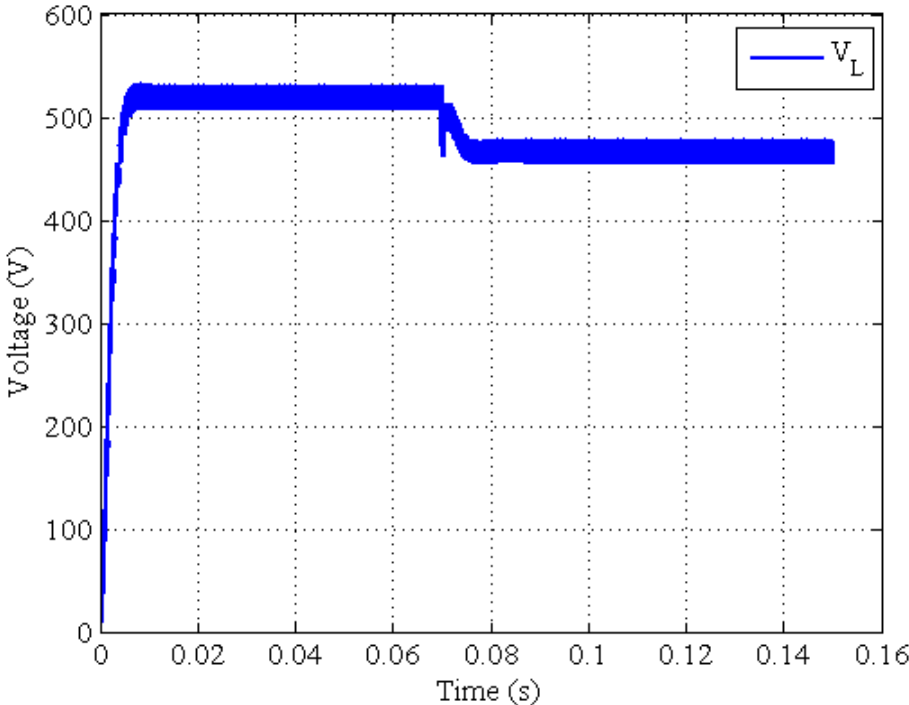


Fig. 50. Load voltage for $R_L = 50\Omega$ to 45Ω .

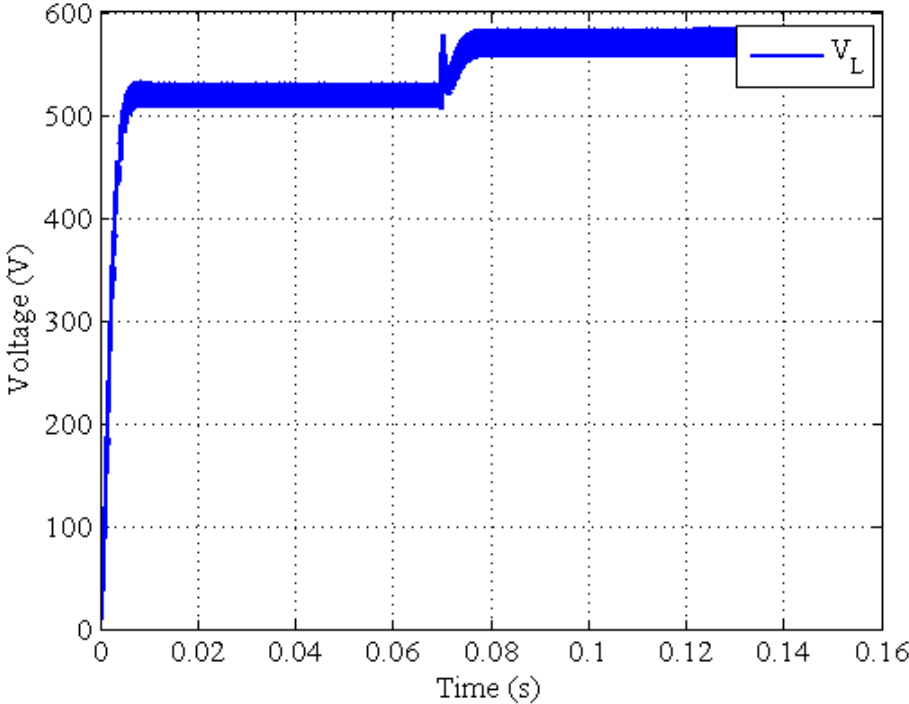


Fig. 51. Load voltage for $R_L = 50\Omega$ to 55Ω .

B. Control Results

By observing how the phase difference angle, input voltage, and load resistance changed the operational characteristics of the Multi-source IDC, a simple yet elegant way to regulate the output voltage and converter 2 input current was obtained and shown in Chapter III. Various control schemes were simulated in order to show that this control method was valid for different variations in load, input current, and input voltage. Each of these simulations have three parts: steady state, 1st variation, and 2nd variation. All simulations were simulated for 0.2s. The control algorithm takes the average value of the measurement in order to determine if converter 2 current or load voltage is within its hysteresis band. These average values are shown along with the actual measured value for that specific element.

1. *Input Voltage Deviation and Load Variation*

For this simulation the first variation comes at 0.04s with the converter 2 voltage, V_2 , changing from 100V to 110V. Once this deviation occurs the controller responds to converter 2 current going out of bounds, greater or less than 27.5 plus hysteresis, and adjusts φ_{23} accordingly. Shortly thereafter, the output voltage goes out of its hysteresis band and φ_{13} is adjusted and φ_{23} is set equal to φ_{13} until the current goes out of its band again. At 0.12s the load resistance is changed from 50 to 45, which causes a voltage spike. The control algorithm then adjusts φ_{13} in order to keep the output voltage regulated and then tends to φ_{23} to monitor the input current of converter 2. This is shown in Fig. 52 – 56. The load was also varied by 20% and is shown in Appendix C.

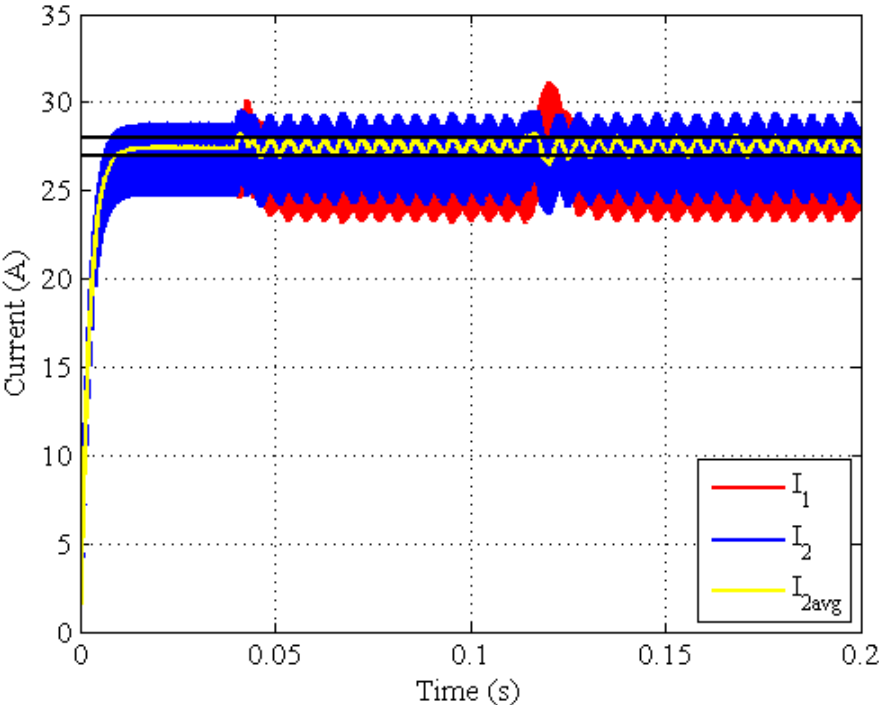


Fig. 52. Source currents for 10% V_2 and 10% R_L variations.

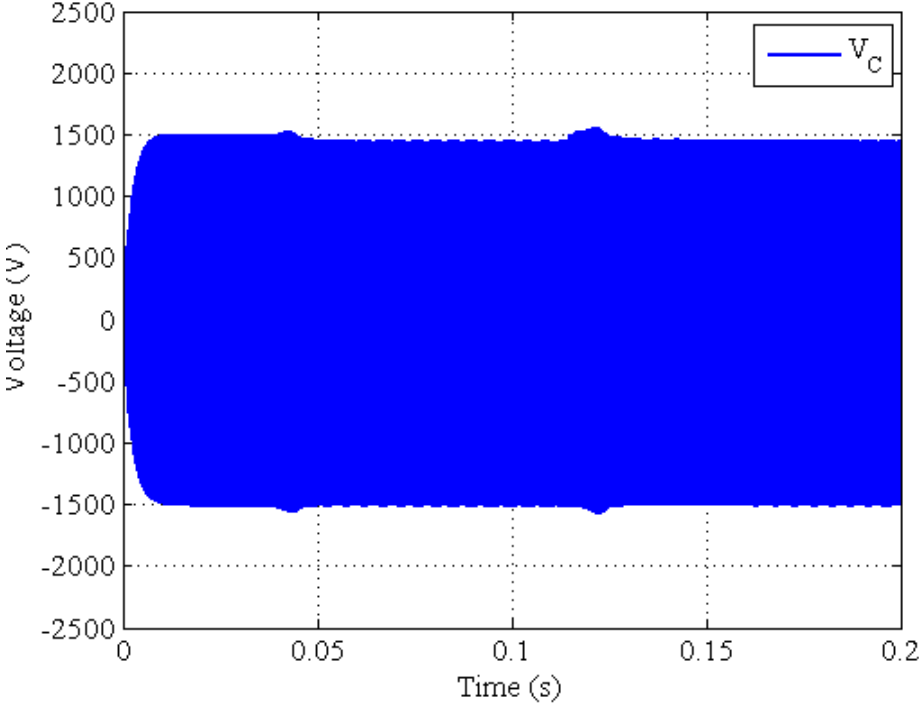


Fig. 53. Center capacitor voltage for 10% V_2 and 10% R_L variations.

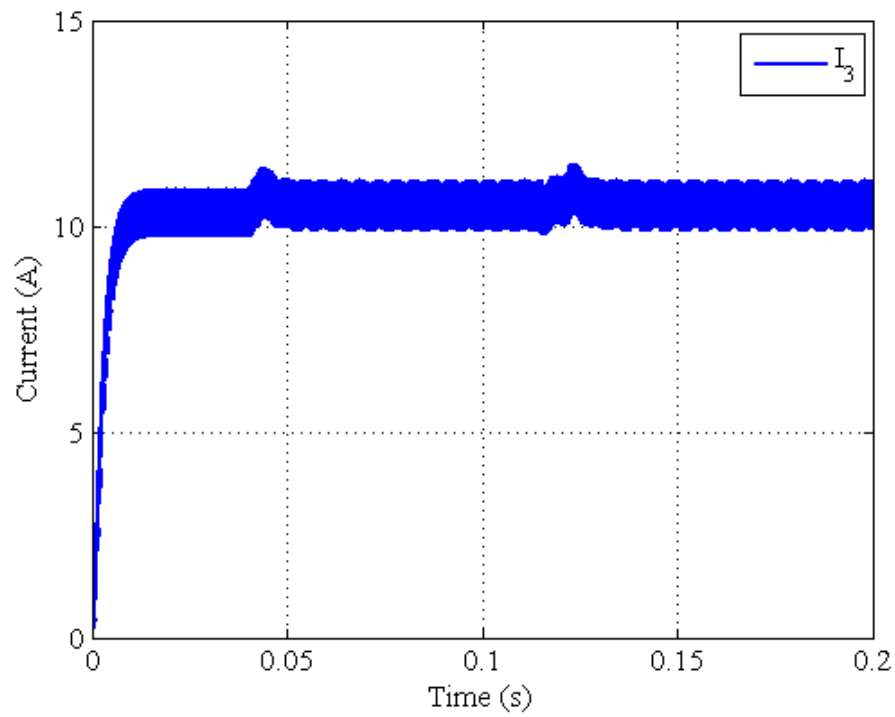


Fig. 54. Load current for 10% V_2 and 10% R_L variations.

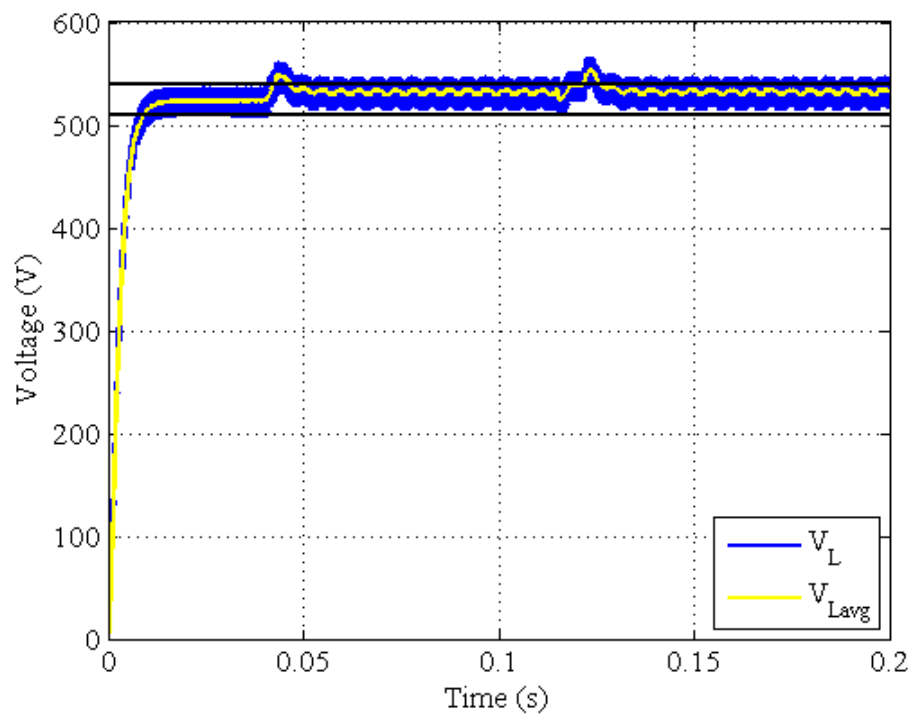


Fig. 55. Load voltage for 10% V_2 and 10% R_L variations.

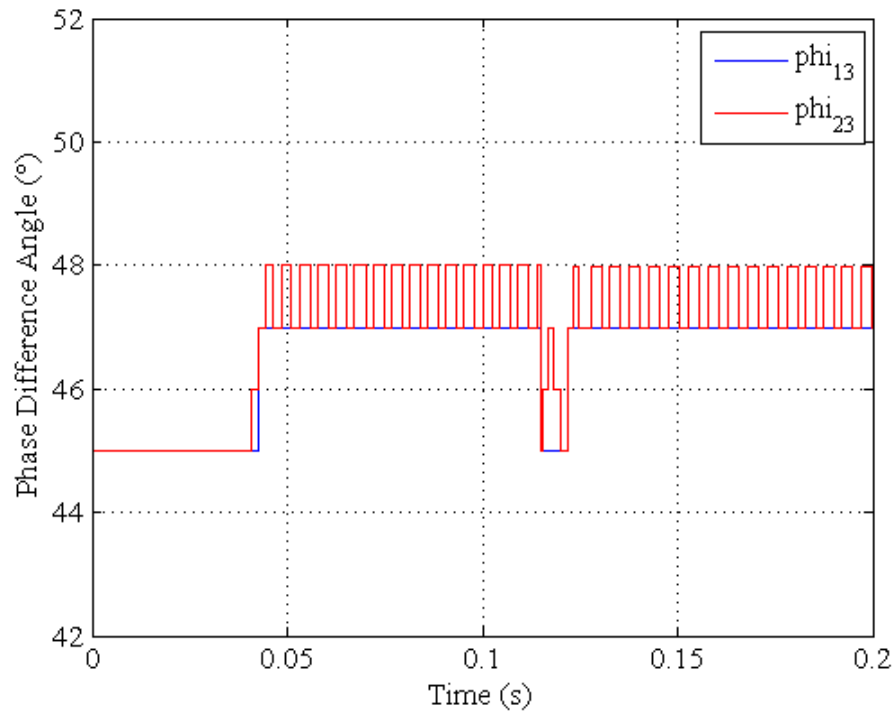


Fig. 56. Phase difference angles for 10% V_2 and 10% R_L variations.

2. *Input Voltage Deviation and Load Voltage Variations*

For this simulation the input voltage was varied from 100V to 110V at 0.03s. In some cases it is desirable to adjust the output voltage to a new value. With this in mind the output voltage was varied from 525V to 600V at 0.12s. In each case the algorithm monitored the average values of the converter 2 current and load voltage along with their respective references and adjusted them accordingly. This is shown in Figs. 57 – 61.

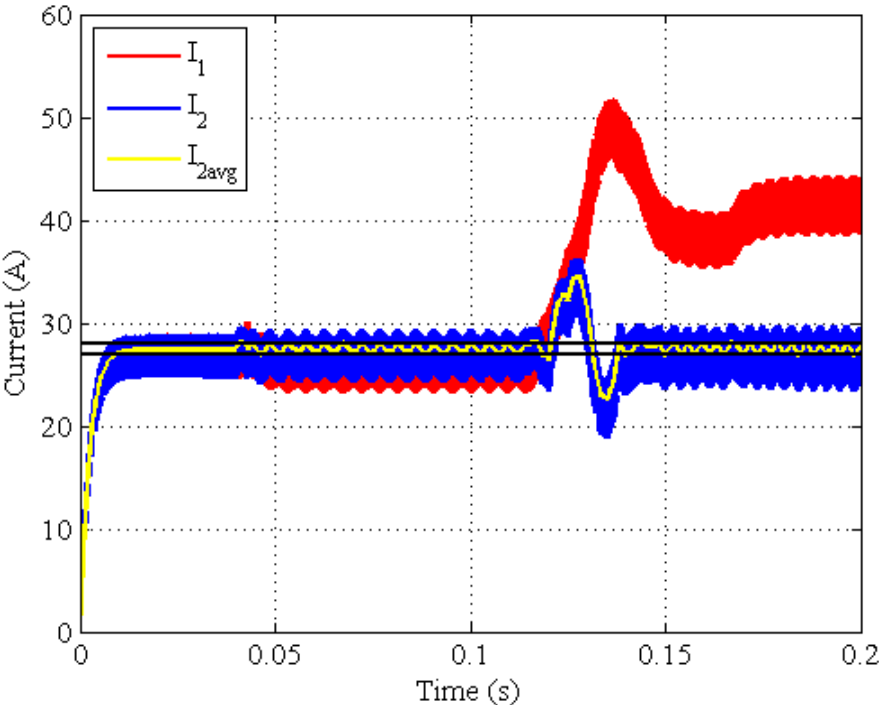


Fig. 57. Source currents for 10% V_2 and 10% V_L variations.

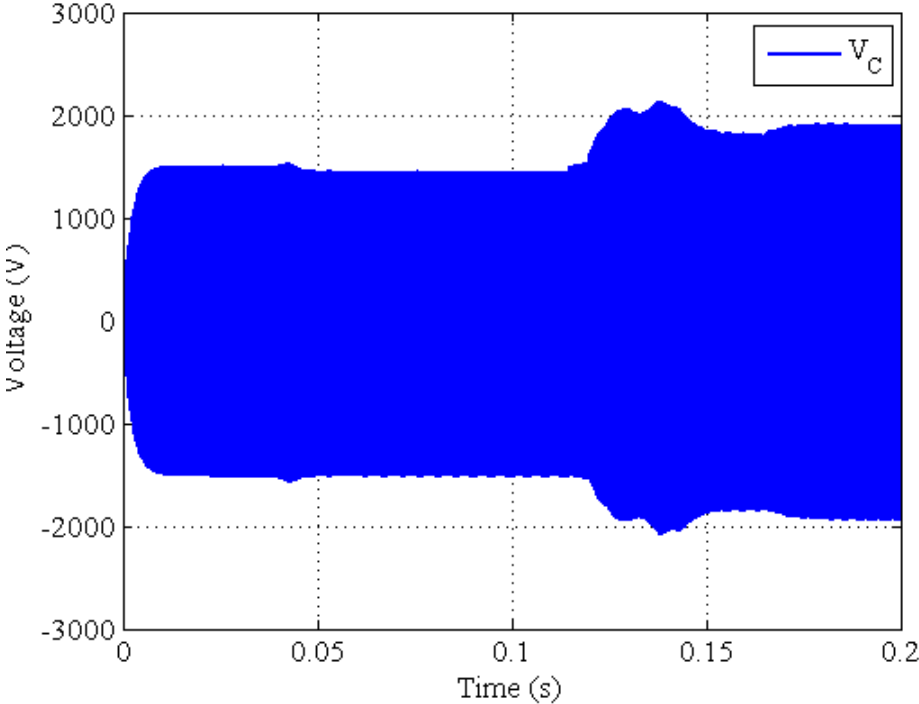


Fig. 58. Center capacitor voltage for 10% V_2 and 10% V_L variations.

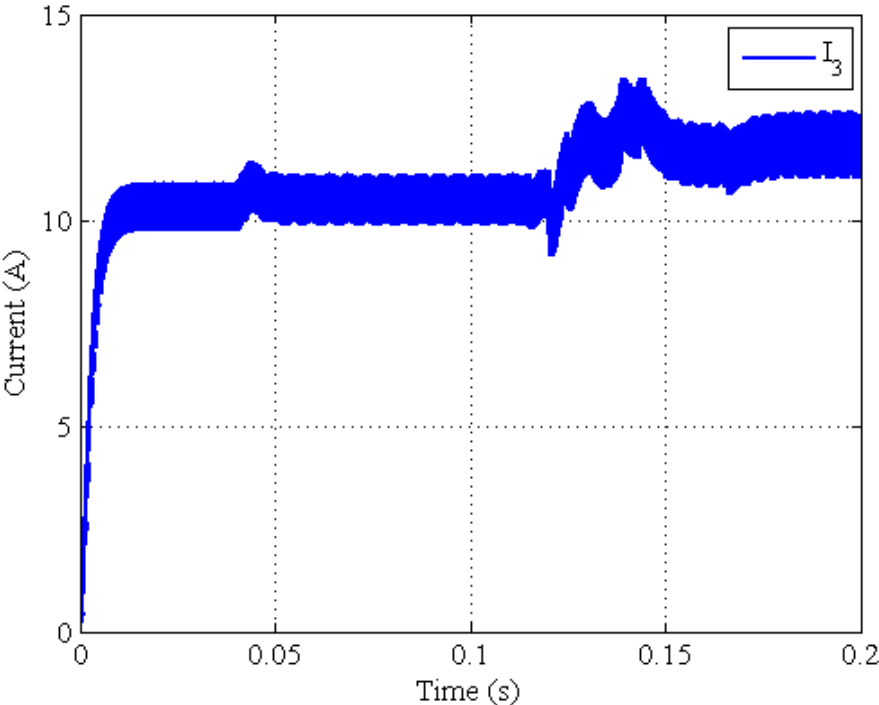


Fig. 59. Load current for 10% V_2 and 10% V_L variations.

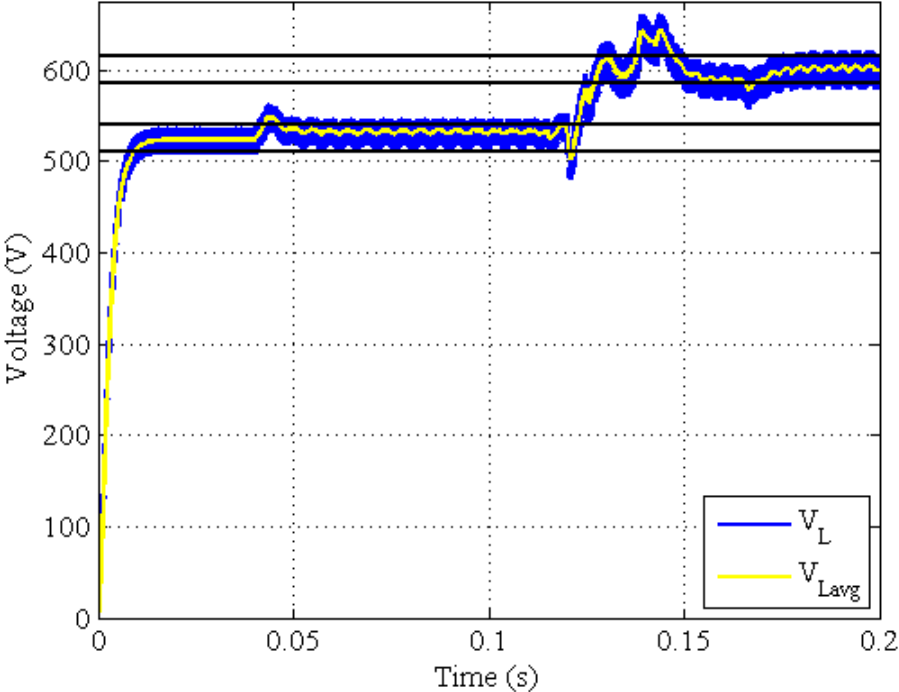


Fig. 60. Load voltage for 10% V_2 and 10% V_L variations.

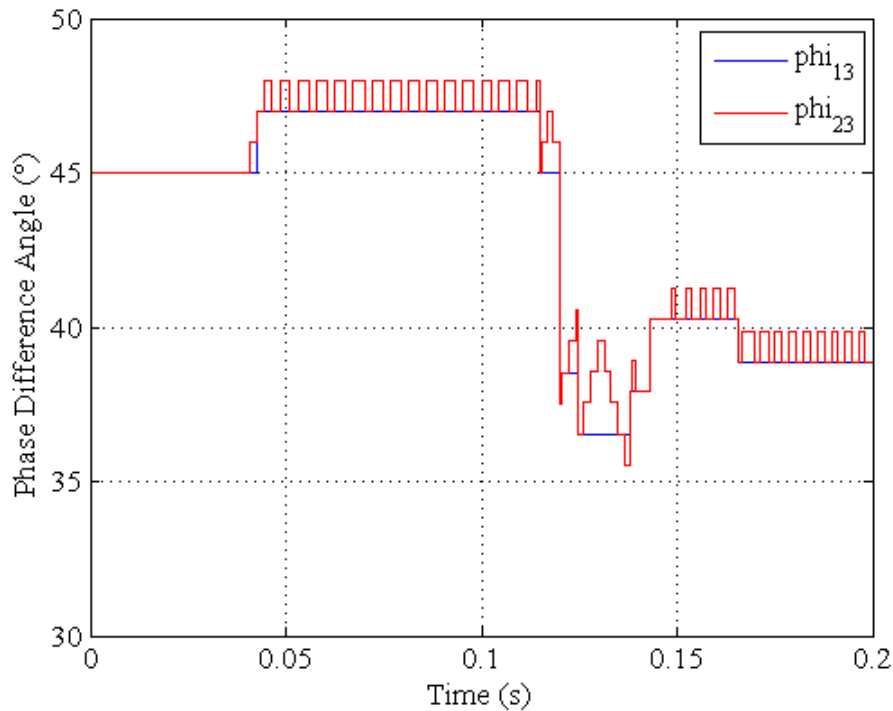


Fig. 61. Phase difference angles for 10% V_2 and 10% V_L variations.

3. *Input Voltage Deviation and Input Current Variations*

For this simulation the input voltage was varied from 100V to 110V at 0.03s. After this three different variations of current control were simulated. This is to show the flexibility of the control to monitor the source that is considered to be the short term source and turn it off through a ramp down sequence or to increase or decrease the current from this source based on its capacity. For the first simulation the input current was stepped down to 20A. The second simulation was a ramp down to near 0A. The third simulation was to ramp down to 0A and then ramp up to 27.5A to show that the source can be turned back on when necessary. This is shown in Figs. 62 – 70. The capacitor voltage and load current are shown in Appendix D.

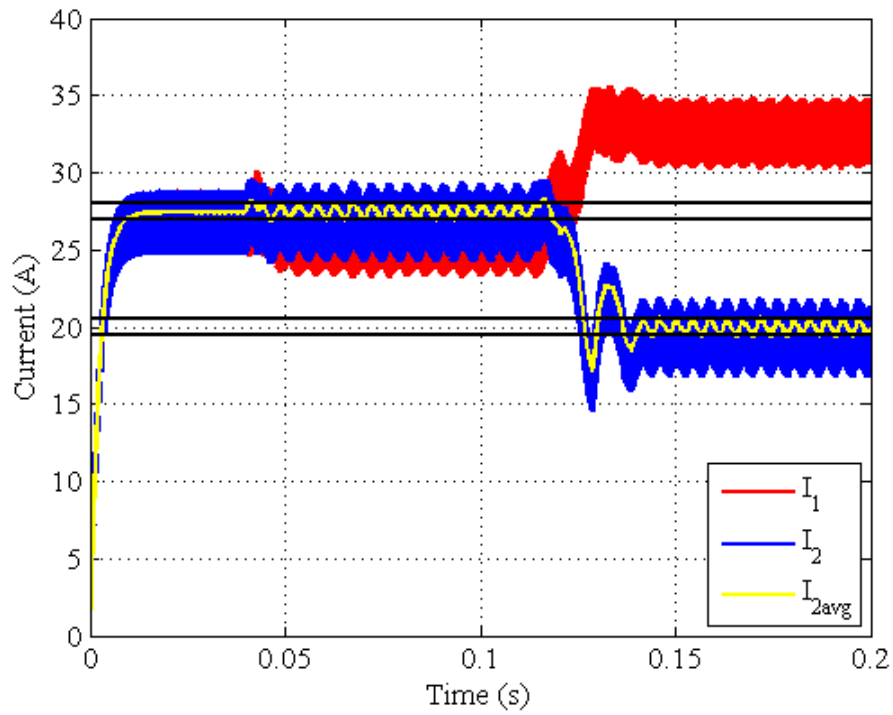


Fig. 62. Source currents for 10% V_2 and 25% I_2 variations.

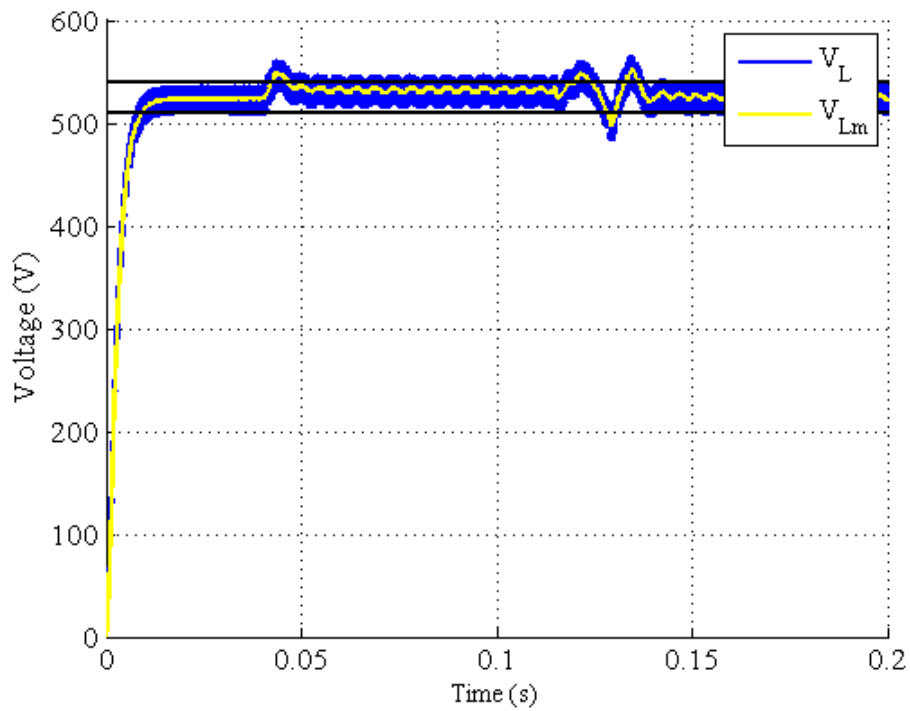


Fig. 63. Load voltage for 10% V_2 and 25% I_2 variations.

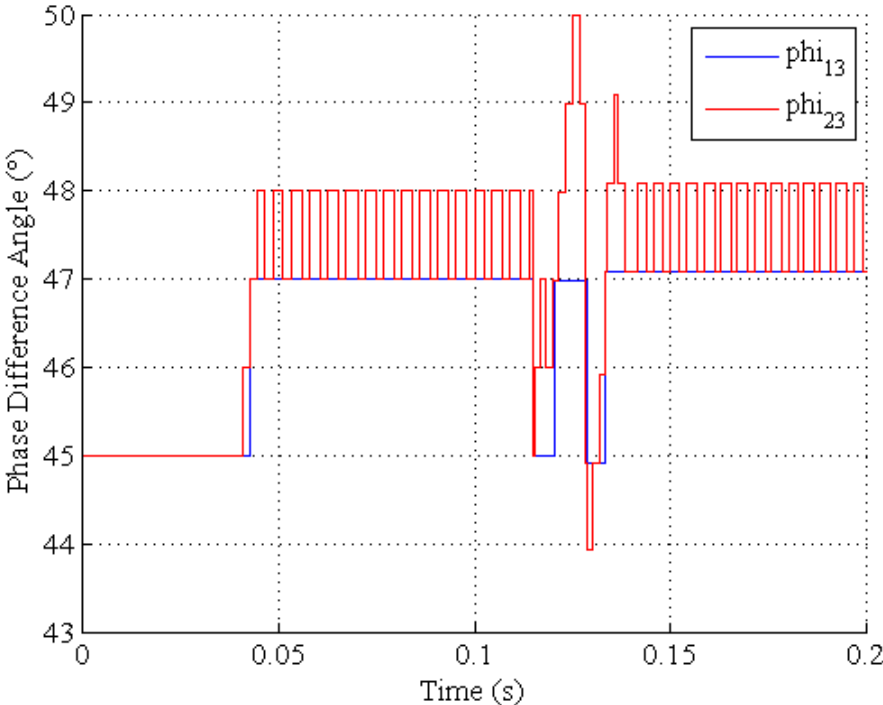


Fig. 64. Phase difference angles for 10% V_2 and 25% I_2 variations.

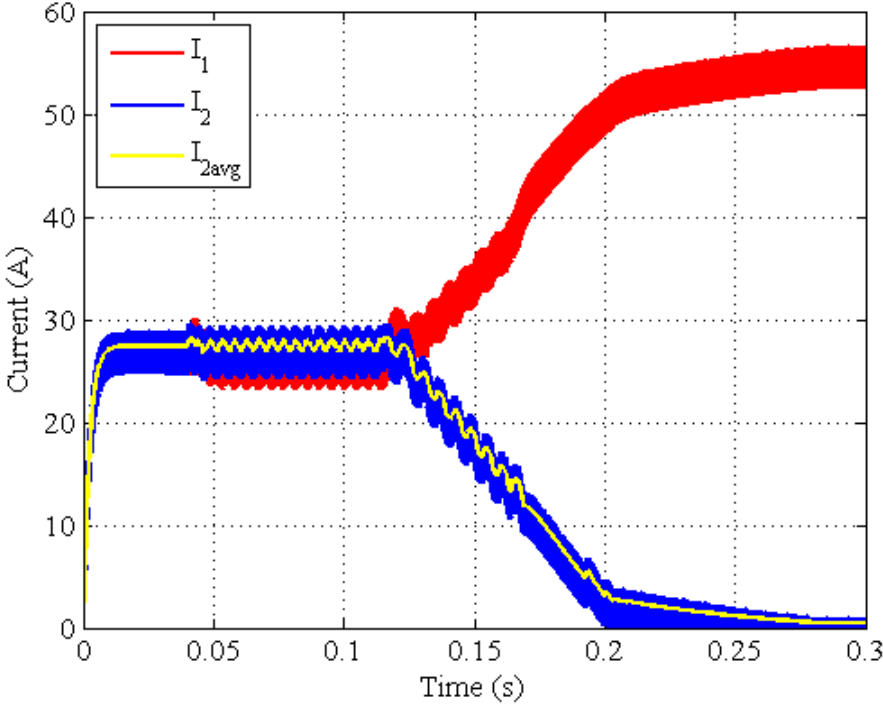


Fig. 65. Source currents for 10% V_2 and ramp down I_2 variations.

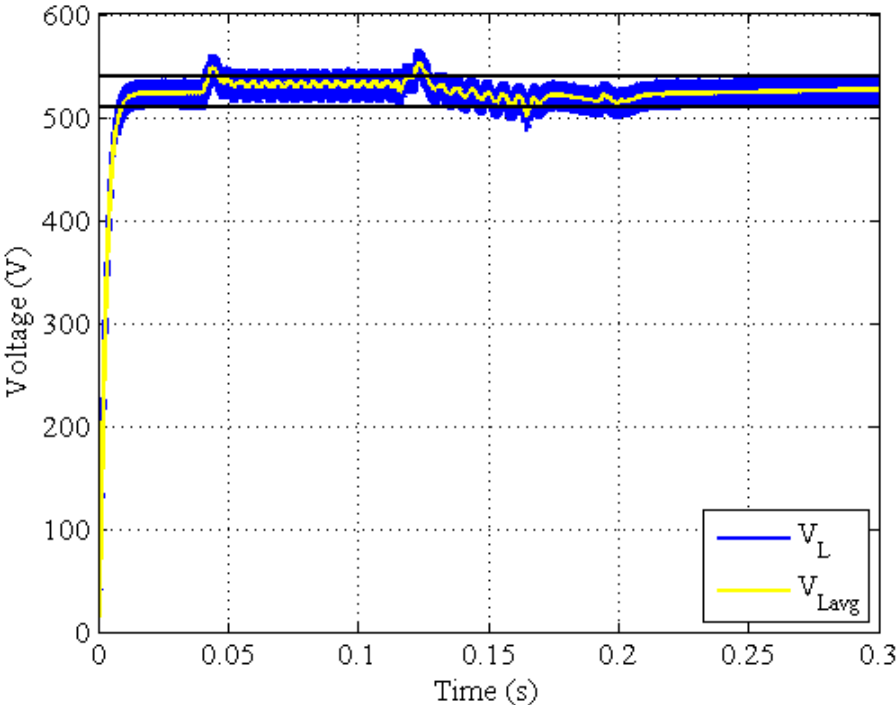


Fig. 66. Load voltage for 10% V_2 and ramp down I_2 variations.

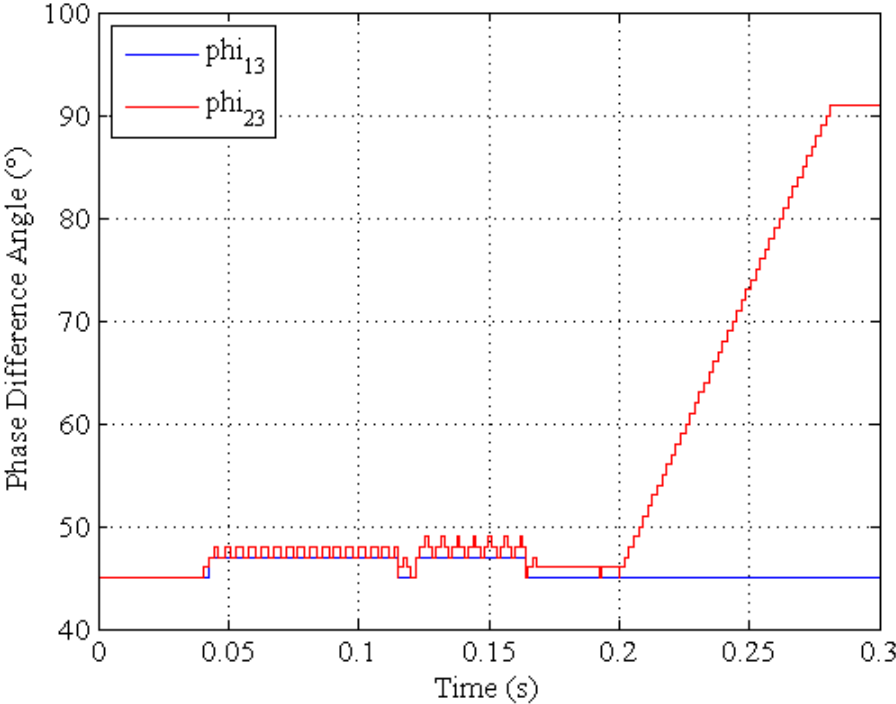


Fig. 67. Phase difference angles for 10% V_2 and ramp down I_2 variations.

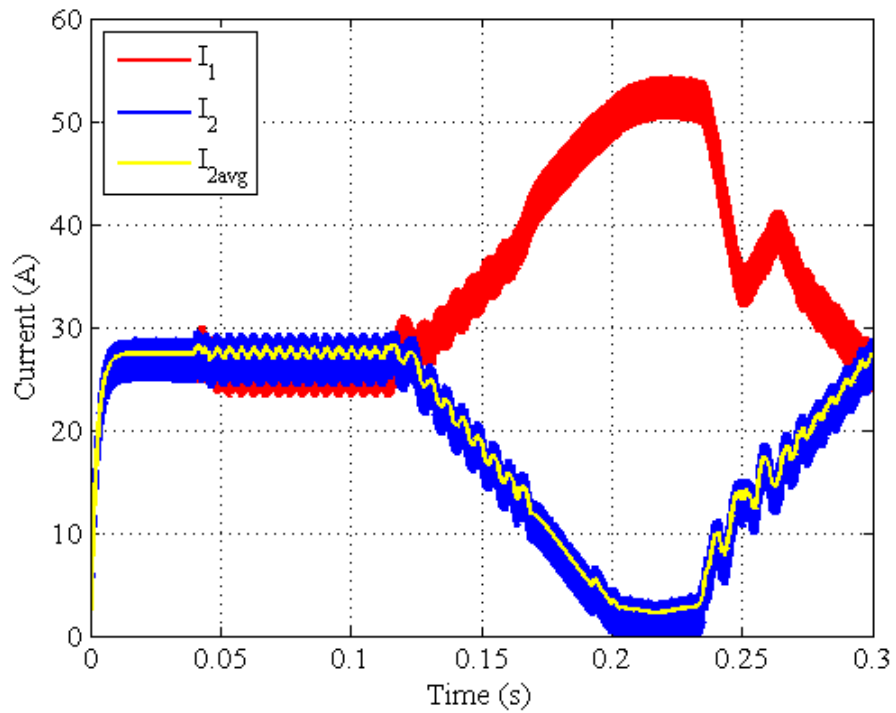


Fig. 68. Source currents for 10% V_2 and ramp down and up I_2 variations.

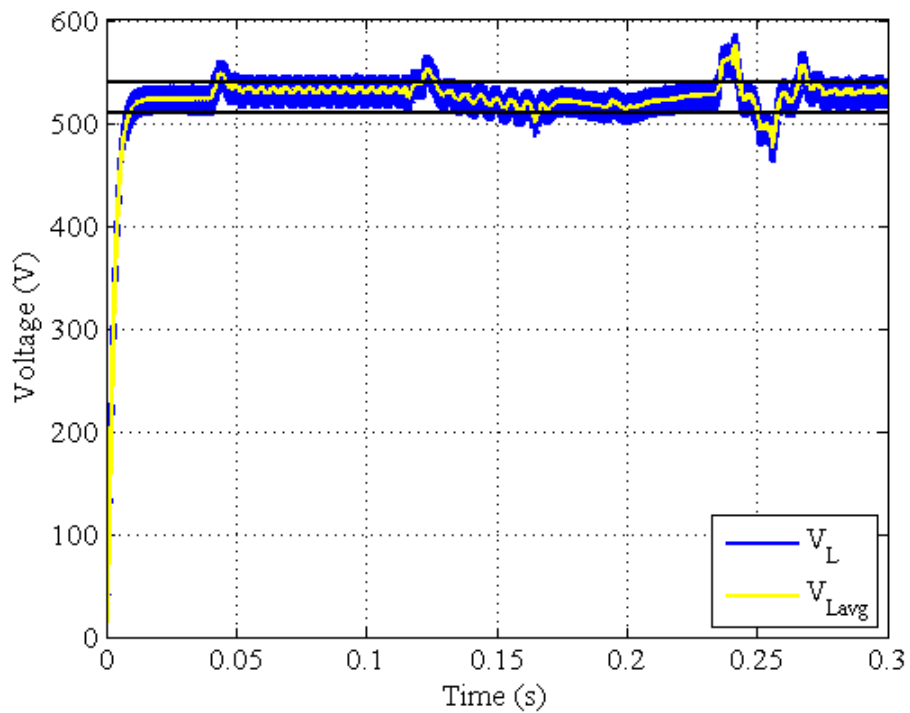


Fig. 69. Load voltage for 10% V_2 and ramp down and up I_2 variations.

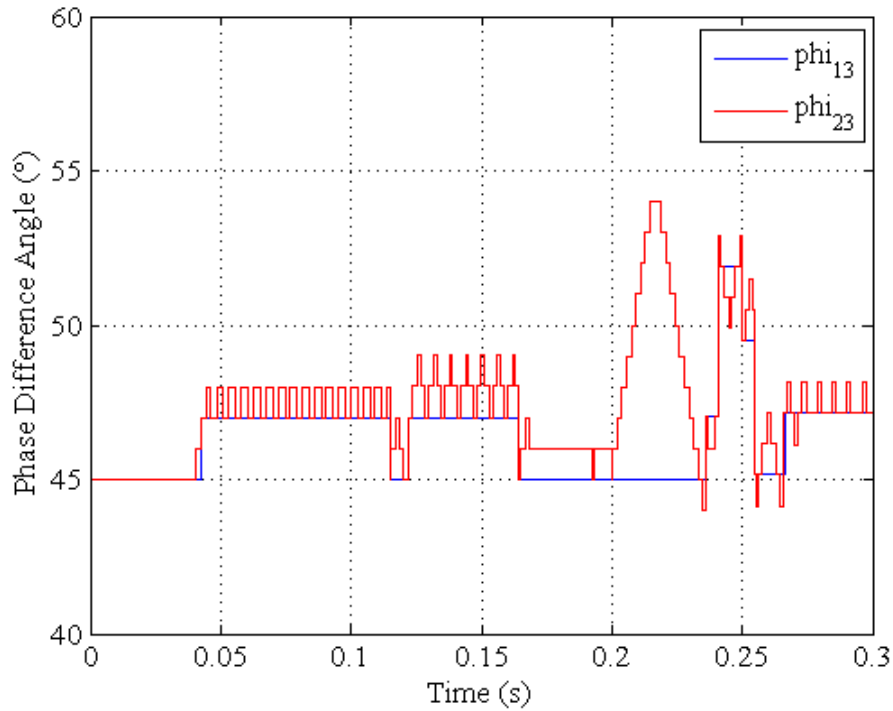


Fig. 70. Phase difference angles for 10% V_2 and ramp down/up I_2 variations.

C. Summary

This chapter has explained the Multi-source operational characteristics and the control strategy to go along with those characteristics. As long as converter 1 can handle the total power requirements of the load then this converter can operate in either load sharing mode or single converter full power mode. This converter works well under various disturbances and continues to regulate the output voltage and input current.

CHAPTER V

CONCLUSIONS AND FUTURE WORK

A. Conclusions

With the need for renewable energy sources in high demand, the technology needed to interface these sources has been a big topic in current research with the creation of new conferences and transactions. This thesis has presented a new DC-DC converter, Multi-source IDC, which can be used with multiple energy sources.

The Multi-source IDC is a topological variation of the original IDC presented in Chapter II. The original IDC is a DC-DC converter with the capability of continuous voltage step up or step down over a wide range without the use of a transformer. This is done by controlling the phase difference angle φ or the switching frequency f . This converter was then modeled using Gyrator theory in order to gain an understanding about its operational characteristics as well as control.

A new DC-DC converter was presented in Chapter III based on the original IDC. This converter, Multi-source IDC, is a topological variation of the IDC. This converter consists of two source converters attached to a center link capacitor and then connected to the load converter. This new converter was then studied based on various disturbances that may occur while operating a multiple source system as well as the responses to similar control techniques from the original IDC.

First this study showed that when the phase difference angles are equal, i.e. $\varphi_{13} = \varphi_{23}$, the Multi-source IDC operates the same as the original IDC with the exception that

the original source current in the IDC is now split between the two converters in the Multi-source IDC. Therefore, this new converter is doing equal load sharing. From this observation it was then desired to operate the converters at different power levels by adjusting their current. This was done by actively controlling the phase difference angle ϕ_{23} in such a way that converter 2 current stayed within the bounds of the desired reference current. It was also desired to control the output voltage across the load during times of disturbance or transients from one power level to the next. This was done by adjusting ϕ_{13} in such a way to keep the output voltage regulated within a tolerable hysteresis band. Both of these controls, input current and output voltage, were then implemented into one controller in order to maintain the input current of converter 2 within a particular set of values as well as hold the output voltage within its set of values. By doing this the Multi-source converter demonstrated that it can be controlled in such a fashion to supply a single load from one limitless supply and one varying supply.

B. Future Work

This project will be extended by placing this converter topology and its control into a particular application. This application will be stand alone power generation via a fuel cell and battery power supply. This study will include but is not limited to: electrical fuel cell modeling in PSIM[®], battery modeling in PSIM[®], battery recharging, and balance of plant control based on energy capacity.

REFERENCES

- [1] H. Tao, A. Kotsopoulos, J.L. Duarte, and M.A.M. Hendrix, "Family of multiport bidirectional DC-DC converters," *IEE Proceedings of Electric Power Applications*, vol. 153, no. 3, pp. 451-458, May 2006.
- [2] J.L. Duarte, M. Hendrix, and M.G. Simoes, "Three-port bidirectional converter for hybrid fuel cell systems," *IEEE Transactions on Power Electronics*, vol. 22, no. 2, pp. 480-487, March 2007.
- [3] Y.M. Chen, Y.C. Liu, S.C. Hung, and C.S. Cheng, "Multi-input inverter for grid-connected hybrid PV/wind power system," *IEEE Transactions on Power Electronics*, vol. 22, no. 3, pp. 1070-1077, May 2007.
- [4] C. Zao, S. Round, and J.W. Kolar, "Buck and boost start-up operation of a three-port power supply for hybrid vehicle applications," in *Proc. 36th Annual Power Electronics Specialists Conference*, 2005, pp. 1851-1857.
- [5] J.G. Kassakian, H.C. Wolf, J.M. Miller, and C.J. Hurton, "Automotive electrical systems circa 2005," *IEEE Spectrum*, vol. 33, no. 8, pp. 22-27, Aug. 1996.
- [6] H. Krishnaswami and N. Mohan, "A Current-fed three-port bi-directional DC-DC converter," in *Proc. 29th International Telecommunications Energy Conference*, Sept. 30, 2007-Oct. 4, 2007, pp. 523-526.
- [7] H. Tao, A. Kotsopoulos, J.L. Duarte, and M.A.M. Hendrix, "Multi-input bidirectional DC-DC converter combining DC-link and magnetic-coupling for fuel cell systems," in *Proc. 40th Annual Meeting Industry Applications Conference*, vol. 3, Oct. 2-6, 2005, pp. 2021-2028.
- [8] Y.M. Chen, Y.C. Liu, and F.Y. Wu, "Multi-input DC/DC converter based on the multiwinding transformer for renewable energy applications," *IEEE Transactions on Industry Applications*, vol. 38, no. 4, pp. 1096-1104, July-Aug. 2002.
- [9] H. Tao, A. Kotsopoulos, J.L. Duarte, and M.A.M. Hendrix, "A soft-switched three-port bidirectional converter for fuel cell and supercapacitor applications," in *Proc. 36th Annual Power Electronics Specialists Conference*, 2005, pp. 2487-2493.

- [10] R.W. De Donker, D.M. Divan, and M.H. Kheraluwala, "A three-phase soft-switched high-power-density DC/DC converter for high-power applications," *IEEE Transactions on Industry Applications*, vol. 27, no. 1, pp. 63-73, Jan.-Feb. 1991.
- [11] M. Ehsani, R.L. Kustom, and R.W. Boom, "A one-phase dual converter for two quadrant power control of superconducting magnets," *IEEE Transactions on Magnetics*, vol. 21, no. 2, pp. 1115-1118, Mar. 1985.
- [12] M. Ehsani and R.L. Kustom, *Converter Circuits for Superconductive Magnetic Energy Storage*, Texas A&M University Press, College Station, Texas, 1988.
- [13] M.O. Bilgiç and M. Ehsani, "Analysis of inductor-converter bridge by means of state-space averaging technique," in *Proc. 19th Annual Power Electronics Specialists Conference*, 1988, pp. 116-121.
- [14] I. Husain, *Analysis and Design of a High Power DC-DC Converter*, M.S. Thesis, Texas A&M University, College Station, 1989.
- [15] S. Singer, "Gyrators in power processing circuits," *IEEE Transactions on Industrial Electronics*, vol. 34, no. 3, pp. 313-318, Aug. 1987.
- [16] M. Ehsani, "Inverse dual converter for high-power applications," U.S. Patent, Patent # 5,208,740, May 4, 1993.

APPENDIX A

STATE SPACE AVERAGING CALCULATIONS FOR MULTI-PORT ICB

There are four different switching states for the multi-port ICB and are shown in Figs.

A.1 – A.4.

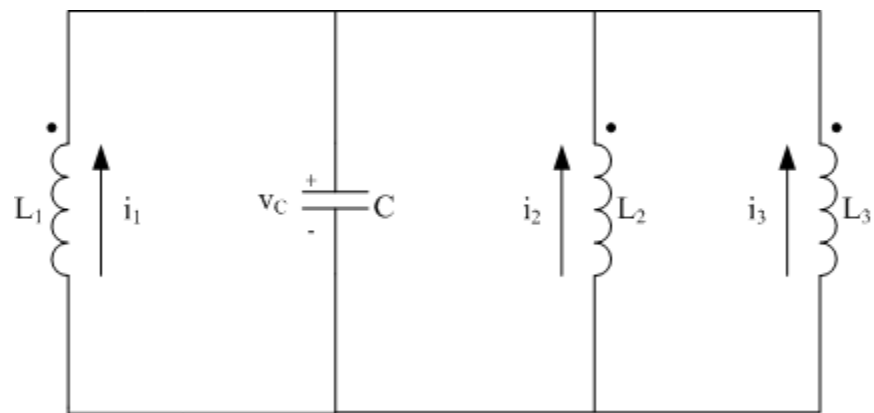


Fig. A.1. Case I: multi-port ICB with S114, S214, S314 switches conducting.

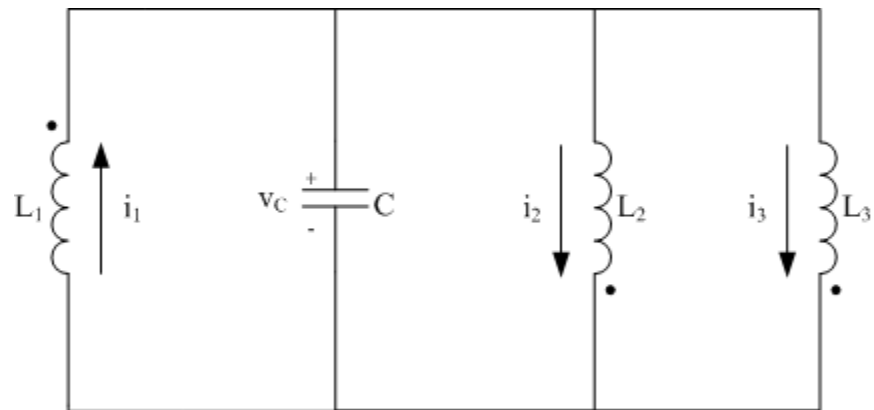


Fig. A.2. Case II: multi-port ICB with S114, S223, and S323 switches conducting.

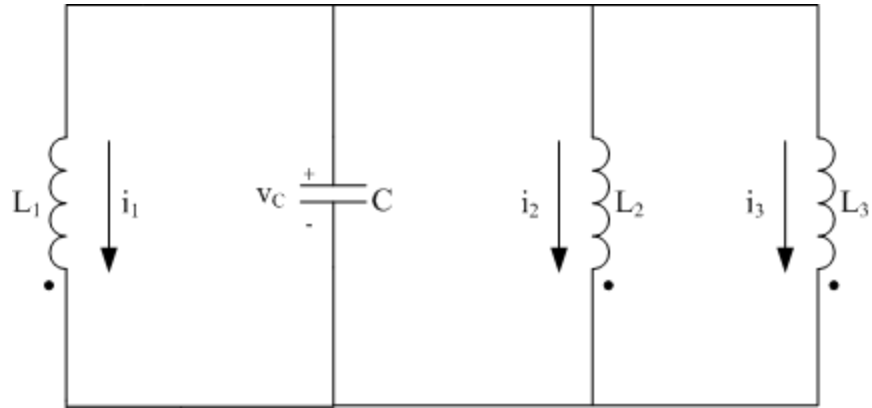


Fig. A.3. Case III: multi-port ICB with S123, S223, and S323 switches conducting.

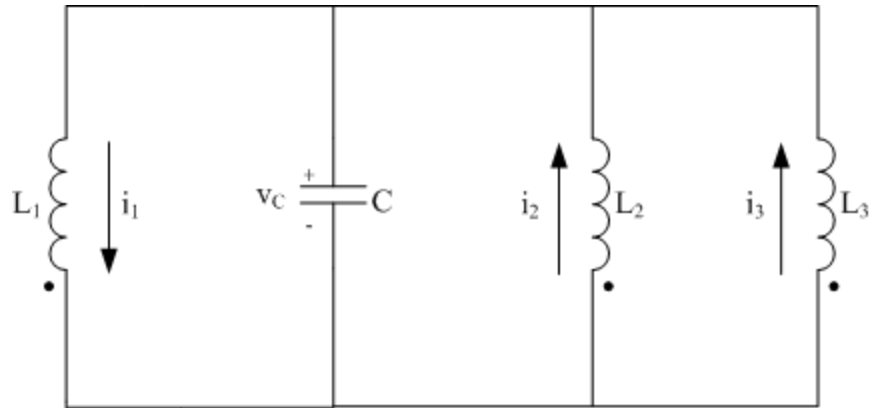


Fig. A.4. Case IV: multi-port ICB with S123, S214, and S314 switches conducting.

Next the equations were written for each of these cases and using the state space averaging approximation technique.

$$\begin{bmatrix} \dot{i}_1 \\ \dot{i}_2 \\ \dot{i}_3 \\ \dot{v}_C \end{bmatrix} = A \begin{bmatrix} i_1 \\ i_2 \\ i_3 \\ v_C \end{bmatrix} \quad (A1)$$

Case 1:

$$L_1 \frac{di_1}{dt} = -v_C \quad (\text{A2})$$

$$L_2 \frac{di_2}{dt} = -v_C \quad (\text{A3})$$

$$L_3 \frac{di_3}{dt} = -v_C \quad (\text{A4})$$

$$C \frac{dv}{dt} = i_1 + i_2 + i_3 \quad (\text{A5})$$

$$A_1 = \begin{bmatrix} 0 & 0 & 0 & -1/L_1 \\ 0 & 0 & 0 & -1/L_2 \\ 0 & 0 & 0 & -1/L_3 \\ 1/C & 1/C & 1/C & 0 \end{bmatrix} \quad (\text{A6})$$

Case II

$$L_1 \frac{di_1}{dt} = -v_C \quad (\text{A7})$$

$$L_2 \frac{di_2}{dt} = v_C \quad (\text{A8})$$

$$L_3 \frac{di_3}{dt} = v_C \quad (\text{A9})$$

$$C \frac{dv}{dt} = i_1 - i_2 - i_3 \quad (\text{A10})$$

$$A_2 = \begin{bmatrix} 0 & 0 & 0 & -1/L_1 \\ 0 & 0 & 0 & 1/L_2 \\ 0 & 0 & 0 & 1/L_3 \\ 1/C & -1/C & -1/C & 0 \end{bmatrix} \quad (\text{A11})$$

Case III

$$L_1 \frac{di_1}{dt} = v_C \quad (\text{A12})$$

$$L_2 \frac{di_2}{dt} = v_C \quad (\text{A13})$$

$$L_3 \frac{di_3}{dt} = v_C \quad (\text{A14})$$

$$C \frac{dv}{dt} = -i_1 - i_2 - i_3 \quad (\text{A15})$$

$$A_3 = \begin{bmatrix} 0 & 0 & 0 & 1/L_1 \\ 0 & 0 & 0 & 1/L_2 \\ 0 & 0 & 0 & 1/L_3 \\ -1/C & -1/C & -1/C & 0 \end{bmatrix} \quad (\text{A16})$$

Case IV

$$L_1 \frac{di_1}{dt} = v_C \quad (\text{A17})$$

$$L_2 \frac{di_2}{dt} = -v_C \quad (\text{A18})$$

$$L_3 \frac{di_3}{dt} = -v_c \quad (\text{A19})$$

$$C \frac{dv}{dt} = -i_1 + i_2 + i_3 \quad (\text{A20})$$

$$A_4 = \begin{bmatrix} 0 & 0 & 0 & 1/L_1 \\ 0 & 0 & 0 & -1/L_2 \\ 0 & 0 & 0 & -1/L_3 \\ -1/C & 1/C & 1/C & 0 \end{bmatrix} \quad (\text{A21})$$

Next using the following approximation to estimate the four different state matrices the final equations can be written.

$$A \cong (A_1 A_2 - A_2 A_1) d d' T \quad (\text{A22})$$

where,

$$d = \frac{\varphi}{2\pi} \quad (\text{A23})$$

$$\omega = \frac{2\pi}{T} \quad (\text{A24})$$

$$d' = 0.5 - \frac{\varphi}{2\pi} \quad (\text{A25})$$

$$A = \begin{bmatrix} 0 & -\left(\varphi - \frac{\varphi^2}{\pi}\right) \frac{1}{L_1 C \omega} & -\left(\varphi - \frac{\varphi^2}{\pi}\right) \frac{1}{L_1 C \omega} & 0 \\ \left(\varphi - \frac{\varphi^2}{\pi}\right) \frac{1}{L_2 C \omega} & 0 & 0 & 0 \\ \left(\varphi - \frac{\varphi^2}{\pi}\right) \frac{1}{L_3 C \omega} & 0 & 0 & 0 \\ 0 & 0 & 0 & 0 \end{bmatrix} \quad (\text{A26})$$

Next these equations were simplified by combining terms into a new variable and writing the equations for the converter currents.

$$k = \left(\varphi - \frac{\varphi^2}{\pi}\right) \frac{1}{\omega C} \quad (\text{A27})$$

$$\dot{I}_1 = -\frac{k}{L_1} I_2 - \frac{k}{L_1} I_3 \quad (\text{A28})$$

$$\dot{I}_2 = \frac{k}{L_2} I_1 \quad (\text{A29})$$

$$\dot{I}_3 = \frac{k}{L_3} I_1 \quad (\text{A30})$$

These were then solved in MATLAB's simulation solver.

$$I_1 = I_o \cos\left(\frac{k\sqrt{L_2 + L_3}}{\sqrt{L_1 L_2 L_3}} t\right) \quad (\text{A31})$$

$$I_2 = I_o \frac{\sqrt{L_1 L_3}}{\sqrt{L_2} \sqrt{L_2 + L_3}} \sin\left(\frac{k\sqrt{L_2 + L_3}}{\sqrt{L_1 L_2 L_3}} t\right) \quad (\text{A32})$$

$$I_3 = I_o \frac{\sqrt{L_1 L_2}}{\sqrt{L_3} \sqrt{L_2 + L_3}} \sin \left(\frac{k \sqrt{L_2 + L_3}}{\sqrt{L_1 L_2 L_3}} t \right) \quad (\text{A33})$$

APPENDIX B

SOURCE CODE FOR FEEDBACK CONTROL OF MULTI-SOURCE IDC

```

// Feedback Control of Multi-Source IDC
// Written by: Billy Yancey

// Defining variables
static double phi13 = 45, phi13_o = 45, phi13_c = 45, phi23_o = 45, phi23_c = 45;
static double pi = 3.1416, theta = 0, m = 0, a = 0, b = 0, V2o = 100, k = 0, n = 0,
del_phi_o = 1, del_phi = 1, c = 0, d = 0, mc1 = 0, mc2 = 0, I2_o = 0;
double Vo, Voref, Vrip, S114, S123, S214, S223, S314, S323, f, phi23, V2, I2, I2ref,
phi223, phi13_r, E, h, g, gnew, grat, w;

// Initializing switching frequency
f = 5000;

// Defining inputs
Vo = x1;
V2 = x2;
I2 = x3;
Voref = x4;
I2ref = x5;

// Defining variables
Vrip = 15; //ripple voltage
w = 2*pi*f; //angular frequency

// Creating a repeating theta from 0 - 360
if (theta >= 360)
{
    theta = 0;
    m++;
}
else
{
    theta = 2*180*f*t - 2*180*m;
}
// Control of Converter 3
if (theta >= 0 && theta <= 180)
{
    S314 = 1;
}

```

```

        S323 = 0;
    }
else
{
    S314 = 0;
    S323 = 1;
}

// Voltage control algorithm
if (t >= 0.025 && a == 0)
{
    if(((Vo > Voref+Vrip) || (Vo < Voref-Vrip)) && m >= mc1+25)
    {
        phi13_r = phi13_o*pi/180;
        g = w*2e-6/(phi13_r-pow(phi13_r,2)/pi);
        grat = Voref/Vo;
        gnew = grat*g;
        E = sqrt(gnew*gnew*pi*pi-4*gnew*w*2e-6*pi);
        //phi_c = 1/2/gnew*(gnew*3.1416-E)*180/3.1416;
        phi13_c = 1/(2*gnew)*(gnew*pi-E)*(180/pi);
        phi23_c = phi13_c;
        //phi_c = grat*phi_r*180/pi;
        h = 0;
        mc1 = m;
    }
else
{
    phi13 = phi13_o;
    h = 1;
}
}
else
{
    phi13 = phi13_c;
    h = 3;
}

if (phi13_c == phi13_o)
{
    phi13_o = phi13;
}
else
{
    if (theta <= 5)

```

```

    {
        a = 1;
    }

    else
    {
        phi13_o = phi13;
    }
}

// Checking for change in input voltage
if (t <= 0.025 && ((I2 > I2ref+0.5) || (I2 < I2ref+0.5)))
//if (((V2o+0.00001) >= V2 && (V2o-0.00001) <= V2)) || (t >= 0.01 && ((I2 >
I2ref+0.5) || (I2 < I2ref+0.5))))
{
    k = 0;
}
else
{
    k = 1;
}

// Current regulation for converter 2 algorithm
if (k == 1 && b == 0)
{
    if ((I2 > I2ref+0.5) && c == 0)
    {
        phi23_c = phi23_o + del_phi_o;
        phi23 = phi23_c;
        del_phi = del_phi_o;
        c = 1;
        d = 0;
        mc2 = m;
        I2_o = I2;
    }
    else if ((I2 < I2ref-0.5) && d == 0)
    {
        phi23_c = phi23_o - del_phi_o;
        phi23 = phi23_c;
        del_phi = del_phi_o;
        c = 0;
        d = 1;
    }
}

```

```

        mc2 = m;
        I2_o = I2;

        //del_phi_o = del_phi;
    }
    else
    {
        if ((I2 < I2ref-0.5) && (m > mc2+8))
        {
            c = 1;
            d = 0;
            phi23 = phi23_c;
            del_phi = del_phi_o;
        }
        else if ((I2 > I2ref+0.5) && (m > mc2+8))
        {
            c = 0;
            d = 1;
            phi23 = phi23_c;
            del_phi = del_phi_o;
        }
        else
        {
            phi23 = phi23_c;
            del_phi = del_phi_o;
        }
    }
    del_phi_o = del_phi;
}
else
{
    phi23 = phi23_c;
    del_phi_o = del_phi;
}

// Checking for duty cycle change of Converter 2
if (phi23 == phi23_o)
{
    phi23_o = phi23;
}
else
{
    if (theta <= 0.05)

```

```

        {
            b = 1;
        }
    else
    {
        }
    }
}

// Firing angle control for Converter 1
if (a == 0)
{
    if (theta >= phi13_o && theta <= (180+phi13_o))
    {
        S114 = 1;
        S123 = 0;
    }
    else if (theta >= (180+phi13_o) && theta <= 360)
    {
        S114 = 0;
        S123 = 1;
    }
    else
    {
        S114 = 0;
        S123 = 1;
    }
}

// Phase shift control for Converter 1
else if (a == 1)
{
    if (theta >= (phi13_o+((phi13-phi13_o)/2)) && theta <=
(180+(phi13_o+((phi13-phi13_o)/2))))
    {
        S114 = 1;
        S123 = 0;
    }
    else if (theta >= (180+(phi13_o+((phi13-phi13_o)/2))) && theta <= 360)
    {
        S114 = 0;
        S123 = 1;
    }
    else

```

```

    {
        S114 = 0;
        S123 = 1;
    }

// Checking to end phase shifting technique
if (theta >= 180)
{
    a = 0;
    phi13_o = phi13;
}
else
{
    a = 1;
}
}

// Firing angle control for Converter 2
if (b == 0)
{
    if (theta >= phi23_o && theta <= (180+phi23_o))
    {
        S214 = 1;
        S223 = 0;
    }
    else if (theta >= (180+phi23_o) && theta <= 360)
    {
        S214 = 0;
        S223 = 1;
    }
    else
    {
        S214 = 0;
        S223 = 1;
    }
}

// Phase shift control for Converter 2
else if (b == 1)
{
    if (theta >= (phi23_o+((phi23-phi23_o)/2)) && theta <=
(180+(phi23_o+((phi23-phi23_o)/2))))
    {
        S214 = 1;
    }
}

```

```
        S223 = 0;
    }
    else if (theta >= (180+(phi23_o+((phi23-phi23_o)/2))) && theta <= 360)
    {
        S214 = 0;
        S223 = 1;
    }
    else
    {
        S214 = 0;
        S223 = 1;
    }
}

// Checking to end phase shifting technique
if (theta >= 180)
{
    b = 0;
    phi23_o = phi23;
}
else
{
    b = 1;
}
}

// Defining outputs
y1 = S114;
y2 = S123;
y3 = S214;
y4 = S223;
y5 = S314;
y6 = S323;
y7 = phi13;
y8 = phi23;
```

APPENDIX C

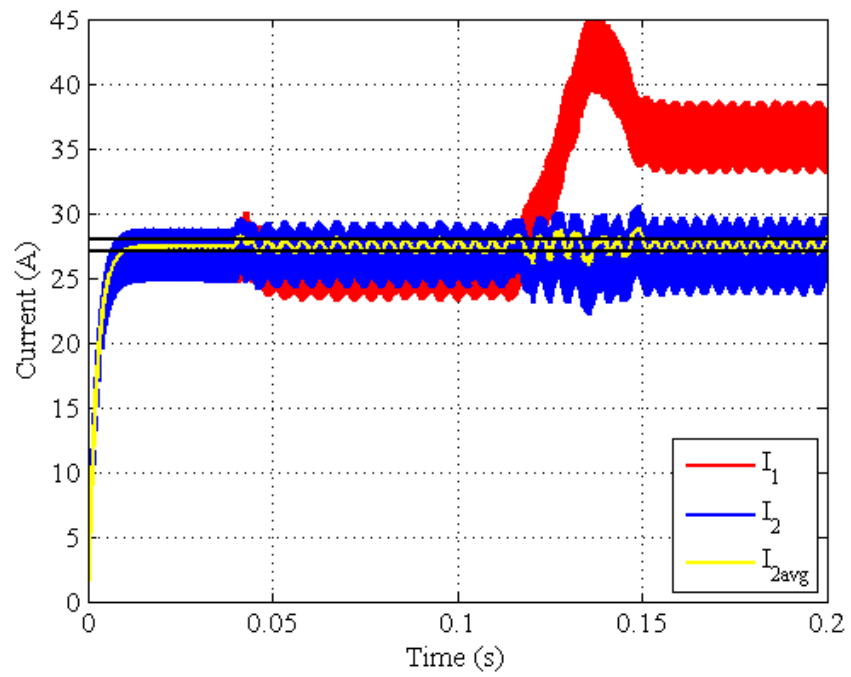
RESULTS FOR 10% V_2 AND 20% R_L VARIATIONS

Fig. C.1. Source currents.

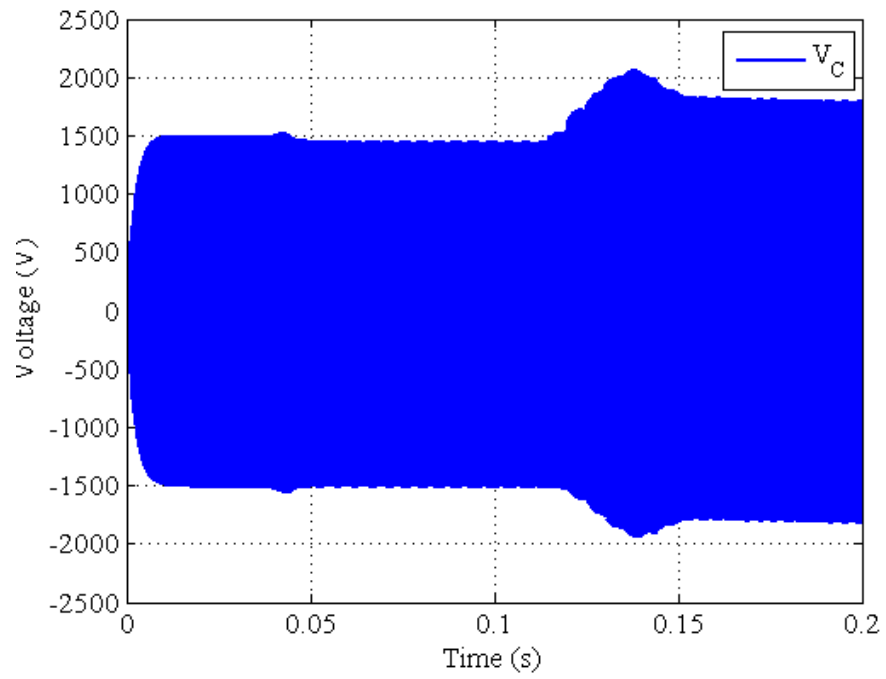


Fig. C.2. Center capacitor voltage.

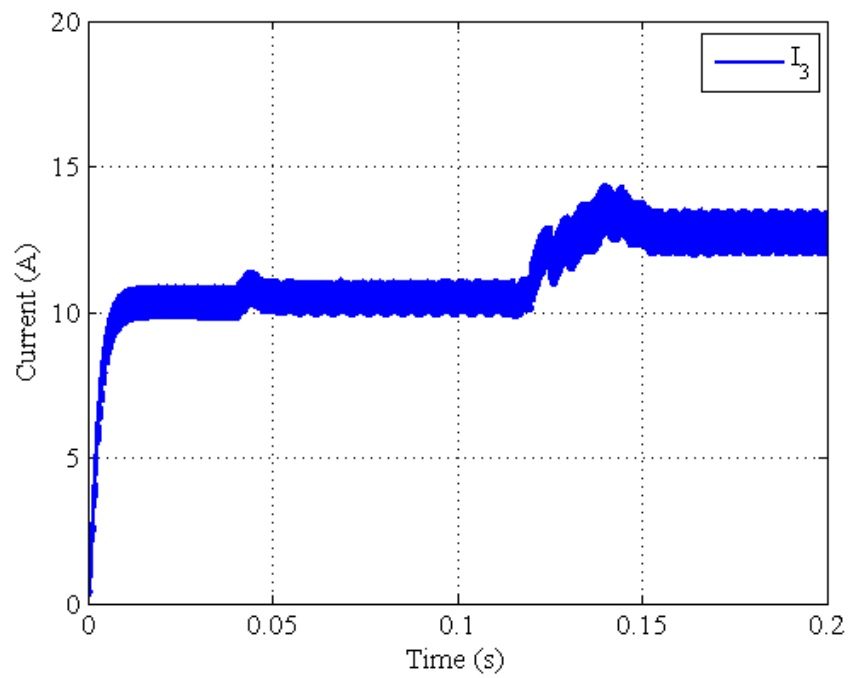


Fig. C.3. Load current.

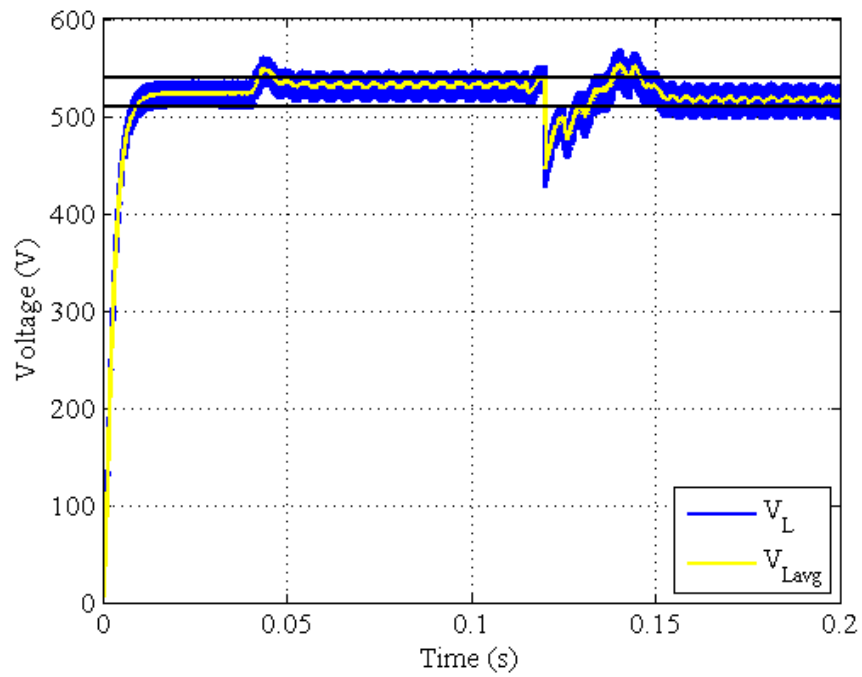


Fig. C.4. Load voltage.

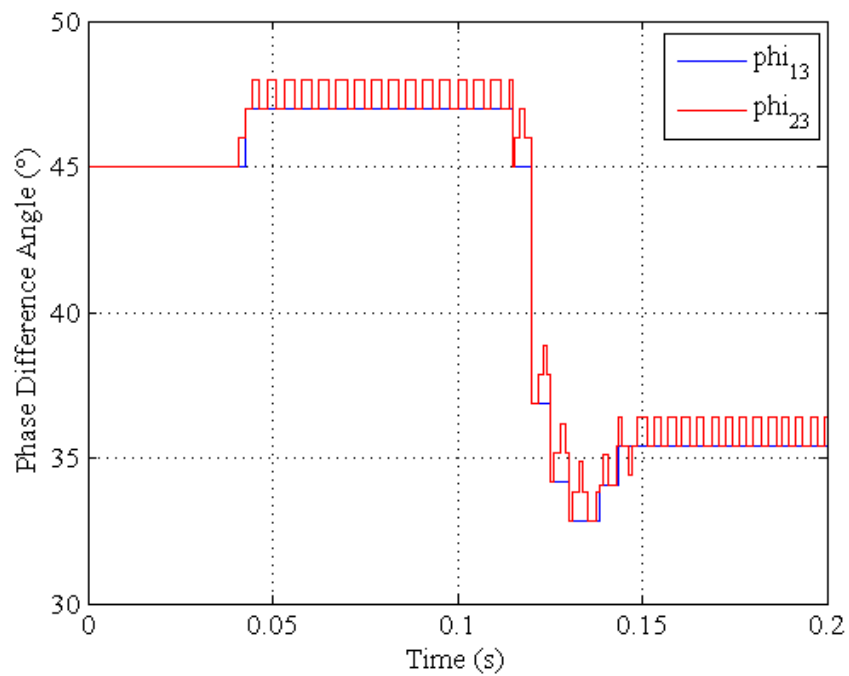
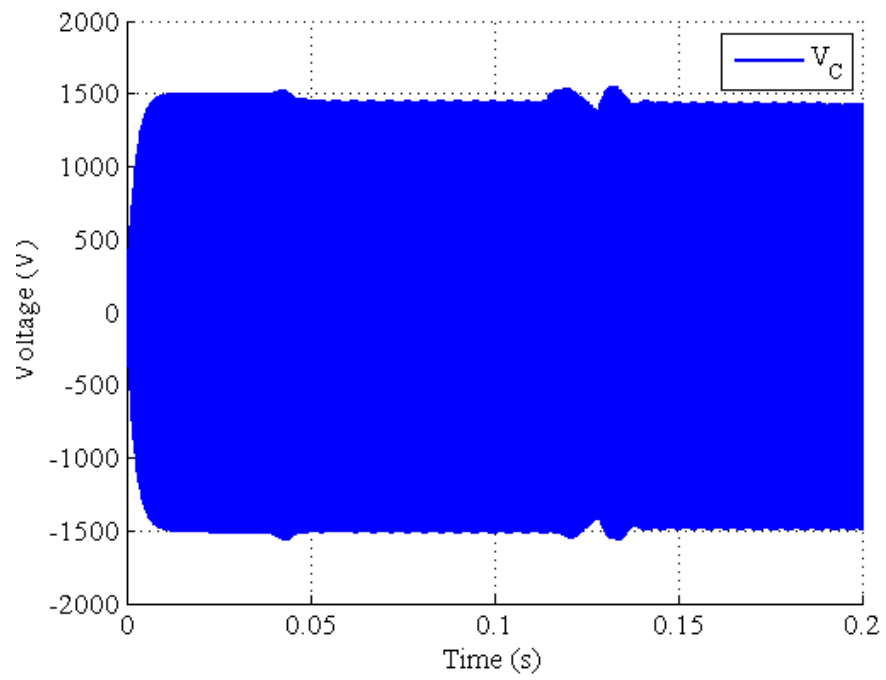


Fig. C.5. Phase difference angles.

APPENDIX D

RESULTS FOR STEP AND RAMP CURRENT VARIATIONS

Fig. D.1. Center capacitor voltage for 10% V_2 and 25% I_2 .

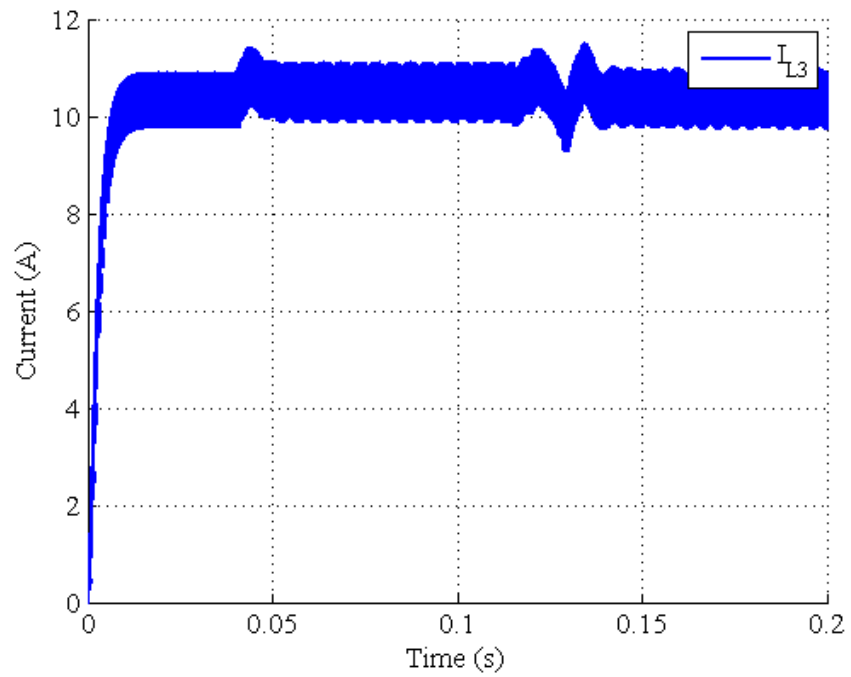


Fig. D.2. Load current for 10% V_2 and 25% I_2 .

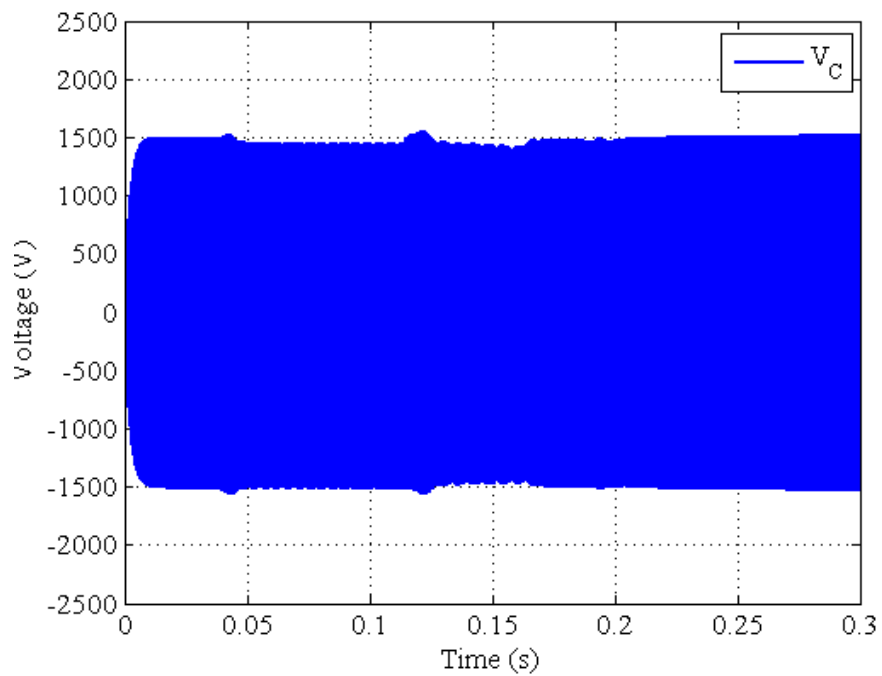


Fig. D.3. Center capacitor voltage for 10% V_2 and ramp down I_2 .

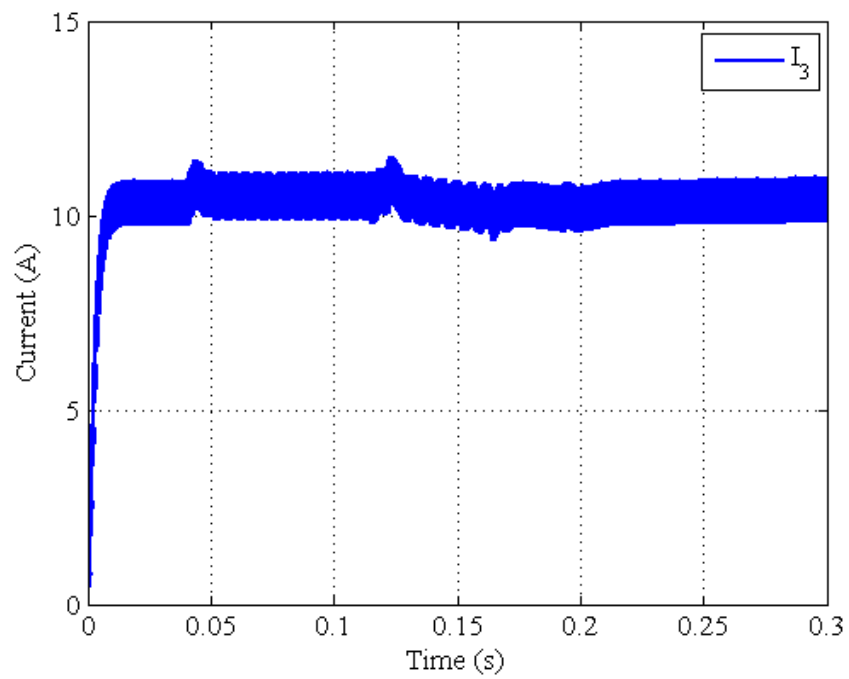


Fig. D.4. Load current for 10% V_2 and ramp down I_2 .

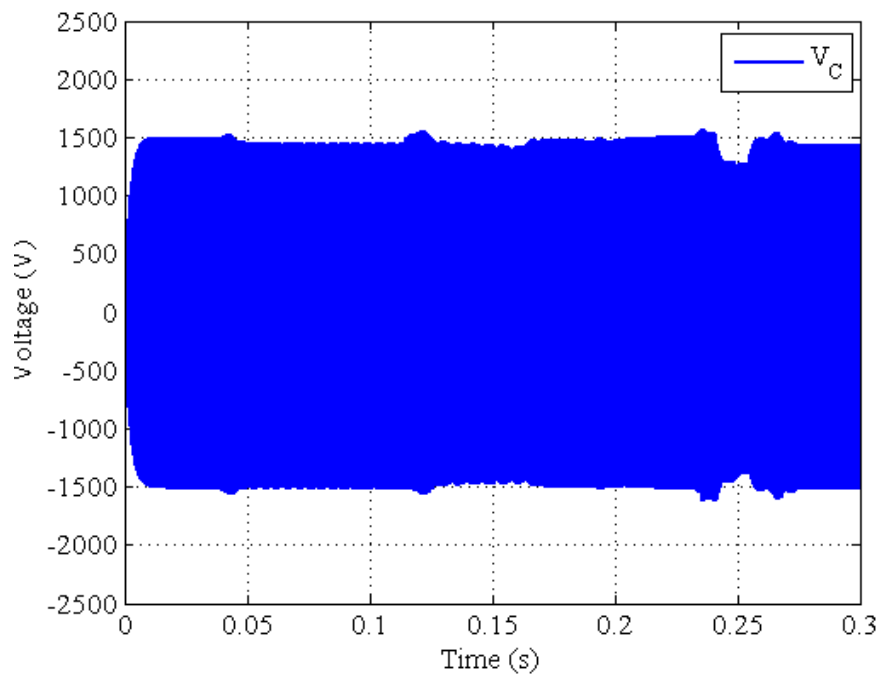


Fig. D.5. Center capacitor voltage for 10% V_2 and ramp down/up I_2 .

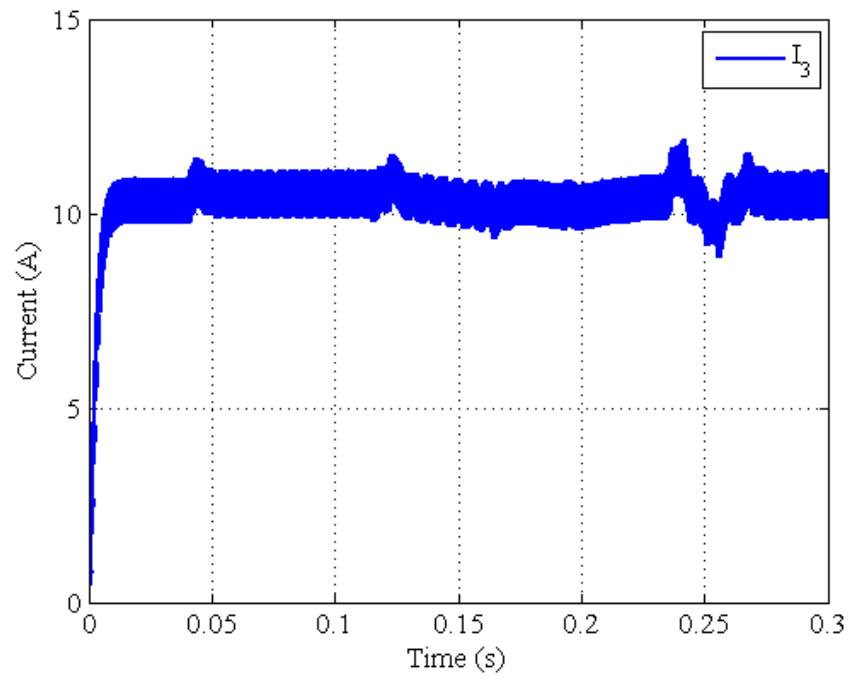


Fig. D.6. Load current for 10% V_2 and ramp down/up I_2 .

VITA

Billy Ferrall Yancey III received his Bachelor of Science in engineering from Arkansas State University in December of 2005. Upon graduation he entered into the graduate program in the Department of Electrical Engineering at University of Missouri-Rolla where he specialized in electromagnetics. After one semester he then transferred to the graduate program in the Department of Computer and Electrical Engineering at Texas A&M University where he specialized in power electronics and motor drives. He received his Master of Science in electrical engineering in May of 2010. His research interests include sustainable energy, power electronic converters for energy storage, and design and control of electrical machines.

He can be reached at billy.yanceyiii@gmail.com or through his advisor Dr. M. Ehsani, Professor, Department of Electrical and Computer Engineering, 3128 TAMU, Texas A&M University, College Station, TX 77843.